Master Thesis

Master's Degree in Energy Engineering

Numerical and computational tools for modern grids with power converters

June 2022

Author: Josep Fanals i Batllori

Supervisors: Oriol Gomis Bellmunt

Eduardo Prieto Araujo

Escola Tècnica Superior
d'Enginyeria Industrial de Barcelona

Abstract

During the last decades, power systems are being transformed in order to move towards decentralized, resilient and sustainable grids. This change of paradigm promotes the integration of power converters as means of coupling renewable generation sources and offering more grid controllability. The appearance of such a novel device at the grid level requires the reformulation of the steady-state system definition. Thus, new techniques and tools are susceptible of appearing so that power systems can be modeled and simulated appropriately.

The work captured in this thesis belongs to two different categories. On the one hand, the current limits of power converters are addressed. A reformulation of the power flow problem is introduced considering their current limits. The methodology is implemented in a large-scale system during fault conditions. In addition, the inclusion of renewable energies is subjected to grid codes, which impose the injection of currents so as to provide voltage-support in the case of faults. The project studies the optimality of conventional grid codes and proposes modifications to improve the voltages under various short-circuit scenarios.

On the other hand, the document deals with the parametrization of the power flow. The power flow can be regarded as a snapshot of the system at a given condition. However, variables are likely to change over time. The parametrized solution to the power flow provides an explicit relationship between the unknown variables and the set of parameters. Multiple techniques are explored, especially the usage of the Galerkin method and the Principal Component Analysis. Although they differ in accuracy and time complexity, both options are adequate to solve realistic grids.

Contents

List of Figures

List of Tables

Glossary

Symbols

$\boldsymbol{A}$	Diagonal matrix formed by eigenvalues
$\boldsymbol{B}$	Imaginary part of the admitance matrix
$\boldsymbol{c^e}$	Vector of coefficients for the real voltage
$\boldsymbol{c^f}$	Vector of coefficients for the imaginary voltage
$\boldsymbol{C}$	Covariance matrix
$\boldsymbol{f}$	Vector of functions
f_o	Objective function
$\boldsymbol{G}$	Real part of the admitance matrix
$\boldsymbol{h_x}$	Observations vector generated with samples
I_{max}	Maximum current of the converter
$\boldsymbol{J}$	Jacobian matrix
k_{isp}	Droop constant for grid-support
M	Number of samples
n	Number of unknowns
N_p	Order of the polymonial
N_d	Number of parameters
$\mathcal{O}$	Time complexity
$\boldsymbol{p}$	Set of parameters
P	Active power injection
Q	Reactive power injection
R	Residual of a given function
$\underline{S}$	Complex power
u_{max}	Voltage upper limit
u_{min}	Voltage lower limit
x	Unknown variable to find
δ	Voltage angle
$\boldsymbol{\Delta x}$	Vector of variations of unknowns
$\boldsymbol{\Delta f}$	Vector of residuals
ϵ	Set tolerance
λ	Eigenvalue
ν	Voltage magnitude
Ω	Parametrization search space
$\boldsymbol{\Psi}$	Primal set of basis

θ	Voltage angle
$\boldsymbol{\Phi}$	Full set of basis
$\boldsymbol{W}$	Matrix of eigenvectors
$\boldsymbol{y}$	Reduced set of meaningful parameters
$\boldsymbol{Y}$	Admittance matrix
$\boldsymbol{Z}$	Generic tensor

Acronyms

AC	Alternating Current
ASD	Alternating Search Directions
CCP	Converter Connection Point
CITCEA	Centre d'Innovació Tecnològica en Convertidors Estàtics i Accionaments
DC	Direct Current
DIS	Disconnected State
FSS	Fully Saturated State
GC	Grid Code
HELM	Holomorphic Embedding Load-Flow Method
IEEE	Institute of Electrical and Electronics Engineers
LU	Lower-Upper decomposition
NR	Newton-Raphson
PCC	Point of Common Coupling
PGD	Proper Generalized Decomposition
PSS	Partially Saturated State
UPC	Universitat Politècnica de Catalunya
USS	Unsaturated State
VSC	Voltage Source Converter

Preface

Traditional techniques to solve power systems in steady-state conditions have existed for decades. Their particularities are well-known to the community, and little to no innovations would be required to analyze conventional systems. The introduction of renewable sources of energy, storage solutions, and demand response mechanisms, among others, cause profound changes in the understanding of the grid. Consequently, mathematical procedures and computational tools have to adapt in order to face the aforementioned challenge.

A relevant issue that modern grids have to confront is the modeling of the system under short-circuit faults. Contrarily to synchronous generators, power converters have to thoroughly control the magnitude of the current they are injecting. By definition, their behavior becomes non-linear once current limits are reached. The classic short-circuit analysis is no longer valid due to the appearance of the non-linear equations modeling the operation of converters. Modeling coherently short-circuits is a non-trivial issue since even popular pieces of software such as PSS/E fail at obtaining the correct steady-state solution.

Another aspect of concern in modern grids is related to the continuous recalculation of the power flow. More grid controllability goes hand in hand with more varying and uncertain system states. Unfortunately, if a single converter setpoint is modified, the whole power flow would have to be calculated again. This comes with an expense of time and computational effort. Instead of solving again the set of non-linear equations, the parametric power flow provides a closed-form expression that relates the parameters (i.e., the variables expected to change) with the unknowns. Much more convenient expressions are derived, which allow the obtention of the steady-state solution in a fraction of the time.

The work developed at the Centre d'Innovació Tecnològica en Convertidors Estàtics i Accionaments (CITCEA) and its spin-off eRoots Analytics attempts to push the existing power systems towards modern grids. The ideas, algorithms and tools developed in this project are set to become a contribution to make this change a reality.

1 Introduction

1.1 Background

Power systems have been typically characterized by centralized generation units powered by fossil fuels and unidirectional power flows [1]. The proliferation of renewable energies ever since the first big oil crisis has carried the immanent challenge of modifying the electrical grid [2], [3]. Modern systems are meant to be reliable, efficient, and at the same time integrate a large penetration of renewables. These are, in short, some of the objectives of the so-called smart grid [4], [5]. Power electronics equipment is expected to become a key driver. In particular, power converters are required to couple renewable energy sources to the grid [6]. They provide controllability, optimize the operation, and ideally help at improving the reliability as well as the stability [7]–[9].

Adding electronics at the grid level has impactful effects on the modeling of the system. Compared to traditional elements such as synchronous generators, the associated control of power converters limits the current during faults to not damage the equipment [10], [11]. Non-linearities arise, and with them, conventional computational tools may no longer be adequate to solve modern systems. Buses have been typically classified as PQ, PV or slack [12], [13], yet current saturation causes the appearance of novel categories. It is also worth mentioning that the traditional approach of modeling converters as current sources during short-circuits may be imprecise given the unknown current angle [11], [14], [15]. Another issue of concern is that converters can operate at multiple states, and hence multiple solutions may exist [16]. Besides, grid codes establish demanding requirements for renewable sources of energy connected through converters [17]. These converters have to help at maximizing voltage-support, although the optimal approach to do so remains unclear.

The grid states are likely to experience variations now more than ever. More controllability is associated with a change in the setpoints, which in turn involves solving repeatedly the power flow problem. Represented by a large set of non-linear equations, obtaining its solution may become a laborious task [18]. The parametric power flow combats this issue by forming a direct relationship between the variable inputs (parameters) and the unknowns (states). The Galerkin method is a mathematical tool that has been long applied to non-electrical domains (see [19] for instance). Recently it has been found useful for parametrizing the power flow [20], [21]. A significant problem it faces is the curse of dimensionality, that is, the bothersome pace at which the computational effort increases with the number of parameters [22]. Techniques based on the Principal Component Analysis combined with a reduction of dimensions are seen as viable options, at the expense of less accuracy [23].

1.2 Objectives

Considering the state of the art, the goals of the thesis are the following:

- To develop a scalable and efficient algorithm to solve the power flow and short-circuit faults considering the current limits of converters. The multiple states in which converters can operate are formulated, along with the associated new set of buses. The program is expected to solve large scale grids.
- To present a methodology that includes the current limits of converters algebraically in the system of non-linear equations.
- To analyze the voltage-support provided by following traditional grid codes for systems under short-circuit fault conditions with power converters. Alternative grid codes are meant to be suggested in case a substantial improvement can be made.
- To explore the set of techniques to parametrize the power flow, focusing on computationally efficient methods that are able to circumvent the curse of dimensionality.
- To apply the decoupled and expanded Galerkin method to the power flow problem. To do so, a generic formulation and the associated program ought to be developed.

1.3 Outline

The structure of the thesis is captured below:

- Chapter 2 covers the definition of converter's states, their modeling, as well as the adapted iterative method to solve grids with power converters. Attention is placed on the short-circuit analysis. Besides, the algebraic inclusion of current limits by employing a Lagrangian function is also discussed in a simple system.
- Chapter 3 is centered around the definition of grid codes for voltage-support during short-circuit faults. The solution provided by conventional grid codes is compared to the optimal one. Two modified grid codes, arguably similar to the traditional one, are suggested to further improve the voltages.
- Chapter 4 establishes the mathematical basis of the Galerkin method combined with Legendre polynomials to be applied in the power flow problem. A generic approach to solve standard grids with parametrized powers is presented.
- Chapter 5 reviews efficient parametric tools that scale better with dimensions than the Galerkin method. The usage of the Principal Component Analysis and a reduction of parameters are studied in greater detail.

- Chapter 6 summarizes the contributions of this work. Potential future lines of work are listed as well.

2 Short-circuit faults with power converters

2.1 Introduction

The integration of renewables and the subsequent penetration of power converters causes profound changes in the operation of power systems. This is especially the case under short-circuit fault conditions. Converters have to operate inside their current and voltage limits, which may force them to become saturated. In such cases, new operating states appear. Hence, the equations that intervene in the power flow problem vary.

The present chapter starts by modeling power converters from a steady-state perspective. The various operating states are described, together with the corresponding equations. Emphasis is placed on the adapted Newton-Raphson method and its Jacobian (see [24] for a simple explanation), as its usage has been found crucial to guarantee a fast calculation. Then, the overall structure of the calculation process is shown. A 2000-bus case study is covered in order to evaluate the performance of the program. The time complexity of the program is assessed to get an idea of how well it scales. In addition, the integration of algebraic limits is derived and exemplified for a simple case.

2.2 Problem definition

In the traditional power flow, buses are either PQ, PV, or slack (commonly reserved for a single one). Power converters also force the presence of these types of buses under normal conditions. However, if abnormal situations arise, such as short-circuit faults, they may reach their current limits or even disconnect. Saturated converters can operate under certain controls. This work considers two current saturation states (PSS and FSS) as described in [25]. All in all, Table 1 displays the four controlled variables depending on the original bus classification and the state of the converter.

Table 1: Possible operating states of the converters in grid-following mode.

	PQ	**PV**
USS	P, Q	P, V
PSS	Q, I_{max}	V, I_{max}
FSS	$P = 0$, I_{max}	$P = 0$, I_{max}
DIS	$P = 0, Q = 0$	$P = 0, Q = 0$

It is important to note that when the converter is at FSS or DIS, it does not matter if it behaves as a PQ or a PV bus since the references are the same. Each converter is therefore capable of operating at six unique states, as can be deduced from Table 1. The description and logic behind the states in Table 1 are summarized below:

1. USS: the converter is unsaturated and can meet the typical references of PQ and PV buses.

2. PSS: the converter is partially saturated. Hence, it can provide the required reactive power (the specified one or the one to reach the desired voltage). However, it cannot surpass the maximum current allowed by the converter, so the active power reference is not met.

3. FSS: the active power is zero while the current is at its maximum. This means the converter provides the maximum possible reactive power.

4. DIS: operating state where the converter is fully disconnected due to an extremely low or high voltage. Hence, no active nor reactive powers are provided. It can be evaluated as if both the active and the reactive powers are at zero, or $P = 0$ and $I_{max} = 0$ for instance. These are equivalent ways to express the same state.

The main challenge converters pose has to do with the new current magnitude equation. This is especially relevant in short-circuit calculations. Some pieces of software such as PSS/E or PowerFactory inject a precalculated current whose angle is unknown and the dependency on the voltage is not considered. Hence, this approach lacks accuracy [26]. Another option is to perform a dynamic simulation, although it may be very time-consuming. The goal of this chapter is to show a methodology to integrate current limits in steady-state calculations.

2.3 Formulation

Consider the traditional power flow, composed of three types of buses: slack, PQ and PV. The slack sets its bus voltage and covers the power mismatches; the PQ bus specifies a given injection of active and reactive power; and in the PV bus, the voltage magnitude as well as the active power injection are established [27]. In matrix form, the power equations are [28]:

$$\begin{cases} \boldsymbol{P} = \Re([\boldsymbol{V}]\boldsymbol{Y}^*\boldsymbol{V}^*), \\ \boldsymbol{Q} = \Im([\boldsymbol{V}]\boldsymbol{Y}^*\boldsymbol{V}^*), \end{cases} \tag{1}$$

where $\boldsymbol{P}$ and $\boldsymbol{Q}$ are the vectors of active and reactive power injections in the buses, $\Re()$ and $\Im()$ are the functions that extract the real and imaginary part respectively, $[\boldsymbol{V}]$ is the diagonal matrix of bus voltages whose elements take the form $\nu_i e^{j\theta_i}$, being ν_i the voltage magnitude and θ_i the voltage angle of a given bus i, $\boldsymbol{Y}^*$ is the complex conjugated bus admittance matrix, and $\boldsymbol{V}^*$ is the complex conjugated vector of voltages.

The system of equations from (1) is solved for the magnitude and the phase of the voltages in the buses where they are unknown. In PQ buses, both the magnitude ν and the angle θ are unknown, whereas in PV buses only the angle θ has to be found. Thus, the total number of unknowns is $2n_{pq} + n_{pv}$, where n_{pq} is the number of PQ buses, and n_{pv} is the number of PV buses. A determined implicit system of equations is obtained since in each PQ bus there are

two equations involved (both active and reactive power), and for each PV bus, the active power equation has to be considered.

The non-linear system of equations is typically solved following the Newton-Raphson method, which generically becomes:

$$\boldsymbol{\Delta f} = -\boldsymbol{J}\boldsymbol{\Delta x}, \tag{2}$$

where $\boldsymbol{\Delta f}$ is the vector of residuals, $\boldsymbol{J}$ is the Jacobian, and $\boldsymbol{\Delta x}$ represents the variations of the unknowns. In the power flow problem:

$$\begin{pmatrix} \boldsymbol{\Delta f_P} \\ \boldsymbol{\Delta f_Q} \end{pmatrix} = - \begin{pmatrix} \frac{d\boldsymbol{f_P}}{d\boldsymbol{\theta}} & \frac{d\boldsymbol{f_P}}{d\boldsymbol{\nu}} \\ \frac{d\boldsymbol{f_Q}}{d\boldsymbol{\theta}} & \frac{d\boldsymbol{f_Q}}{d\boldsymbol{\nu}} \end{pmatrix} \begin{pmatrix} \boldsymbol{\Delta\theta} \\ \boldsymbol{\Delta\nu} \end{pmatrix}, \tag{3}$$

where the left-hand side vector contains the following residuals:

$$\begin{cases} \boldsymbol{\Delta f_P} = -\boldsymbol{P_{\text{set}}} + \Re([\boldsymbol{V}]\boldsymbol{Y}^*\boldsymbol{V}^*), \\ \boldsymbol{\Delta f_Q} = -\boldsymbol{Q_{\text{set}}} + \Im([\boldsymbol{V}]\boldsymbol{Y}^*\boldsymbol{V}^*), \end{cases} \tag{4}$$

where $\boldsymbol{P_{\text{set}}}$ and $\boldsymbol{Q_{\text{set}}}$ are the vectors of set active and reactive power respectively, in the corresponding PQ and PV buses.

Equation (3) is solved for the increments of phase and magnitude, that is, $\boldsymbol{\Delta\theta}$ and $\boldsymbol{\Delta\nu}$. This way, at each iteration, the unknowns are updated as:

$$\begin{cases} \boldsymbol{\theta}^{(k+1)} = \boldsymbol{\theta}^{(k)} + \boldsymbol{\Delta\theta}, \\ \boldsymbol{\nu}^{(k+1)} = \boldsymbol{\nu}^{(k)} + \boldsymbol{\Delta\nu}, \end{cases} \tag{5}$$

where k denotes the index of the previous iteration.

The matrix in (3) is the so-called Jacobian. Compactly, its entries are the following (for more details, see [28]):

$$\begin{cases} \frac{d\boldsymbol{f_P}}{d\boldsymbol{\theta}} = \Re(j[\boldsymbol{V}]([\boldsymbol{Y}^*\boldsymbol{V}^*] - \boldsymbol{Y}^*[\boldsymbol{V}^*])), \\ \frac{d\boldsymbol{f_Q}}{d\boldsymbol{\theta}} = \Im(j[\boldsymbol{V}]([\boldsymbol{Y}^*\boldsymbol{V}^*] - \boldsymbol{Y}^*[\boldsymbol{V}^*])), \\ \frac{d\boldsymbol{f_P}}{d\boldsymbol{\nu}} = \Re([\boldsymbol{V}]([\boldsymbol{Y}^*\boldsymbol{V}^*] + \boldsymbol{Y}^*[\boldsymbol{V}^*])[\boldsymbol{\nu}]^{-1}), \\ \frac{d\boldsymbol{f_Q}}{d\boldsymbol{\nu}} = \Im([\boldsymbol{V}]([\boldsymbol{Y}^*\boldsymbol{V}^*] + \boldsymbol{Y}^*[\boldsymbol{V}^*])[\boldsymbol{\nu}]^{-1}). \end{cases} \tag{6}$$

2.3.1 Adapted Newton-Raphson method

In contrast with the conventional power flow described until now, the inclusion of power converters involves the treatment of current as a magnitude to be controlled. Hence, the power flow solver has to contain an additional set of equations responsible for limiting the current of

converters when short-circuit faults occur. States in which the current is limited will be referred to as saturation states.

Figure 1 shows the scheme from where the equation of the converter current magnitude is derived. The bus i under study has a current source, a power source, a converter, and impedances (a shunt element and links to other buses) connected to it.

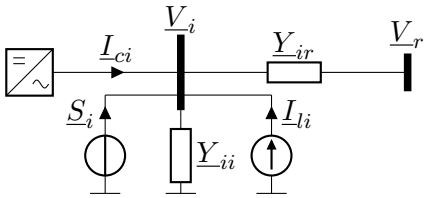

Figure 1: Generic bus with a converter, a power source, a current source, and impedances.

By Kirchhoff's current law, the current balance in bus i is:

$$\underline{I}_{ci} = \underline{V}_i \underline{Y}_{ii} + \sum_{r \neq i} \underline{Y}_{ir} \underline{V}_r - \underline{I}_{li} - \underline{S}_i^* / \underline{V}_i^*, \tag{7}$$

or in matrix form:

$$\boldsymbol{I_c} = \boldsymbol{YV} - [\boldsymbol{V}^*]^{-1} \boldsymbol{S}^* - \boldsymbol{I_l}. \tag{8}$$

The phase of the converter current $\boldsymbol{I_c}$ is constructively irrelevant. It affects the distribution of current between active and reactive components, yet it is the absolute value of the current that determines if the converter ends up damaged under short-circuit conditions. One approach to work with the absolute value of the current is to compute the product between the current and the complex conjugated current:

$$\boldsymbol{f_{I^2}} = \boldsymbol{I_c} \boldsymbol{I_c^*}. \tag{9}$$

Hence, the new squared current residual becomes:

$$\boldsymbol{\Delta f_{I^2}} = -\boldsymbol{I^2_{c,max}} + (\boldsymbol{YV} - [\boldsymbol{V}^*]^{-1} \boldsymbol{S}^* - \boldsymbol{I_l}) \cdot (\boldsymbol{YV} - [\boldsymbol{V}^*]^{-1} \boldsymbol{S}^* - \boldsymbol{I_l})^*, \tag{10}$$

where $\boldsymbol{I^2_{c,max}}$ is the vector of squared maximum currents supported by the converters.

The remaining unknowns are still the phase and the voltage magnitude. The terms of the Jacobian to be calculated are:

$$\begin{cases} \frac{d\boldsymbol{f_{I^2}}}{d\boldsymbol{\theta}} = [\boldsymbol{I_c}](\frac{d\boldsymbol{I_c}}{d\boldsymbol{\theta}})^* + [\boldsymbol{I_c}]^*(\frac{d\boldsymbol{I_c}}{d\boldsymbol{\theta}}), \\ \frac{d\boldsymbol{f_{I^2}}}{d\boldsymbol{\nu}} = [\boldsymbol{I_c}](\frac{d\boldsymbol{I_c}}{d\boldsymbol{\nu}})^* + [\boldsymbol{I_c}]^*(\frac{d\boldsymbol{I_c}}{d\boldsymbol{\nu}}), \end{cases} \tag{11}$$

where the derivatives are:

$$\begin{cases} \frac{d\boldsymbol{I_c}}{d\boldsymbol{\theta}} = j(\boldsymbol{Y}[\boldsymbol{V}] - [\boldsymbol{S}]^*[\boldsymbol{V}^*]^{-1}), \\ \frac{d\boldsymbol{I_c}}{d\boldsymbol{\nu}} = ([\boldsymbol{S}]^*[\boldsymbol{V}^*]^{-1} + \boldsymbol{Y}[\boldsymbol{V}])[\boldsymbol{\nu}]^{-1}. \end{cases} \tag{12}$$

With this, the whole system of equations becomes:

$$\begin{pmatrix} \boldsymbol{\Delta f_P} \\ \boldsymbol{\Delta f_Q} \\ \boldsymbol{\Delta f_{I^2}} \end{pmatrix} = - \begin{pmatrix} \frac{d\boldsymbol{f_P}}{d\boldsymbol{\theta}} & \frac{d\boldsymbol{f_P}}{d\boldsymbol{\nu}} \\ \frac{d\boldsymbol{f_Q}}{d\boldsymbol{\theta}} & \frac{d\boldsymbol{f_Q}}{d\boldsymbol{\nu}} \\ \frac{d\boldsymbol{f_{I^2}}}{d\boldsymbol{\theta}} & \frac{d\boldsymbol{f_{I^2}}}{d\boldsymbol{\nu}} \end{pmatrix} \begin{pmatrix} \boldsymbol{\Delta\theta} \\ \boldsymbol{\Delta\nu} \end{pmatrix}. \tag{13}$$

Equation (13) is solved to find the variations of the unknowns. The unknowns are then updated as indicated in (5). Then, if the residuals are still too large, these steps are repeated until convergence is reached.

As mentioned, converters are supposed to be able to operate in four different states [16], which affects the associated type of bus. In the unsaturated state (USS), the converter operates as a regular PQ/PV bus. When working in the partially saturated state (PSS), the converter injects the maximum current and specifies a given voltage magnitude or reactive power. If fully saturated (FSS), then the converter works at the maximum current and injects no active power ($P = 0$) [29]. Thus, the current equation has to be taken into account in both PSS and FSS. The fourth state corresponds to a disconnected (DIS) converter, as if it was non-existent. It can be modeled by setting $P = 0$ and $Q = 0$, for instance. Table 2 summarizes the type of bus in accordance with the converter state.

Table 2: Traditional types of buses and mapping to types of buses depending on the converter state.

Converter State	PQ Control	PV Control
USS	PQ	PV
PSS	QI	VI
FSS	PI	PI
DIS	PQ	PQ

Notice that traditional PQ and PV buses are mapped to PQ, PV, QI, PI, and VI buses. In this regard, the current limits of converters force the presence of the novel PI, QI, and VI buses.

The diagram depicted in Figure 2 illustrates the procedure to obtain the solution of the system of equations from the initial objects. The iterations stop once the maximum residual (or mismatch) is no longer greater than an established tolerance ϵ.

2.3.2 Iteration of states

Regarding the operation of converters, on one side, they could be tripped off in case of losing the voltage reference. On the other side, the converter control saturates the current to avoid being overloaded (assuming it remains connected). The potential current saturation modifies the converter operation. Hence, the different states of converters should be considered in the

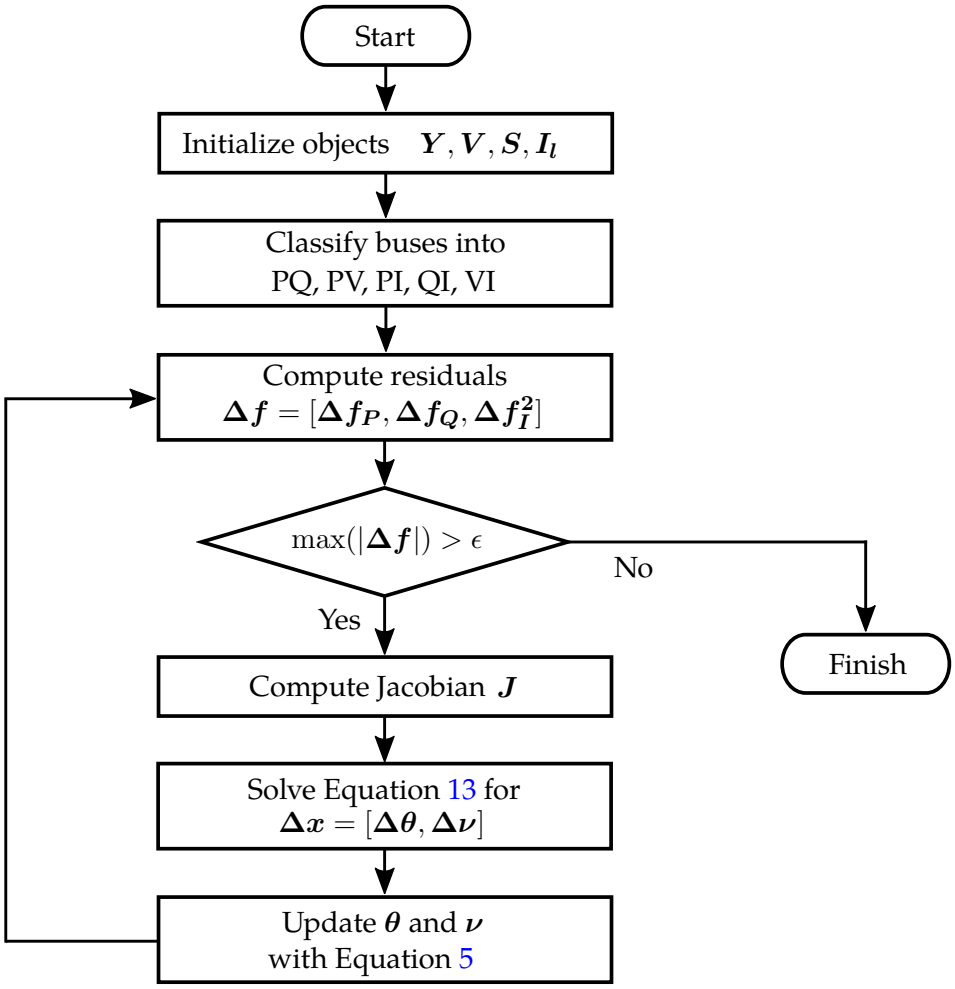

Figure 2: Steps to solve the power flow problem.

computation of system operation points. This is especially critical for short-circuit calculation as the converters close to the fault location will be operated with a reduced voltage, which makes them disconnected or operated with a limited current.

Usually, the operation state of a converter in a specific scenario is uncertain. Therefore, an iterative algorithm has been proposed to obtain the converters' operation states to calculate the system operation points that satisfy all converter limits. This iterative process serves as the outer loop that updates converters' operation states. On the other hand, the inner loop defines and solves the equations modeling the studied system corresponding to the given states of converters, which has been explained in the previous section. In particular, the outer loop updates the converters' states for each outer loop iteration $n + 1$ based on the solution obtained from the previous iteration n, which is calculated by the inner loop solver.

The converter will be tripped off when the converter connection point (CCP) voltage is lower

than the threshold value. Therefore, the connection status of a converter can be updated as follows based on the obtained solution such that:

$$x_i = \begin{cases} \text{Connected} & \text{if } u_i \geq u_i^{\text{inf}} \text{ and } u_i \leq u_i^{\text{sup}} \\ \text{Disconnected} & \text{if } u_i < u_i^{\text{inf}} \text{ or } u_i > u_i^{\text{sup}} \end{cases} \tag{14}$$

where x_i is the activation state of the converter connected to bus i, u_i is the voltage magnitude of bus i (which is also the CCP voltage magnitude), and u_i^{inf} and u_i^{sup} are the established lower and upper voltage limits to trip off the converter. A disconnected converter would fall under the DIS state, and thus, it can simply be eliminated from the model.

When a converter has been identified as remaining connected to the AC grid following the criterion expressed in (14) for the iteration $n+1$, it is also necessary to update its current saturation states. A similar scheme can be adopted to update the converters current saturation states based on the solution obtained from the previous iteration n.

The current saturation states for the converter in PQ control are updated based on the limits in terms of its CCP voltage magnitudes such that:

$$\begin{cases} \underbrace{\sqrt{p_{ref}^2 + q_{ref}^2}/i_{vsc}^{\max}}_{u_{lim}^{USS}} \leq u_{con} & \text{if USS} \\ \underbrace{|q_{ref}|/i_{vsc}^{\max}}_{u_{lim}^{FSS}} \leq u_{con} < \underbrace{\sqrt{p_{ref}^2 + q_{ref}^2}/i_{vsc}^{\max}}_{u_{lim}^{USS}} & \text{if PSS} \\ u_{con} \leq \underbrace{|q_{ref}|/i_{vsc}^{\max}}_{u_{lim}^{FSS}} & \text{if FSS} \end{cases} \tag{15}$$

where u_{lim}^{USS} is the upper limit of the CCP voltage magnitude for converter operated in USS, u_{lim}^{FSS} is the upper limit for FSS, and p_{ref} and q_{ref} are the active and reactive power references respectively. The current saturation state of a converter, x_i, can be updated based on an obtained solution, sol, utilizing a function, $DS(sol, i)$, which is expressed as follows:

$$x_i = \begin{cases} \text{USS} & \text{if } u_{lim}^{USS} \leq u_n \\ \text{PSS} & \text{if } u_{lim}^{FSS} \leq u_n < u_{lim}^{USS} \\ \text{FSS} & \text{if } u_n \leq u_{lim}^{FSS} \end{cases} \tag{16}$$

where u_n is the voltage solution obtained at the iteration n.

The heuristics related to PV are not as straightforward. However, some possible paths to transition between states are depicted in Figure 3. It has to be mentioned that these heuristics provide no guarantee that a feasible solution will be found. However, they are a convenient first step towards finding a suitable state configuration.

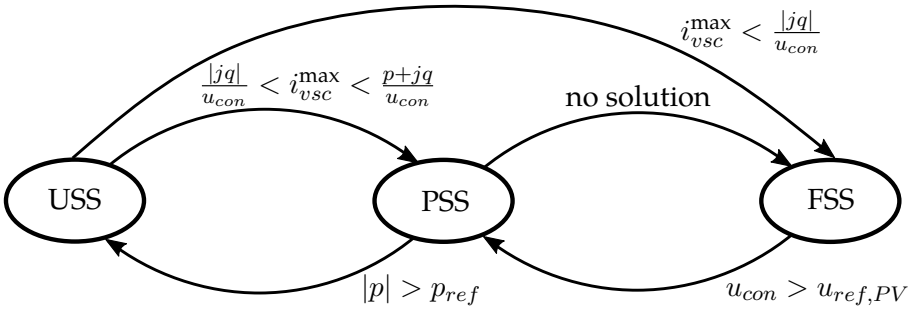

Figure 3: Heuristics to determine the states of PV converters.

The overall workflow of the proposed methodology is summarized as shown in Figure 4. The process starts with a set of initial states of all converters in the studied system, $\boldsymbol{X}_0$. The equations modeling the studied system are defined and solved in the first iteration using the solver presented in Figure 2. The states of all converters for the upcoming iteration, $n+1$, will be updated based on the solution obtained from the current iteration. In particular, the connection states is updated primarily following (14). Then, for those converters who have been identified as connected, their current saturation states will be updated also. In this regard, the current saturation states of the converter in PQ control are obtained as expressed in (16), and the states of VSCs in PV mode obey Figure 3. The iterative process will be terminated when the states remain unchanged for all converters, which means an operation point that satisfies all converters' limits has been obtained.

2.3.3 Hybrid solver for short-circuit faults

Traditional power systems are composed of synchronous generators and loads. During symmetrical fault conditions, synchronous generators are typically modeled with a Thévenin equivalent as the induced electromotive force is assumed to be constant [30]. Besides, synchronous generators do not include controls to limit the current in the case of faults. They can stand peaks of current during short periods of time [31]. Loads are represented by shunt impedances that consume the prespecified power at nominal voltage conditions. Therefore, the initial system represented by non-linear equations is transformed into a grid formed only by voltage sources and impedances. By definition, this is a linear system to be solved using the superposition principle (considering pre-fault and post-fault conditions) and well-known circuit theory techniques [32]. There is no need to rely on iterative schemes such as the Newton-Rapshon method.

On the other hand, voltage source converters (VSCs) have to carefully limit the current so as not to surpass their limitations, which are in turn imposed by their semiconductors [33], [34]. VSCs invalidate the possibility of solving the short-circuit by adding the pre-fault and post-fault results. It could be the case that VSCs operate unsaturated before the fault, only to become saturated after the fault. The control references will invariably change, hence VSCs would have

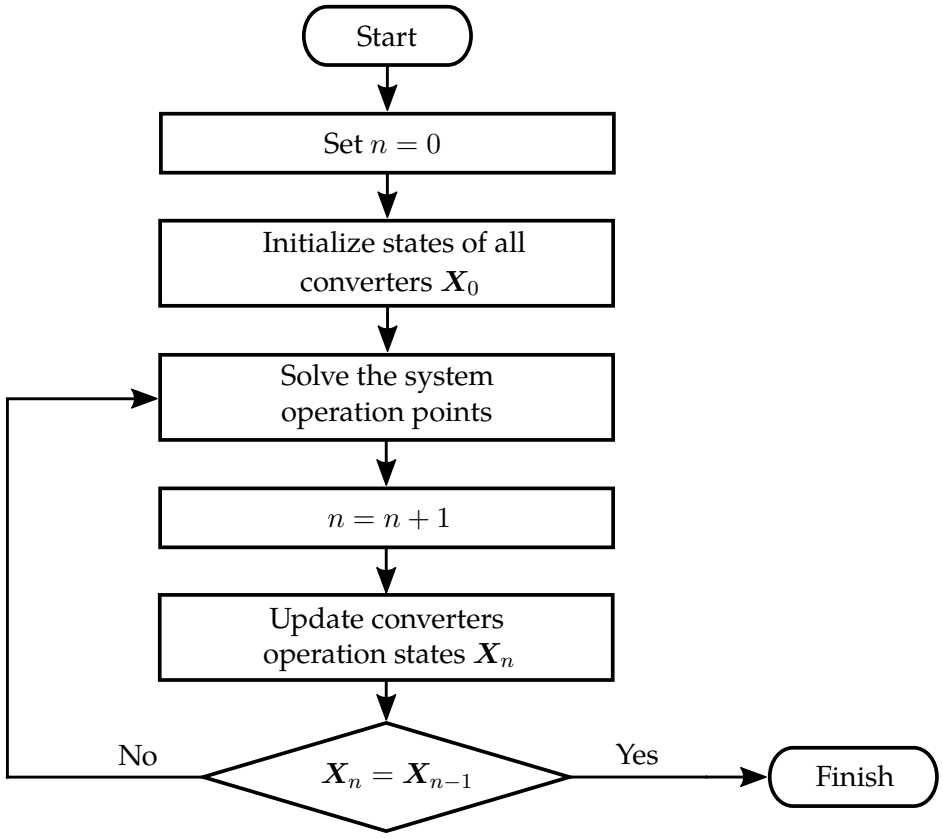

Figure 4: Overall workflow to identify the converter states.

to somehow remain connected in the post-fault analysis.

Figure 5 exemplifies the proposed pre-fault and post-fault situations.

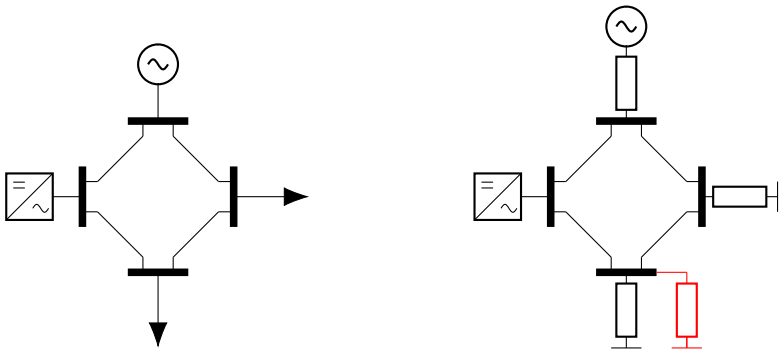

(a) Pre-fault. (b) Faulted system.

Figure 5: Representation of the pre-fault and post-fault equivalent systems, with a converter.

The pre-fault system includes a converter, a synchronous generator, and a couple of loads. They are viewed as non-linear elements due to the non-linearities found in the P and Q equations (see (1)). During the short-circuit fault, which is represented by an impedance in red, loads and

synchronous generators are modeled as linear devices. However, VSCs have to be treated as non-linear elements according to the states defined in Table 2. Perhaps the converter becomes saturated due to the heavy inrush of current, although even if it remains unsaturated, it will act as a non-linear device. This justifies the assigned name of "hybrid solver" since some elements are viewed as linear and others as non-linear. Table 3 summarizes the modeling of the elements.

Table 3: Modeling of loads, synchronous machines and VSCs for normal conditions and short-circuits.

Element	**Normal operation**	**Short-circuits**
Load	PQ node	Constant impedance
Synchronous machines	PQ/PV node	Thévenin equivalent
VSC	Depending on the state	Depending on the state

Due to the presence of a single non-linear device, the system of equations becomes non-linear by definition. It is meant to be solved by the procedure described in Figure 2. The linearization of the loads obeys:

$$\underline{Z}_i = \frac{V_i^2}{\underline{S}_i^*}, \tag{17}$$

where $\underline{Z}_i$ is the impedance by which a load of value $\underline{S}_i$ is transformed into a linear device, and V_i^2 is the squared absolute value of the voltage at the bus where the load is connected. Equation (17) applies to all i loads.

The Thévenin equivalent of synchronous generators is composed of an impedance of the form $R_g + jX_g$ as well as the induced electromotive force $\underline{E}$. While the impedance is a known magnitude provided by the manufacturer, $\underline{E}$ is found with:

$$\underline{E}_i = \underline{V}_i + (R_{g,i} + jX_{g,i})\underline{I}_{\text{inj},i}, \tag{18}$$

where i is the index that covers all generators, $\underline{V}_i$ is the pre-fault voltage at the bus where the generator i is connected, and $\underline{I}_{\text{inj},i}$ is the injected current by the generator in pre-fault conditions.

The steps covered by the hybrid solver are summarized below:

1. Initialize the objects $\boldsymbol{Y}$, $\boldsymbol{V}$, $\boldsymbol{S}$, $\boldsymbol{I_l}$ and classify the buses into PQ, PV, PI, QI, VI.

2. Solve the non-linear system of equations iteratively until a low error is reached. It basically implies following the steps inside the loop of Figure 2. With this, the pre-fault solution is obtained.

3. Linearize loads with (17), synchronous generators with their corresponding Thévenin equivalent (see (18)), and modify $\boldsymbol{Y}$ to include the fault impedance.

4. Solve the hybrid system formed by linear synchronous generators and loads and non-linear converters. Objects $\boldsymbol{Y}$, $\boldsymbol{V}$ and $\boldsymbol{S}$ are modified and the looping steps in Figure 2 are followed.

It is worth mentioning that modeling synchronous generators with Thévenin equivalents causes the addition of one extra bus for each generator. Even if they are essentially the same, Norton equivalents are preferable because they do not introduce an additional bus. Thus, the size of the hybrid system becomes identical to the size of the non-linear system.

2.3.4 Novel ideas

The theory developed up to this point contains some relevant contributions that revolve around the idea of considering the current limits of converters. The most important ideas are the following:

1. A method to solve the power flow problem with converters operating in multiple states is proposed. It relies on adding a new set of equations in the Newton-Raphson formulation to take into account the absolute value of the currents.

2. There is a need to consider the new types of buses PI, QI and VI, apart from the traditional PQ, PV and slack buses. In turn, these new buses depend on the states of the converters.

3. An approach to identify a suitable solution, considering the multiple combinations of operating states, is described.

4. A hybrid model where converters act as non-linear devices and synchronous generators and loads are treated as linear elements is proposed.

2.4 Algorithm overview

As previously illustrated, the program is composed of an inner and an outer loop. The outer loop is crucial to iterate on the converter states. Likely, the initially expected configuration does not yield a solution as a divergent state is reached. Therefore, some decision rules have to be established. Let `states` be a list of all converters states, `snap` a class with all the information of the grid, `success` a boolean variable that indicates if the system has been successfully solved, and ϵ the maximum permitted error. A general picture of the solver is described in Algorithm 1.

The inner loop is limited to iterating in order to find a solution for the given conditions. Contrarily, the outer loop is responsible for updating the states of the converters through the `update_states` function. Since there is no predetermined rule to find the states of the converters, some heuristics are developed. The chosen rules to select the states of a converter have been presented in Section 2.3.2. In particular, converters in PQ mode follow the rules captured in (15) while PV converters obey Figure 3. The internal loop follows the proposed Newton-Rapshon methodology.

Algorithm 1: Full solver algorithm

Data: `snap`, `states`, ϵ

Result: Solved system in `snap`

`success` $\leftarrow$ `False`

`states_old` $\leftarrow$ `states`

Initialize objects in `snap`;

while `success`$=$ `False` or `states` $\neq$ `states_old` **do**

  `states_old` $\leftarrow$ `states`

  while $\max(|\boldsymbol{\Delta f}|) > \epsilon$ **do**

    `snap` $\leftarrow$ `inner_loop(snap)`

  end

  `success` $\leftarrow$ `True`

  `states` $\leftarrow$ `update_states(snap)`

end

Mainly, the inner loop calculates the residuals and the Jacobian to compute the variation of the unknowns. Algorithm 2 depicts its basic structure.

Algorithm 2: Iteration inside the `inner_loop` function

Data: `snap`

Result: Updated `snap` after one iteration

$\boldsymbol{\Delta f} \leftarrow$ `calc_residuals(snap)`

$\boldsymbol{J} \leftarrow$ `calc_jacobian(snap)`

Solve $\boldsymbol{\Delta f} = -\boldsymbol{J}\boldsymbol{\Delta x}$ for $\boldsymbol{\Delta x}$;

Update `snap` with $\boldsymbol{\Delta x}$;

It has to be noted that objects such as the Jacobian or the admittance matrix are highly sparse in large systems [35]. This promotes the usage of sparse matrices since relying on dense matrices would require more memory and cause longer computational times. The produced code employs the `scipy.sparse` library [36]. Inversion of matrices is avoided at all costs. Hence, the system $\boldsymbol{\Delta f} = -\boldsymbol{J}\boldsymbol{\Delta x}$ is solved with the built-in function `linalg.spsolve`. Just as a visual reference, Figure 6 depicts the first 100 rows and columns of the Jacobian for the ACTIVSg2000 grid.

White squares identify non-null elements, whereas black entries indicate a zero value. Sparse matrices are characterized by storing the non-null elements and their position in the matrix. This is a much more efficient approach when it comes to storing large matrices of this nature.

2.5 Case study

The case under study covers the ACTIVSg2000 system. It is a 2000-bus synthetic grid representative of the state of Texas. Synthetic grids are fictional, yet they can be functionally similar to

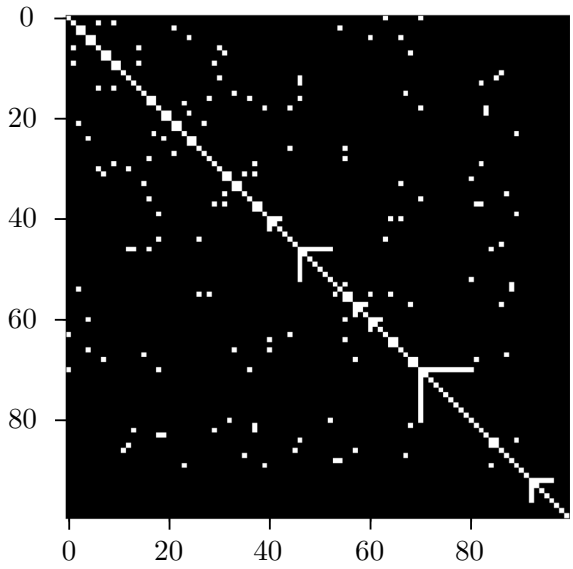

Figure 6: First 100 rows and columns for the 2000-bus Jacobian.

realistic grids [37]. The dataset corresponding to the aforementioned particular system can be found in [38], and the base power is 100 MVA.

Figure 7 depicts the state of Texas and an approximate placement of the three added converters. They are distributed far apart one from another so that they will most likely not reach the current limits simultaneously.

Table 4 indicates the input data of the three converters, such as the type and control references. One additional expression to be used in order to provide grid-support is:

$$q = q_{ref} + v k_{isp}(v_{ref} - v), \tag{19}$$

where q_{ref} is the initial reactive power, v is the actual voltage of the converter, k_{isp} is a droop constant for grid-support, and v_{ref} is the reference voltage.

Table 4: Input data of the converters for the ACTIVSg2000 system.

bus	**type**	**state**	p_{ref}	q_{ref}	v_{ref}	i_{max}	v_{min}	v_{max}	k_{isp}
1001	PQ	USS	-5.0	3.026	1.0	7.0	0.05	1.3	1.0
4023	PQ	USS	-1.0	0.973	1.0	2.0	0.05	1.3	1.0
8073	PQ	USS	6.0	1.458	1.0	8.0	0.05	1.3	1.0

2.5.1 Results analysis

Three situations are covered in this case study. In order to validate the tool, faults are provoked at the buses where the VSCs are connected. Large fault impedances should cause the VSC to

Figure 7: Approximate location of the three converters. Image from [39].

remain unsaturated (USS) or operate partially saturated (PSS) at most. Strong faults should require the affected VSC to be fully saturated (FSS) or perhaps directly disconnected (DIS).

The first case corresponds to a normal situation where no faults have been produced. The power flow results are captured in Table 5.

Table 5: Power flow results for the converters under normal conditions.

VSC	State	ν	θ (°)	$\lvert I\rvert$	P	Q	$\lvert S\rvert$
vsc1	USS	1.0073	-40.7924	5.8017	-5.0000	3.0260	5.8443
vsc2	USS	1.0050	-63.9565	1.3882	-1.0000	0.9731	1.3953
vsc3	USS	1.0200	-48.6301	6.0529	6.0000	1.4580	6.1746

The voltages remain near 1.0 pu, just as expected in normal conditions. Since the voltage is sufficiently high, the converters inject currents below their limits. This causes them to operate in an unsaturated state (USS). Note that in this case VSCs could have been modeled as traditional generators that specify a given active and reactive power.

Table 6 shows the results for short-circuit conditions with a relatively small fault impedance $\underline{Z}_f$ of $0.002j$. The fault is caused at bus 1001, that is, at the terminals of the converter vsc1.

Table 6: Short-circuit results for the converters with $\underline{Z}_f = 0.002j$.

VSC	State	ν	θ (°)	$\lvert I\rvert$	P	Q	$\lvert S\rvert$
vsc1	FSS	0.0633	-14.1576	7.0000	0.0000	0.4431	0.4431
vsc2	USS	0.9997	-63.3836	1.3958	-1.0000	0.9732	1.3954
vsc3	USS	0.9997	-46.1701	6.1764	6.0000	1.4582	6.1746

The first converter has to operate at fully saturated conditions (FSS). Otherwise, no solution is feasible. The modified Newton-Raphson method is capable of imposing the current saturation of this converter given the current of 7 pu, which coincides with the maximum specified in Table 4. Being fully saturated, its active power is null so all the current is devoted to injecting reactive power. The voltage at bus 1001 is extremely low due to the extreme fault. The other two VSCs are apparently quite unaffected. They still behave unsaturated and their injections are practically the same as in the power flow scenario shown in Table 5.

A non-extremely severe fault with $\underline{Z}_f = 0.05j$ is again provoked at bus 1001. Table 7 gathers the results.

Table 7: Short-circuit results for the converters with $\underline{Z}_f = 0.05j$.

VSC	State	ν	θ (°)	$\lvert I\rvert$	P	Q	$\lvert S\rvert$
vsc1	PSS	0.6423	-34.1962	7.0000	-3.1009	3.2557	4.4962
vsc2	USS	1.0050	-63.9565	1.3882	-1.0000	0.9696	1.3928
vsc3	USS	1.0200	-48.6301	6.0529	6.0000	1.4453	6.1716

In this case, vsc1 operates saturated as well, even though only partially. This implies that some active power can be injected while the current limit is reached. Its voltage is of course higher than for $\underline{Z}_f = 0.002j$. As the converters vsc2 and vsc3 are topologically far from the fault, their voltages and powers are roughly the same as if no fault had taken place. Overall the results suggest that the expanded Newton-Raphson method is useful in dealing with saturated VSCs.

2.5.2 Dynamic validation

The results obtained for the two faults are validated dynamically. PSS/E is employed for this purpose. The goal is to reach the same steady-state values, thus confirming that the steady-state calculations derived from the proposed formulation are correct. Figure 8 shows the evolution of the variables over time for the severe fault.

The fault is provoked at $t = 1$ s. There is a drastic change in the powers as well as the voltage. It is observed that it converges to the steady-state value computed with the adapted Newton-Raphson, hence validating the results.

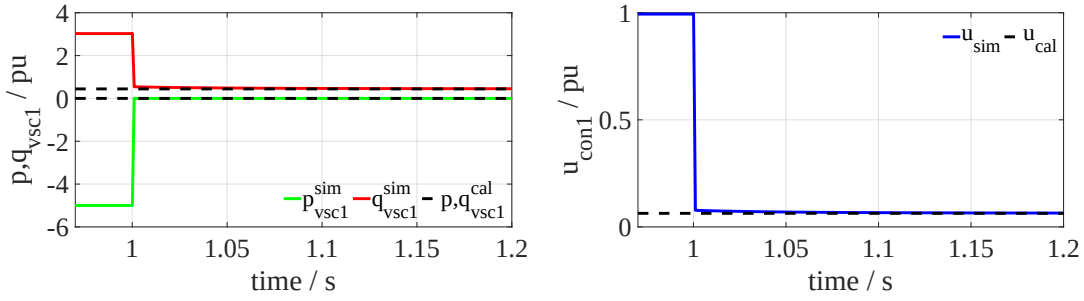

(a) vsc1 power injections. (b) Fault voltage.

Figure 8: Dynamic simulation for a severe fault with $\underline{Z}_f = j0.002$ pu.

Similarly, the moderate fault where $\underline{Z}_f = 0.05j$ is analyzed. Figure 9 depicts the evolution of the magnitudes until steady-state conditions are reached.

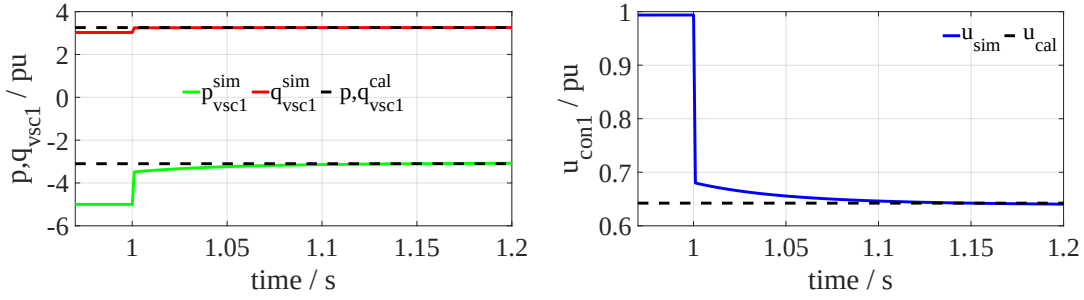

(a) vsc1 power injections. (b) Fault voltage.

Figure 9: Dynamic simulation for a moderate fault with $\underline{Z}_f = j0.05$ pu.

The dynamic simulation results tend to reach again the steady-state values given in Table 7. With this, the proposed methodology is concluded to work accurately. Performing the simulation with the custom software instead of the dynamic simulation offers the advantage of shorter calculation times.

2.5.3 Comparison with PSS/E steady-state results

Apart from dynamic simulations, the software PSS/E provides the option of performing steady-state calculations for short-circuits. However, converters are not modeled as converters per se. Instead, they are either represented by generators or FACTS. Table 8 shows the results obtained with the proposed converter model (and associated software), compared to the results provided by PSS/E modeling the converters differently.

The short-circuit values do not match as expected. The reason is that the steady-state simulation integrated into PSS/E does not model realistically the converters. Rather, they are represented by generators or FACTS, which end up being equivalent up to a certain extent.

Table 8: Comparison of short-circuit results with the proposed method and PSS/E.

$\underline{Z}_f$ \ I_{sc}	**Proposed method**	**PSS/E VSCs as generators**	**PSS/E VSCs as FACTS**
$j0.05$	12.75	13.40	12.17
$j0.002$	31.40	32.57	25.91

Given that the steady-state simulation in PSS/E fails at obtaining the right values, the only valid option is to opt for its dynamic simulation. As previously anticipated, a relevant aspect is the computational time. Figure 10 presents the time simulation required to reach the steady-state values for a fault at bus 6111 with $\underline{Z}_f = 0.05j$ pu.

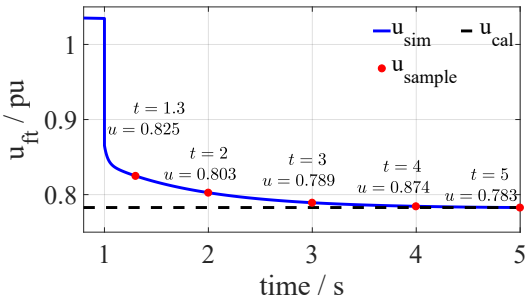

Figure 10: PSS/E simulation with $\underline{Z}_f = j0.05$ pu inserted at bus 6111.

It has been tested that when the system is dominated by synchronous machines instead of VSCs, a longer time is required to achieve steady-state conditions in fault simulations. This is due to their high inertia. Notice that in this particular example about 4 seconds would be required in reality in order to achieve a representative value. Dynamic simulations are generally much slower than steady-state calculations since the system states are computed at various points in time. This explains why it is preferable to directly employ steady-state computations when possible.

The computing efficiency of the PSS/E dynamic simulation is compared with the proposed method. Table 9 depicts the required simulation times and the maximum errors. A relative tolerance of $1 \cdot 10^{-4}$ has been selected in the PSS/E simulation.

The proposed methodology, highlighted in gray, achieves much shorter calculation times. The dynamic simulation has to solve the system at each time step, which is very computationally intensive. More than 10 s are required to obtain an error of less than $1 \cdot 10^{-3}$. In short, the custom approach for solving short-circuit faults with power converters is both more accurate and faster than the dynamic simulation of PSS/E.

Table 9: Comparison of efficiency with PSS/E dynamic simulation.

t_{sim} after fault (s)	Calculation time (s)	Error $\lvert u_{sample} - u_{cal} \rvert$ (pu)
0.3	1.43	42×10^{-3}
1	3.52	19.8×10^{-3}
2	6.81	6.5×10^{-3}
3	10.07	1.6×10^{-3}
4	13.14	$< 0.1 \times 10^{-3}$
Proposed method	0.085	6.17×10^{-11}

2.6 Time complexity

The main mathematical operations to perform in the Newton-Raphson method are the computation of the residuals, the calculation of the Jacobian, and the obtention of the variation of the unknowns. It is suggested that the computational effort C should depend on the size n of a given system as [40]:

$$C \propto n^{1+2\gamma}, \tag{20}$$

where γ is expected to be 0.2 more or less. This means that the required time is not directly proportional to the size of the system, yet it should scale moderately well.

Calculating the inverse of the Jacobian has to be avoided in all conditions. Computing an inverse matrix has a complexity of $\mathcal{O}(n^3)$ and can be optimized up to $\mathcal{O}(n^{2.x})$, where x has been reported to be 2.37286 [41]. In any case, this would be considerably slower than the baseline $\mathcal{O}(n^{1.4})$. The employed `sparse.linalg.spsolve` function from `scipy` relies on the UMFPACK. It is a sparse direct solver which performs the Lower-Upper (LU) factorization of the Jacobian [42]. Thus, the Jacobian is not inverted directly.

The goal of this section is to briefly show the time complexity of the proposed algorithm. For this purpose, several systems of increasing size have been analyzed. The data of the converters are generally irrelevant since the focus is placed on the time to solve the inner loop for a maximum error $\epsilon = 10^{-10}$ pu. Table 10 shows the required time depending on the size.

Table 10: Average computational time for different systems including converters.

System	Time (ms)
IEEE14	21.69
IEEE39	25.52
IEEE118	32.38
Pegase1354	69.48
ACTIVSg2000	82.42

Even though some time is spent on initializing the objects (there seems to be some offset), the increase is quite linear. It is relatively complicated to determine a fitting curve. However, the complexity seems to be better than $\mathcal{O}(n^{1.4})$. It is concluded that the proposed solver scales efficiently. Compared to other software packages such as GridCal, a competitive time in large-scale systems is achieved.

2.7 Inclusion of algebraic limits

This section introduces the concept of the Lagrangian for the power flow. Expressions to embed limits (such as power limits) into the traditional power flow equations are derived. This is particularly interesting as using conditionals to check the state of a device lacks flexibility and robustness. Instead, it is much more beneficial to encapsulate the states of a device in a single algebraic equation.

The idea of operating with algebraic limits is exemplified in the case of the DC power flow. First, the equations extracted from the Lagrangian formulation are presented. Then, they are applied to a simple case study to observe the advantages of this approach. Figure 11 shows a generic bus of a DC system.

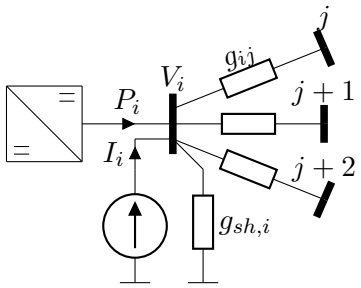

Figure 11: Scheme of a DC bus with a power injection, a current injection, and connections to other buses.

Any given bus can have an injection of power and current coming from devices. This bus is connected to other buses through conductances of the form g_{ij}, and can have attached a shunt conductance such as $g_{sh,i}$. The current balance becomes:

$$\sum_j g_{ij}(V_i - V_j) + V_i g_{sh,i} = \frac{P_i}{V_i} + I_i, \tag{21}$$

where the voltage V_i can be set to a specified value V_i^{sp}, and the power P_i is restricted to be between $P_i^{\max}$ and $P_i^{\min}$. For this purpose, the problem can be viewed as a minimization problem, where the difference between both sides of the equality in (21) has to be reduced:

$$\mathcal{F} = \sum_j g_{ij}(V_i - V_j) + V_i g_{sh,i} - \frac{P_i}{V_i} - I_i = 0. \tag{22}$$

In a minimization problem, the Lagrangian $\mathcal{L}$ is derived and is set equal to zero to find the optimal points. Therefore:

$$\mathcal{L} = \int \mathcal{F} d\{V_i\}, \tag{23}$$

where $\{V_i\}$ denotes the set of V_i voltages which are in fact the unknowns of the problem.

The Lagrangian of the whole system becomes:

$$\mathcal{L} = \frac{1}{2}\sum_i \sum_{j<i} g_{ij}(V_i - V_j)^2 + \frac{1}{2}\sum_i V_i^2 g_{sh,i} - \sum_k P_k \ln V_k - \sum_i I_i V_i, \tag{24}$$

where k identifies all indices of controlled buses.

The minimization problem to be formulated is:

$$\begin{aligned} \min_{\{V_i\}} \quad & \frac{1}{2}\sum_i \sum_{j<i} g_{ij}(V_i - V_j)^2 + \frac{1}{2}\sum_i V_i^2 g_{sh,i} - \sum_k P_k \ln V_k - \sum_i I_i V_i, \\ \text{s.t.} \quad & V_k^{sp} - V_k = 0, \\ & P_k^{\min} \leq P_k \leq P_k^{\max}. \end{aligned} \tag{25}$$

2.7.1 Power limits formulation

The voltage equalities and power inequalities have to be introduced somehow into the problem. For the equalities, it is equivalent to say that the minimization problem evolves into:

$$\begin{aligned} \min_{\{V_i\}} \quad & \frac{1}{2}\sum_i \sum_{j<i} g_{ij}(V_i - V_j)^2 + \frac{1}{2}\sum_i V_i^2 g_{sh,i} - \sum_k P_k \ln \frac{V_k}{V_k^{sp}} - \sum_i I_i V_i, \\ \text{s.t.} \quad & P_k^{\min} \leq P_k \leq P_k^{\max}, \end{aligned} \tag{26}$$

since the derivative would still be the same.

The inequalities can become part of the objective equation with the usage of barrier functions. A barrier function takes an extremely high value (ideally infinity) if the condition is not met, while it tends to zero if the constraint is respected. Logarithmic barrier functions can be a suitable choice. The dual problem reads as follows:

$$\begin{aligned} \max_{\{P_k\}} \quad & \frac{1}{2}\sum_i \sum_{j<i} g_{ij}(V_i - V_j)^2 + \frac{1}{2}\sum_i V_i^2 g_{sh,i} - \sum_k P_k \ln \frac{V_k}{V_k^{sp}} - \sum_i I_i V_i \\ & + \mu_1 \ln (P_k^{\max} - P_k) + \mu_2 \ln (P_k - P_k^{\min}), \end{aligned} \tag{27}$$

where μ_1 and μ_2 are barrier parameters. From now on they are considered to take the same value, hence $\mu_1 = \mu_2 = \mu$. The point is that the barrier parameter has to progressively decrease towards 0. In this condition, (27) becomes equivalent to (26) as desired.

For instance, one rule that can be established to determine the value of μ at each iteration is:

$$\mu^{(r)} = \frac{1}{2(r+1)^r}, \tag{28}$$

where r denotes the iteration index, starting from 0. In this manner, μ will decrease relatively fast so that after a dozen iterations it will become practically zero for our problems of interest.

The powers P_k can be treated as the Lagrangian multipliers. Maximizing (27) with respect to this powers P_k yields [43]:

$$-\ln \frac{V_k}{V_k^{sp}} - \frac{\mu}{P_k^{\max} - P_k} + \frac{\mu}{P_k - P_k^{\min}} = 0, \tag{29}$$

so the final expression to employ becomes:

$$(\ln(V_k) - \ln(V_k^{sp}))(P_k^{\max} - P_k)(P_k - P_k^{\min}) = \mu(P_k^{\max} + P_k^{\min} - 2P_k). \tag{30}$$

Using (30) in the power flow formulation, where μ is progressively decreased, allows to include controls and their subsequent saturations in a full compacted expression. This has been derived for the DC power flow, but a similar approach can be followed for the AC power flow.

2.7.2 Power limits results

Suppose there is a simple three-bus radial system as the one in Figure 12. It is formed by two DC generators and a converter. Bus 3 is treated as the slack bus, where the voltage is set and the corresponding DC generator attached to it has no power limits. Bus 1 acts as a PV bus, yet its converter has active power limits initially of $P_1^{\max} = 0.5$ and $P_1^{\min} = 0.1$. It is assumed beforehand that the voltage of $V_1 = 1.01$ can be achieved without surpassing the limits.

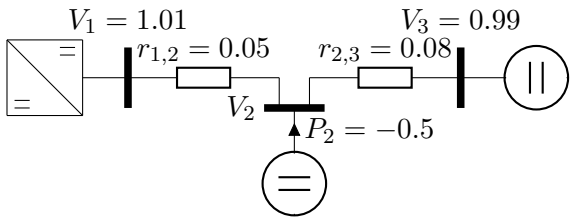

Figure 12: Simplistic case study for the DC power flow.

Explicitly, the three equations that intervene are:

$$\begin{cases} (V_1 - V_2)g_{1,2} = P_1/V_1, \\ (V_2 - V_1)g_{2,1} + (V_2 - V_3)g_{2,3} = P_2/V_2, \\ (V_3 - V_2)g_{3,2} = P_3/V_3, \end{cases} \tag{31}$$

where $g_{x,y}$ is the reciprocal of $r_{x,y}$, and $g_{x,y} = g_{y,x}$. The third expression in (31) is of little interest as P_3 is a slack variable. Hence, the problem lies on solving the first two expressions for P_1 and

V_2. Although this is a very simple case, solving equations of this form is not straightforward as they are nonlinear due to the term P_k/V_k.

Solving the system of equations yields the results shown in Table 11. Notice that the power P_1 is inside the limits. Thus, this is a valid solution and there would be no need to consider the expressions from the Lagrangian.

Table 11: Results for the DC power flow base case.

Magnitude	Value
V_1	1.0100
P_1	0.4703
V_2	0.9867
P_3	0.0406

In order to force the active power upper limit to be reached, it can be set to $P_1^{\max} = 0.4$. Under these conditions, the new results are gathered in Table 12.

Table 12: DC power flow results considering an upper limit $P_1^{\max} = 0.4$.

Magnitude	Value
V_1	1.0011
P_1	0.4000
V_2	0.9811
P_3	0.1089

Now instead of meeting the voltage reference, since the active power upper limit is reached, it is the power that is set. Relying on (30) allows to always use the same equation, independently on the state of the converter. Not opting for this approach, an incorrect solution may be reached depending on the seed values. With the logarithmic barrier functions, the same result has been obtained in spite of employing very different seeds.

Also, it could be hypothesized that the following expression would do the job as well:

$$(V_k - V_k^{sp})(P_k^{\max} - P_k)(P_k - P_k^{\min}) = 0. \tag{32}$$

This has been tested to not be useful for the same reason as before: an incorrect solution may be reached. It is too drastic to set it to zero even at the first iteration. Instead, decreasing the barrier parameter permits obtaining a feasible operating point that is realistic.

2.7.3 Current limits formulation

Expressions of the same nature have to be derived when the bus has a limited injection of current. Denote the current I_k as the injected current in bus k, and $I_k^{\max}$ and $I_k^{\min}$ the maximum and

minimum allowed currents respectively. Recall that the full original Lagrangian is:

$$\mathcal{L} = \frac{1}{2}\sum_i \sum_{j<i} g_{ij}(V_i - V_j)^2 + \frac{1}{2}\sum_i V_i^2 g_{sh,i} - \sum_i P_i \ln V_i - \sum_i I_i V_i. \tag{33}$$

It can be divided into a term that does not contain the involved Lagrangian multipliers, and a sum of terms that include the Lagrangian multipliers. These multipliers are the currents of the form I_i in this particular case. The minimization problem becomes:

$$\begin{aligned} \min_{\{V_i\}} \quad & \frac{1}{2}\sum_i \sum_{j<i} g_{ij}(V_i - V_j)^2 + \frac{1}{2}\sum_i V_i^2 g_{sh,i} - \sum_i P_i \ln V_i - \sum_i I_i V_i, \\ \text{s.t.} \quad & V_i^{sp} - V_i = 0, \\ & I_i^{\min} \leq I_i \leq I_i^{\max}, \end{aligned} \tag{34}$$

where the restrictions only apply in the buses where the voltage is an input variable. Notice that there are the upper and lower limits of the current. As the direction of the current is irrelevant from the point of view of protection of the device, a recommendation is to set $I_i^{\min} = -I_i^{\max}$.

The voltage equality constraints are introduced in the terms where I_i is present, that is:

$$\begin{aligned} \min_{\{V_i\}} \quad & \frac{1}{2}\sum_i \sum_{j<i} g_{ij}(V_i - V_j)^2 + \frac{1}{2}\sum_i V_i^2 g_{sh,i} - \sum_i P_i \ln V_i - \sum_i I_i (V_i - V_i^{sp}), \\ \text{s.t.} \quad & I_i^{\min} \leq I_i \leq I_i^{\max}. \end{aligned} \tag{35}$$

No natural logarithms are employed when introducing this restriction because the nature of the expressions is preserved. It has been tested that simply employing (30) where powers are replaced by currents yields unrealistic results. The current limitations are treated as barrier functions in order to enter them into the dual problem:

$$\begin{aligned} \max_{\{I_i\}} \quad & \frac{1}{2}\sum_i \sum_{j<i} g_{ij}(V_i - V_j)^2 + \frac{1}{2}\sum_i V_i^2 g_{sh,i} - \sum_i P_i \ln V_k - \sum_i I_i (V_i - V_i^{sp}) \\ & + \mu_1 \ln (I_i^{\max} - I_i) + \mu_2 \ln (I_i - I_i^{\min}). \end{aligned} \tag{36}$$

Deriving (36) with respect to the currents I_i produces the final expression to add as an algebraic equation in the reformulated power flow:

$$-(V_i - V_i^{sp}) - \frac{\mu}{I_i^{\max} - I_i} + \frac{\mu}{I_i - I_i^{\min}} = 0, \tag{37}$$

which can be further developed as:

$$-(V_i - V_i^{sp})(I_i^{\max} - I_i)(I_i - I_i^{\min}) - \mu(I_i - I_i^{\min}) + \mu(I_i^{\max} - I_i) = 0. \tag{38}$$

2.7.4 Current limits results

Treating bus 1 as a point of connection where the injection of current is limited, instead of the power, has no effect on the conventional power flow equations. The only modification is the

replacement of (30) for (38). Then, a similar scenario is studied. The base results are exactly the same, and the current $I_1 = 0.4657$. Considering $I_1^{\max} = 0.4$ and $I_1^{\min} = -0.4$, the upper limit should be reached. Then, the results are the ones in Table 13.

Table 13: DC power flow results considering current limits of ± 0.4.

Magnitude	Value
V_1	1.0012
I_1	0.4000
V_2	0.9812
P_3	0.1084

There has been no observed dependence on the final results between choosing one seed or another. The estimated initial current can be far from the final result, yet the right solution is obtained. Again, if an expression different from (38) is employed, this has been tested not to be the case.

Future work could involve experimenting with these sorts of expressions in the AC power flow. One limitation is that various programmable operating states may not be possible as conditionals are completely removed from the problem formulation. It may not be the best idea to implement it for VSCs. However, it could be useful for synchronous generators where there is simply a voltage setpoint and reactive power limits.

2.8 Conclusion

The inclusion of power converters adds certain complexity to the modeling of the systems since converters can operate at different states. The chapter has described all possible states, their particularities, and how to determine the working state. As the converters saturate their current, new expressions for the squared absolute value of the currents have been derived. The formulation of an extended Jacobian has been shown as well.

In order to test the performance of the solver, the ACTIVSg2000 system has been studied. Faults have been provoked at the buses where the converters are directly connected. It has been justified that converters change their state in accordance with the fault impedance. Besides, the analysis of systems with a different number of buses results in a satisfactory time complexity thanks to working with sparse matrices.

Future work should cover more appropriate rules to determine the operating states of the converters. At the moment, some contradictions could appear and the state of the converter may never converge. The usage of the Lagrangian to algebraically embed the limits has worked successfully in a small-scale DC system. It would be convenient to test a similar methodology for AC systems.

3 Analysis of grid codes for short-circuits considering saturation

3.1 Introduction

The rise in renewable energies has been achieved with the inclusion of Voltage Source Converters (VSC) as means of coupling energetic resources to the grid while providing controllability [44]–[46]. The high flexibility of VSC control enables advanced grid voltage-support control, which could enhance the system performance during the fault and ensure a fast recovery after the fault clearance. However, compared to conventional electrical machines, VSCs cannot withstand overloads for a long period [47]. Such current limitation modifies the operation modes of the VSCs and must be considered in the power system computational analysis.

VSCs have to saturate the currents to not exceed their limitations, but should also contribute to improving the voltage profile [48]. This becomes visible when looking at the requirements imposed by Transmission System Operators (TSO) in their grid codes [49], [50]. Such requirements are recent, as they have emerged together with the incorporation of renewables. As a consequence, nowadays renewable power plants have to control active and reactive power [51]. Focusing on power converters, they have to provide support in case of short-circuit faults, and therefore they are usually forced to remain connected even under strong fault conditions. This latter aspect is often referred to as low voltage ride through [52]–[54]. A traditional approach to raise the voltage is to inject reactive current proportionally to the voltage drop [51], [55]. As for the analysis of faults, it is often the case that voltages are decomposed into positive, negative, and zero sequence values to deal with unbalanced conditions [56]. The influence of the sequence current components on the voltages can be assessed. In this sense, both positive and negative sequence currents have to be thoroughly controlled by power converters as discussed in [55], [57].

To provide voltage-support means rising the positive sequence voltage close to the nominal value and decreasing the negative sequence voltage so that it approaches zero. The majority of support strategies are compared and summarized in [58]. Grid codes generally require the injection of only reactive power [59], [60]. This is because transmission networks are often considered to have an inductive characteristic. Reference [57] presents expressions to maximize the positive sequence voltage, minimize the negative sequence voltage, or maximize the difference between both. The power injection is given as a function of the voltage at the point of common coupling (PCC) and the connecting impedance to the grid. However, this is only intended to be used in a simple system with a single converter directly connected to the grid. Expressions of the same nature are proposed in [61], where instead of solving the optimization problem, a control parameter is introduced. This takes various values to prioritize the positive or the negative sequence voltages but does not guarantee that the system is operating in an optimal state. The effect of varying this control parameter is studied in [62], although it is not computed with a

systematic approach, but rather, manually. Reference [63] proposes a maximum allowed support (MAS) control scheme that could provide the maximum voltage-support and simultaneously satisfy the current limitations. This study does not explicitly indicate how to obtain the current angle, and variations in input parameters are rather limited. Another voltage-support scheme is presented in [64], where the influence that the active power and the resistive part of the impedance connecting the VSC to the grid have on the injected currents has been neglected. In addition, positive and negative sequence grid voltage values are imposed, which makes the obtention of the steady-state current values rather trivial. A variation of the grid code requirements is depicted in [65], where the authors found that it provided better results than conventional grid codes by dynamically adjusting the positive and negative sequence voltage references. However, the presented analysis is limited to a system with a purely inductive circuit.

This chapter identifies the optimized system equilibrium point during faults considering converters' current limitations. From a voltage-support perspective, the optimal state is where the positive sequence voltage is as close as possible to the nominal value while the negative sequence voltage tends to zero. The optimized operation points are compared with the results obtained from a conventional grid code. In short, conventional grid codes specify the current to be injected as a function of the voltage drop, as long as the fault is not extremely severe. Otherwise, the maximum current has to be injected (see [51] for details). On the other hand, two potential adaptations of the conventional grid code are suggested. One prioritizes positive sequence current whereas the other prioritizes negative sequence current. Both are restricted to only injecting reactive power and permit injecting the maximum possible current for grid-support during faults.

This chapter presents two main contributions. On the one hand, two adaptations derived from typical grid codes are described. On the other hand, a comparison is made between the optimal solution, the operation points given by traditional grid codes, and the result of the adapted grid codes. The adapted grid codes have been found to provide near-optimal solutions. Hence, they are generally superior to the conventional grid codes while their implementation is arguably simple. Overall, the chapter indicates the preferable injected currents under diverse short-circuit fault conditions. An assessment of the convenience of grid codes to support faults is derived, which provides fundamental information when proposing future improvements in order to evolve towards more resilient grids.

The optimized solution, the conventional grid code, and the modified grid codes are tested for different types and depths of short-circuit faults. First, a basic system with a single converter is studied. Then, the analysis is performed for a system derived from the IEEE 9-bus case with two converters to show that the proposed methodology can be extended to larger systems with several converters. Variations in the impedances are introduced to evaluate the performance of the strategies under different conditions. The methods have been tested in multiple scenarios,

yet just a few are shown for illustrative purposes.

3.2 Formulation

3.2.1 System modeling

VSCs are elements that interconnect AC and DC grids. As shown in Figure 13, VSCs can be modeled following the so-called average model [66]. The VSC has been assumed to be connected to the AC grid through a filter denoted by $\underline{Z}_z$. The control strategy of the VSC consists of controlling powers by imposing current references. Then, voltages are properly adjusted to meet these current references with an inner current loop [67].

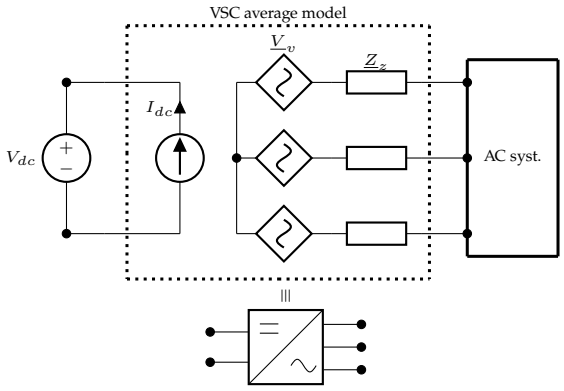

Figure 13: Average model of a three-wire VSC connected to the grid.

Power systems are likely to involve more than a single converter. Therefore, the modeling is approached from a generalized perspective. Figure 14 presents the generic modeling for a system with n converters. Converters are active elements connected to a grid through impedances of the form $\underline{Z}_{vk}$. The grid has been split into a passive part, only formed by impedances and denoted by its admittance matrix $\mathbf{Y_g}$, and an active part, modeled with a Thévenin equivalent constituted by $\underline{V}_t$ and $\underline{Z}_t$. The connection point between the passive and the active part of the grid is denoted as node g. Using a Norton equivalent would be valid as well, and in fact, it simplifies the formulation since it does not create an additional bus between $\underline{V}_t$ and $\underline{Z}_t$. Therefore, the mathematical model presented in this chapter ends up using a Norton equivalent. The analysis of faults can be performed in the natural reference frame or in symmetrical components as in [68]. For convenience, in this chapter, the circuits are modeled following the natural reference frame.

VSCs are treated as current sources that inject currents of the form of $\mathbf{I_k}$ $\forall k \in [1, ..., n]$. These current vectors, expressed in the natural reference frame, are further developed as:

$$\mathbf{I_k} = \left[\underline{I}_k^a, \underline{I}_k^b, \underline{I}_k^c\right]^T . \tag{39}$$

Since this chapter assumes VSCs to be connected to the system by only three wires (as this

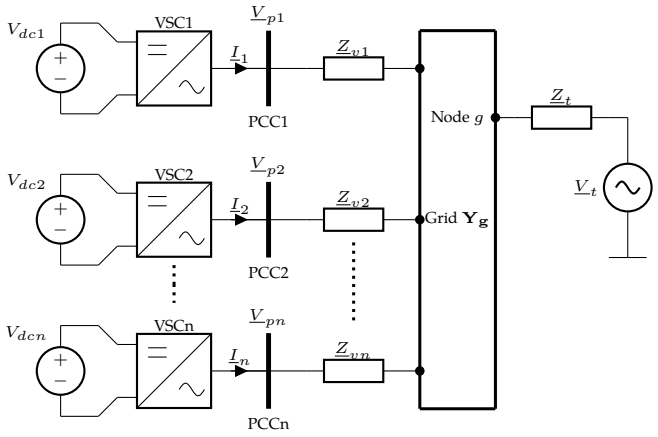

Figure 14: Single-phase representation of a complete system.

is the most typical configuration in transmission systems), there is no zero sequence current component. Thus, the formulation of the problem also imposes:

$$\underline{I}_k^a + \underline{I}_k^b + \underline{I}_k^c = 0 \; \forall k \in [1, ..., n] \; . \tag{40}$$

The PCC is precisely where the voltages $\mathbf{V_{pk}}$ ought to be controlled by the converter. Again, these vectors are constituted by the three phase voltages as:

$$\mathbf{V_{pk}} = \left[\underline{V}_{pk}^a, \underline{V}_{pk}^b, \underline{V}_{pk}^c\right]^T \; . \tag{41}$$

Voltages and currents are related via admittance submatrices of the form $\mathbf{Y_{vk}}$, which in normal operating conditions, given that the system circuit is symmetrical, become:

$$\mathbf{Y_{vk}} = \begin{pmatrix} \frac{1}{\underline{Z}_{vk}} & 0 & 0 \\ 0 & \frac{1}{\underline{Z}_{vk}} & 0 \\ 0 & 0 & \frac{1}{\underline{Z}_{vk}} \end{pmatrix} \; . \tag{42}$$

In case a fault occurs at the buses interconnected by $\underline{Z}_{vk}$, elements $1/\underline{Z}_f$ are added by observation, where $\underline{Z}_f$ denotes the fault impedance.

The admittance matrix $\mathbf{Y_g}$ has dimensions $3n_g \times 3n_g$, where n_g is the number of buses found in this passive $\mathbf{Y_g}$ grid. The vector $\mathbf{I_t}$ has a length of $3 \times n_g$ and accounts for the injected currents into the grid $\mathbf{Y_g}$.

Consequently, the magnitudes depicted in Figure 14 are finally related by:

$$\begin{pmatrix} \mathbf{I_1} \\ \mathbf{I_2} \\ \vdots \\ \mathbf{I_n} \\ \mathbf{I_t} \end{pmatrix} = \begin{pmatrix} \mathbf{Y_{v1}} & \mathbf{0} & \dots & \mathbf{0} & -\mathbf{Y'_{v1}} \\ \mathbf{0} & \mathbf{Y_{v2}} & \dots & \mathbf{0} & -\mathbf{Y'_{v2}} \\ \vdots & \vdots & \ddots & \vdots & \vdots \\ \mathbf{0} & \mathbf{0} & \dots & \mathbf{Y_{vn}} & -\mathbf{Y'_{vn}} \\ -\mathbf{Y'^T_{v1}} & -\mathbf{Y'^T_{v2}} & \dots & -\mathbf{Y'^T_{vn}} & \mathbf{Y_g} \end{pmatrix} \begin{pmatrix} \mathbf{V_{p1}} \\ \mathbf{V_{p2}} \\ \vdots \\ \mathbf{V_{pn}} \\ \mathbf{V_g} \end{pmatrix} , \tag{43}$$

where matrices of the form $\mathbf{Y'_{vk}}$ are $3 \times 3n_g$ objects constituted by zeros and only three $1/\underline{Z}_{vk}$ elements. For instance, considering $\underline{Z}_{v1}$ is connected to the first bus of the grid $\mathbf{Y_g}$, the corresponding $\mathbf{Y'_{v1}}$ matrix becomes:

$$\mathbf{Y'_{v1}} = \begin{pmatrix} \frac{1}{\underline{Z}_{v1}} & 0 & 0 & 0 & 0 & 0 & \dots & 0 & 0 & 0 \\ 0 & \frac{1}{\underline{Z}_{v1}} & 0 & 0 & 0 & 0 & \dots & 0 & 0 & 0 \\ 0 & 0 & \frac{1}{\underline{Z}_{v1}} & 0 & 0 & 0 & \dots & 0 & 0 & 0 \end{pmatrix} . \tag{44}$$

The final goal of the modeling approach is the obtention of voltages. They are computed from (43) by operating the product between the inverse of the full admittance matrix and the currents vector. In order to have a clearer comprehension of the voltages, they are eventually converted into symmetrical components by means of Fortescue's transformation [69]:

$$\begin{pmatrix} \underline{V}^0_{pk} \\ \underline{V}^+_{pk} \\ \underline{V}^-_{pk} \end{pmatrix} = \frac{1}{3} \begin{pmatrix} 1 & 1 & 1 \\ 1 & \underline{a} & \underline{a}^2 \\ 1 & \underline{a}^2 & \underline{a} \end{pmatrix} \begin{pmatrix} \underline{V}^a_{pk} \\ \underline{V}^b_{pk} \\ \underline{V}^c_{pk} \end{pmatrix} , \tag{45}$$

where $\underline{a} = e^{j\frac{2\pi}{3}}$.

3.2.2 Optimization problem

It can be typically assumed that positive sequence voltages have to approach the nominal voltage while negative sequence voltages have to be minimized. The zero sequence component of the voltages is a magnitude likely to be different from zero under asymmetrical faults. Nevertheless, as three-wire VSCs are unable to inject zero sequence currents, it will remain an uncontrolled variable. In this sense, no efforts will be made towards reducing it. Current saturation restrictions imposed by the VSC characteristics have to be considered in fault conditions. This applies to each phase of each converter. Therefore, the generic optimization problem is expressed as:

$$\begin{aligned} \min_{\mathbf{I_1},\dots,\mathbf{I_n}\in\mathbf{I}} \quad & f_o = \sum_{k=1}^{n} \left[\lambda_k^+ |(1 - V_{pk}^+(\mathbf{I}))| + \lambda_k^- |(0 - V_{pk}^-(\mathbf{I}))| \right] , \\ \text{s.t.} \quad & \max\left(I_k^a, I_k^b, I_k^c\right) \leq I_{\text{max},k} \; \forall k \in [1, ..., n] , \end{aligned} \tag{46}$$

where f_o is the objective function, $\mathbf{I_1}, ..., \mathbf{I_n}$ respectively denote the current injection from the n converters, $\mathbf{I}$ is the left-hand side vector in (43), k identifies a given converter out of the total n converters, λ_k^+ and λ_k^- denote weighting factors for positive and negative voltage magnitudes, $I_{\text{max},k}$ is the maximum phase current allowed by the converter k, and V_{pk}^+ and V_{pk}^- are the positive and negative sequence voltages of the converter k at the PCC. These voltages are expressed as a function of the currents, as they are related in the natural reference frame by (43), and are eventually transformed to positive and negative sequence using (45). Ideally, they should tend to 1.0 and 0.0 pu respectively. It has been assumed that voltages at each phase of the converter do not surpass the limitations, which seems a fair assumption considering that AC voltages

decrease substantially during faults. In any case, this assumption is numerically validated in the case studies. The solution to (46) is equivalent to the result of the strategy C shown in [57], although it is not limited to a single converter. This solution is not meant to be implemented in practice; rather, it will act as a benchmark representing the ideal case.

3.2.3 Conventional Grid Codes (GC)

In order to improve the voltage profile during faults, grid code control rules often impose injection requirements for positive and negative sequence currents proportional to the positive and negative sequence voltage drops respectively [51], [70]. In the case of positive sequence, a generic piecewise function can be defined as:

$$f^+(V_{pk}^+) := \begin{cases} I_k^+ = 0 & V_{pk}^+ \geq V_{\text{high}}^+ \\ I_k^+ = k_p(V_{\text{high}}^+ - V_{pk}^+) & V_{\text{low}}^+ \leq V_{pk}^+ < V_{\text{high}}^+ \\ I_k^+ = I_{\text{max},k} & V_{pk}^+ < V_{\text{low}}^+ \end{cases} \tag{47}$$

The most basic of the four voltage-support strategies analyzed in this chapter will be denoted by GC. It is precisely the application of (47), i.e., only positive sequence current is injected.

A similar proportionality can be established in the negative sequence:

$$f^-(V_{pk}^-) := \begin{cases} I_k^- = 0 & V_{pk}^- \leq V_{\text{low}}^- \\ I_k^- = k_n(V_{pk}^- - V_{\text{low}}^-) & V_{\text{low}}^- < V_{pk}^- \leq V_{\text{high}}^- \\ I_k^- = I_{\text{max},k} & V_{pk}^- > V_{\text{high}}^- \end{cases} \tag{48}$$

Constants k_p and k_n, which represent the slope of the droop, are set as fixed quantities [55]. The unfavorable consequence of applying (47) and (48) simultaneously is that the nominal current of the converter could be exceeded due to imbalances. Indeed, during extreme faults, the positive sequence voltage could reach the lower threshold V_{low}^+ and the negative sequence voltage could surpass the upper threshold V_{high}^-. Then, both I_k^+ and I_k^- would be set at $I_{\text{max},k}$. Consequently, some of the currents in the natural reference frame could become larger than $I_{\text{max},k}$. One way to address this problem consists of injecting only positive or negative sequence currents (the GC option is based on this idea). However, this strategy is likely to be suboptimal if the maximum voltage-support has to be provided. In case the voltages do not exceed these lower or upper thresholds, the converter would still be capable of injecting some current in the non-prioritized sequence up to reaching saturation.

3.2.4 Improved Grid Codes (GCP and GCN)

The two adaptations of the conventional grid code, which are a central contribution of this work, basically consist of determining the available current margin. The two direct prioritizations

are covered. One strategy is to have the positive sequence current following (47) and injecting the remaining maximum allowed current in the negative sequence. This methodology will be commonly referred to as GCP.

The other option, abbreviated as GCN, prioritizes the negative sequence. It obeys (48) and analogously injects the maximum positive sequence current that respects the limits. During all situations, the converters work under saturated conditions (current limits reached) as the non-prioritized current is set to the allowed maximum.

Also, only reactive power is injected in both GCP and GCN. It is generally accepted that since transmission systems are mainly inductive, injecting reactive current has a larger impact on the voltages than injecting active current. Hence, leaving aside stability issues, it is beneficial to prioritize reactive currents. The procedure to determine the non-prioritized current is the main challenge in GCP and GCN. Thus, it is depicted in detail below.

Consider a generic distribution of positive and negative sequence voltages in the complex plane, as in Figure 15.

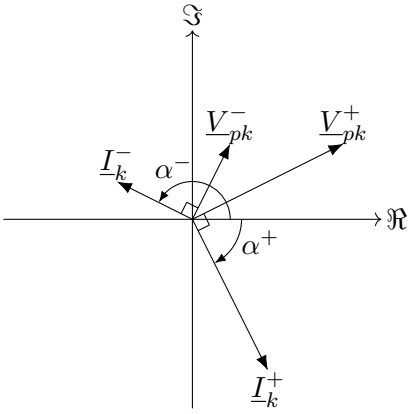

Figure 15: Overview of positive and negative sequence voltages and currents following grid code rules.

Phase currents are related to sequence components as follows:

$$\begin{pmatrix} \underline{I}^a \\ \underline{I}^b \\ \underline{I}^c \end{pmatrix} = \begin{pmatrix} 1 & 1 & 1 \\ 1 & \underline{a}^2 & \underline{a} \\ 1 & \underline{a} & \underline{a}^2 \end{pmatrix} \begin{pmatrix} \underline{I}^0 \\ \underline{I}^+ \\ \underline{I}^- \end{pmatrix} \tag{49}$$

where $\underline{I}^0$ is zero as the three-wire VSC is incapable of injecting it. The k index that identifies a

given VSC has been omitted to alleviate the notation. Explicitly, (49) becomes:

$$\begin{cases} \underline{I}^a = \underline{I}^+ + \underline{I}^- \\ \underline{I}^b = \underline{a}^2\underline{I}^+ + \underline{aI}^- \\ \underline{I}^c = \underline{aI}^+ + \underline{a}^2\underline{I}^- \end{cases} \tag{50}$$

The goal is to determine the maximum current that respects the converter limits. It is known beforehand that not all the three phases of a particular converter will operate with a saturated current; most likely, only one phase will reach saturation. The phase currents in (50) are squared in order to express them as functions of I_{re}^+, I_{im}^+, I_{re}^- and I_{im}^-:

$$g \coloneqq \begin{cases} I_{\text{max}}^2 \geq (I_{re}^+ + I_{re}^-)^2 + (I_{im}^+ + I_{im}^-)^2 \\ I_{\text{max}}^2 \geq (-\frac{1}{2}I_{re}^+ + \frac{\sqrt{3}}{2}I_{im}^+ - \frac{1}{2}I_{re}^- - \frac{\sqrt{3}}{2}I_{im}^-)^2 \\ \qquad +(-\frac{1}{2}I_{im}^+ - \frac{\sqrt{3}}{2}I_{re}^+ - \frac{1}{2}I_{im}^- + \frac{\sqrt{3}}{2}I_{re}^-)^2 \\ I_{\text{max}}^2 \geq (-\frac{1}{2}I_{re}^+ - \frac{\sqrt{3}}{2}I_{im}^+ - \frac{1}{2}I_{re}^- + \frac{\sqrt{3}}{2}I_{im}^-)^2 \\ \qquad +(\frac{\sqrt{3}}{2}I_{re}^+ - \frac{1}{2}I_{im}^+ - \frac{\sqrt{3}}{2}I_{re}^- - \frac{1}{2}I_{im}^-)^2 \end{cases} \tag{51}$$

It is also convenient to define the angles of the positive and negative sequence currents, which are denoted by α^+ and α^- respectively:

$$\begin{cases} \alpha^+ = \angle(\underline{V}_p^+) - \frac{\pi}{2} \\ \alpha^- = \angle(\underline{V}_p^-) + \frac{\pi}{2} \end{cases} \tag{52}$$

where $\angle(\cdot)$ indicates the function that extracts the angle of a complex magnitude. By shifting the current angle $\pm\frac{\pi}{2}$ rad with respect to the corresponding voltages $\underline{V}_p^+$ and $\underline{V}_p^-$, only reactive power is injected. As transmission systems are mostly inductive, providing only reactive power is expected to boost the voltages magnitude. This is verified in the results section where the suitability of these adaptations is assessed by means of varying the angle of the impedances.

A procedure to find the four components I_{re}^+, I_{im}^+, I_{re}^- and I_{im}^- is presented. Contrarily to traditional grid codes where the grid-support current is only specified in one sequence, the algorithms that follow provide the currents in both positive and negative sequences. First, Algorithm 3 contains the methodology to be employed when the positive sequence is prioritized (GCP).

Similarly, Algorithm 4 details the procedure to follow in case the negative sequence is prioritized (GCN).

In essence, Algorithms 3 and 4 compute one sequence current with the basic grid codes (positive and negative respectively). The other sequence current (negative and positive respectively) is found by solving the g function shown in (51), which is implemented with a $solve$ function in Algorithms 3 and 4. Since there would be infinite solutions, it is forced that at least in one phase

Algorithm 3: Current calculation for the GCP strategy.

Data: V_p^+, V_p^-, α^+, α^-, $I_{\max}$
Result: I_{re}^+, I_{im}^+, I_{re}^-, I_{im}^-
$I^+ \leftarrow f^+(V_p^+)$ // use (47) ;
$I^- \leftarrow f^-(V_p^-)$ // use (48) ;
$(I_{re}^-, I_{im}^-) \leftarrow solve(g)$ s.t. $\angle(I_{re}^- + jI_{im}^-) = \alpha^-$ and $(I^a = I_{\max}$ or $I^b = I_{\max}$ or $I^c = I_{\max})$;
$I^- \leftarrow \min(I^-, |I_{re}^- + jI_{im}^-|)$;
$I_{re}^+ \leftarrow \Re(I^+\angle\alpha^+)$; $I_{im}^+ \leftarrow \Im(I^+\angle\alpha^+)$;
$I_{re}^- \leftarrow \Re(I^-\angle\alpha^-)$; $I_{im}^- \leftarrow \Im(I^-\angle\alpha^-)$;

Algorithm 4: Current calculation for the GCN strategy.

Data: V_p^+, V_p^-, α^+, α^-, $I_{\max}$
Result: I_{re}^+, I_{im}^+, I_{re}^-, I_{im}^-
$I^+ \leftarrow f^+(V_p^+)$ // use (47) ;
$I^- \leftarrow f^-(V_p^-)$ // use (48) ;
$(I_{re}^+, I_{im}^+) \leftarrow solve(g)$ s.t. $\angle(I_{re}^+ + jI_{im}^+) = \alpha^+$ and $(I^a = I_{\max}$ or $I^b = I_{\max}$ or $I^c = I_{\max})$;
$I^+ \leftarrow \min(I^+, |I_{re}^+ + jI_{im}^+|)$;
$I_{re}^+ \leftarrow \Re(I^+\angle\alpha^+)$; $I_{im}^+ \leftarrow \Im(I^+\angle\alpha^+)$;
$I_{re}^- \leftarrow \Re(I^-\angle\alpha^-)$; $I_{im}^- \leftarrow \Im(I^-\angle\alpha^-)$;

the current magnitude is equal to $I_{\max}$. In this sense, one inequality is turned into an equality. This is done in an iterative fashion until a solution that validates all three inequalities is found. The algorithm also makes sure that the resulting current does not surpass the one obtained from (48) for GCP or from (47) for GCN.

3.3 Single converter case study

The analysis is first performed considering a one-converter case study as the one depicted in Figure 16. Unless noted otherwise, the corresponding baseline parameters are indicated in Table 14. It has been decided to model a transmission system rather than a distribution grid since the operation under faults is much more critical there. A fault is forced at the grid-equivalent terminals. The impedances that model the fault are set accordingly to the type of fault, i.e., balanced or unbalanced. Most of the case studies correspond to unbalanced faults as they have a higher probability of occurrence [71]. The goal is to improve the voltage $\underline{V}_{p1}$ by injecting the optimal $\underline{I}_1^a$, $\underline{I}_1^b$ and $\underline{I}_1^c$ currents. Three parametric studies are covered:

1. The fault impedance experiences variations. This case is explicitly described in order to exemplify the formulation.

2. The ratio R_1/X_1, which stands for the proportion between the resistive and the inductive

parts that compose the impedance $\underline{Z}_{v1}$, takes a range of values. In any case, the absolute value of the impedance $\underline{Z}_{v1}$ is kept constant.

3. The length of a hypothetical submarine cable is increased. As it is represented by a π line model, both the magnitude and the angle of the impedance change.

Table 14: System parameters for the one-converter case.

Parameter	Value	Parameter	Value
$\underline{V}_t$	1.00	$I_{\max}$	1.00
$\underline{Z}_{v1}$	$0.01 + j0.05$	$\underline{Z}_t$	$0.01 + j0.1$
λ_1^+	1.00	λ_1^-	1.00

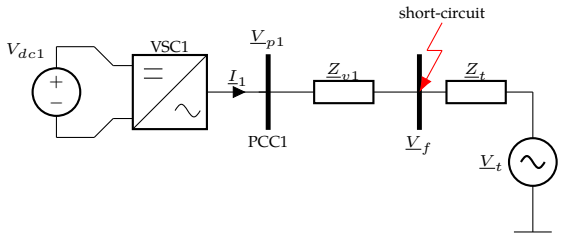

Figure 16: Single-phase representation of the single converter system under study.

Regarding the grid codes, the values of the constants are gathered in Table 15. They remain the same for all studies. Both the weighting factors λ_1^+ and λ_1^- have been set to the same value to attribute the same importance to each sequence, and take the same values as in [72]. The optimal results can change significantly in case one sequence is prioritized. The results obtained in this chapter are computed with Python 3.9.1 using the Mystic package, a highly constrained non-convex optimization framework [73], [74]. A differential global optimization solver has been employed with a relative precision up to $1 \cdot 10^{-6}$. Nevertheless, other software packages capable of handling complex convex problems can be adopted as well.

Table 15: Generic grid code parameters.

Parameter	Value	Parameter	Value
V_{high}^+	0.9	V_{low}^+	0.4
V_{high}^-	0.6	V_{low}^-	0.1
k_p	2.0	k_n	2.0

3.3.1 Fault impedance variation analysis

For a single converter system as the one depicted in Figure 16, the fault impedance connected to the bus at voltage $\underline{V}_f$ represents the event of short-circuit in this case. Explicitly, voltages and

currents are related by:

$$\begin{pmatrix} \underline{I}_1^a \\ \underline{I}_1^b \\ \underline{I}_1^c \\ \underline{I}_t^a \\ \underline{I}_t^b \\ \underline{I}_t^c \end{pmatrix} = (\mathbf{Y_v} + \mathbf{Y_f}) \begin{pmatrix} \underline{V}_{p1}^a \\ \underline{V}_{p1}^b \\ \underline{V}_{p1}^c \\ \underline{V}_f^a \\ \underline{V}_f^b \\ \underline{V}_f^c \end{pmatrix}, \tag{53}$$

where the admittance matrix has been splitted into two parts: $\mathbf{Y_v}$ represents the non-faulted admittance matrix of the system, whereas $\mathbf{Y_f}$ is constituted by the admittances that intervene in the fault and has the same size as $\mathbf{Y_v}$. This way, the admittance matrices are defined as:

$$\mathbf{Y_v} = \begin{pmatrix} \underline{Y}_{v1} & 0 & 0 & -\underline{Y}_{v1} & 0 & 0 \\ 0 & \underline{Y}_{v1} & 0 & 0 & -\underline{Y}_{v1} & 0 \\ 0 & 0 & \underline{Y}_{v1} & 0 & 0 & -\underline{Y}_{v1} \\ -\underline{Y}_{v1} & 0 & 0 & \underline{Y}_{v1} + \underline{Y}_t & 0 & 0 \\ 0 & -\underline{Y}_{v1} & 0 & 0 & \underline{Y}_{v1} + \underline{Y}_t & 0 \\ 0 & 0 & -\underline{Y}_{v1} & 0 & 0 & \underline{Y}_{v1} + \underline{Y}_t \end{pmatrix} \tag{54}$$

where $\underline{Y}_{v1} = 1/\underline{Z}_{v1}$ and $\underline{Y}_t = 1/\underline{Z}_t$.

On the other hand, the fault admittance matrix $\mathbf{Y_f}$ is fully dependent on the type and depth of the fault. All its elements are zero except for a few entries that contain the fault admittance connected to their respective bus. The optimization problem for the one case converter, particularized from (46), reads:

$$\begin{aligned} \min_{\mathbf{I_1} \in \mathbf{I}} \quad & f_o = \lambda_1^+ |(1 - V_{p1}^+(\mathbf{I}))| + \lambda_1^- |(0 - V_{p1}^-(\mathbf{I}))| \,, \\ \text{s.t.} \quad & \max(I_1^a, I_1^b, I_1^c) \leq I_{\text{max},1} \,, \end{aligned} \tag{55}$$

where $\mathbf{I_1}$ contains the currents $\underline{I}_1^a, \underline{I}_1^b, \underline{I}_1^c$ for which the optimization problem is actually solved for, and $\mathbf{I}$ is the left-hand side vector in (53). Because of the nature of the three-wire converter, it is also imposed that the sum of the three-phase currents becomes zero.

The procedure to solve the optimization problem is the following:

- Initialize the admittance matrices $\mathbf{Y_v}$ as in (54), and then, construct $\mathbf{Y_f}$.
- Currents are initialized to a random array of values.
- The Mystic package is called to solve the optimization problem stated in (55).
- Positive and negative sequence voltages are evaluated to determine the optimality of the solution by means of (45).

- In the case of sweeping a range of m scenarios with different fault impedance values, the above presented steps are repeated m times.

- Currents are transformed into positive and negative sequence values since the final goal is to evaluate their values in this reference frame.

Solving the problem with the aforementioned steps for a balanced fault yields the results shown in Figure 17, where impedance $\underline{Z}_f$ denotes the fault impedance connected to each phase, which is considered to be fully resistive in this case. The results suggest that the optimal case (OPT) is the preferred one, as its associated objective function f_o is always the smallest. In other words, the positive and negative sequence voltages tend to be closer to the references of 1 and 0 pu respectively (see (55)). This optimal solution is achieved by distributing the currents between the real and imaginary parts. The real part of the current is the so-called active current, whereas the imaginary part represents the reactive current. It has to be noted that the phase of the positive and negative currents is referred to their corresponding positive and negative voltages. In this case, the imaginary current remains slightly larger than the real current (in absolute value). This is the main difference between OPT and the grid code implementations found in GCP, GCN, and GC. These three strategies require the converter to employ its full capability on the imaginary positive sequence current. Therefore, their objective functions and voltage profiles become identical in this case with a balanced fault.

Significantly different results are obtained in the case of a line-to-line fault, as shown in Figure 18. This unbalanced fault causes the optimal currents to be almost zero in the positive sequence, so the majority of the current capability is employed in the negative sequence. Severe faults require a large real current (in absolute value), whereas in the case of less extreme faults, the imaginary current tends to the maximum, i.e, 1.0. Even though the active current is kept at zero for GCP, GCN, and GC, their reactive currents vary significantly across the range of $\underline{Z}_f$ values. GCP tends to approach the results provided by OPT for large $\underline{Z}_f$, whereas GCN evolves on the contrary direction. This finding was not forced, but rather, it happens to be the case that GCP closely follows the optimal trajectory.

For small purely resistive fault impedances, GCP prioritizes injecting current in the positive sequence whereas GCN does the same for the negative sequence, as expected. As a consequence, positive sequence voltages in the case of GCP are initially superior to the ones obtained with GCN. The situation is reversed around $\underline{Z}_f \approx 0.1$. Since the fault is not that severe, much of the current capability is employed in the non-prioritized sequence in order to reach saturation. In the end, there is an almost constant minimal difference between OPT and GCP, as their objective functions f_o are nearly the same. The fundamental grid code GC is usually the suboptimal choice. Even though it specifies a similar I_{im}^{+} current compared to GCP, the negative sequence voltage is not minimized since by definition $I^{-} = 0$.

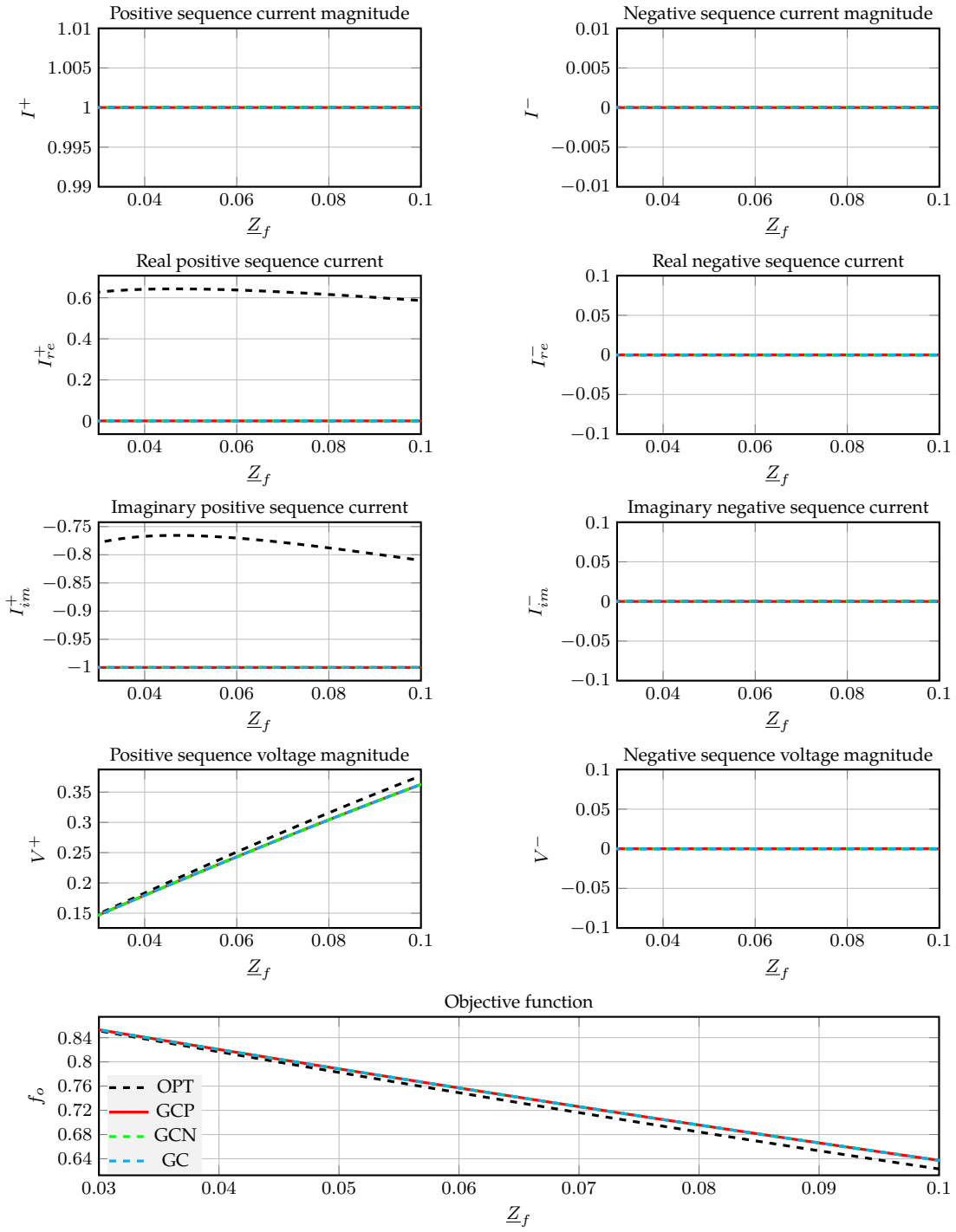

Figure 17: Influence of the currents for a balanced fault with a varying fault impedance, one-converter case.

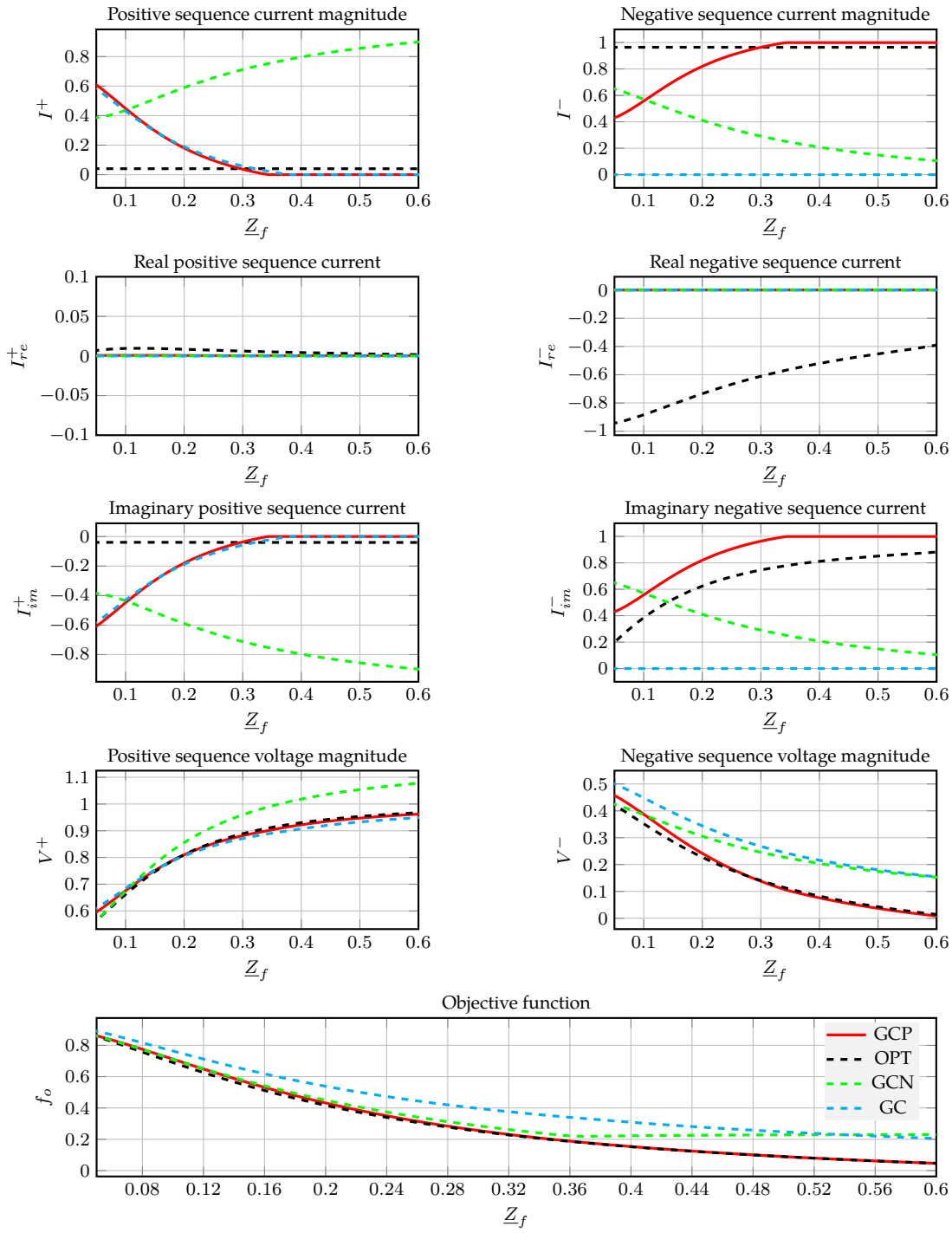

Figure 18: Influence of the currents for a line-to-line fault with a varying fault impedance, one-converter case.

3.3.2 R_1/X_1 variation analysis

The R_1/X_1 variation analysis performs a sweep for a range of angles of the $\underline{Z}_{v1}$ impedance, while the absolute value is preserved. The goal of this study is to determine how this affects the

distribution of currents between the real and the imaginary part. The results in Figure 19 for the OPT case show that despite an increase in the resistive part of the impedance, the currents remain nearly constant for all the range of values. Most of the current capability is dedicated to I_{im}^{+} and I_{im}^{-}.

Differences among the objective functions of OPT and the rest of the options are more significant for a large R_1/X_1 value since it has been established that GCP, GCN, and GC cannot inject any active current. In particular, the OPT option achieves a larger positive sequence voltage than both GCP and GC for all ranges of values. Regarding the negative sequence voltage, OPT is usually the best choice despite having placed the same importance on the positive and the negative sequence voltages. GC does not make any effort to minimize V^{-}, and this is why it remains significantly superior to the other strategies. Despite the fact that GCP prioritizes active current, as the fault is not severe and it has been imposed that the converter has to operate under saturated conditions, the GCP strategy injects more current in the negative sequence than in the positive sequence. The contrary applies to the GCN option. Therefore, GCN yields larger V^{+} and V^{-} voltages compared to GCP. In the end, the objective function is practically the same for GCP and GCN. The positive aspect of employing GCP and GCN is that given that power systems are mainly inductive (i.e., R/X ratios tend to be small) [75], the injection of zero active power is not that crucial, as shown in Figure 19 for $R_1/X_1 < 1$.

3.3.3 Cable length variation analysis

Figure 20 represents the third parametric study regarding single converter systems, which deals with a hypothetical submarine cable modeled with its π equivalent. The data selected to model the cable are extracted from [76] and adapted to per-unit values, which are shown in Table 16. The base values are a power of 100 MVA and a voltage of 220 kV. The followed approach to analyze the system is identical to the previous ones, except for the reduction to a Thévenin equivalent of the set of elements including the cable and the grid. With this reduction, the system in Figure 20 takes the form of the system in Figure 16. The corresponding Thévenin equivalent is defined by:

$$\begin{cases} \underline{V}_t' = \frac{\underline{Z}_p\underline{Z}_p}{2\underline{Z}_t\underline{Z}_p+\underline{Z}_p\underline{Z}_s+\underline{Z}_p\underline{Z}_p+\underline{Z}_t\underline{Z}_s} \\ \underline{Z}_t' = \frac{\underline{Z}_p\underline{Z}_p\underline{Z}_t+\underline{Z}_p\underline{Z}_p\underline{Z}_s+\underline{Z}_p\underline{Z}_s\underline{Z}_t}{2\underline{Z}_p\underline{Z}_t+\underline{Z}_s\underline{Z}_p+\underline{Z}_s\underline{Z}_t+\underline{Z}_p\underline{Z}_p} \end{cases} \tag{56}$$

Similarly as before, a Norton equivalent is preferred. The current $\underline{I}_t'$ is simply equal to $\underline{V}_t'/\underline{Z}_t'$.

Table 16: Cable parameters for the one-converter case.

Parameter	Value	Units
$\underline{Z}_s$	$6.674 \cdot 10^{-5} + j2.597 \cdot 10^{-4}$	pu/km
$\underline{Z}_p$	$-j77.372$	pu·km

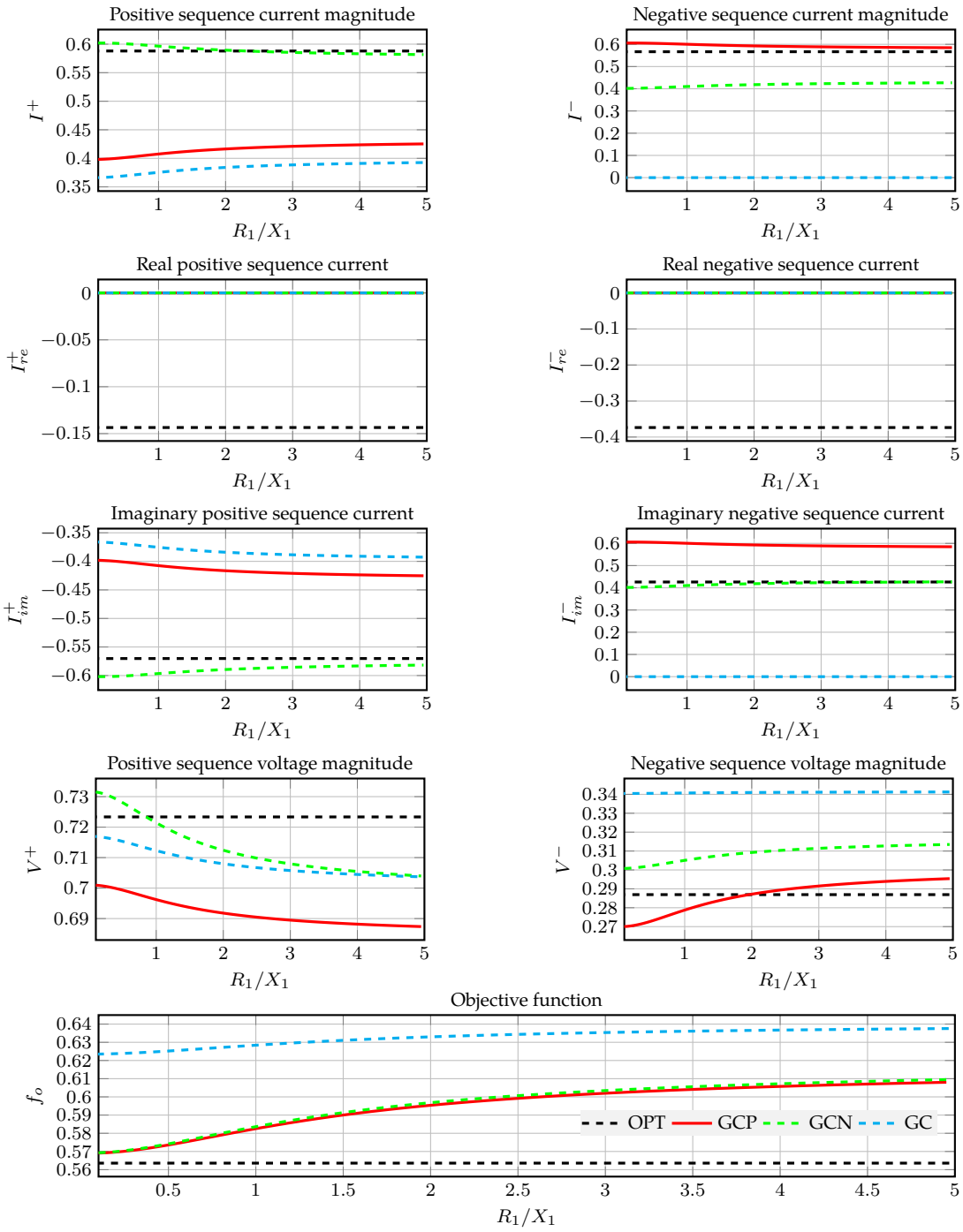

Figure 19: Influence of the currents for the line-to-ground fault with a varying R_1/X_1 ratio and a fault impedance $\underline{Z}_{ag} = 0.01$, one-converter case.

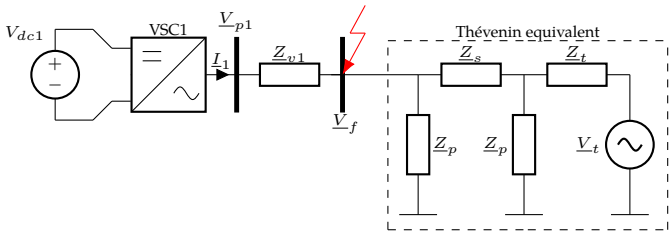

Figure 20: Single-phase representation of the single converter connected to a system with a cable.

The analysis performed considers a cable with a varying length, up to 100 km. Its impact on the Thévenin equivalent parameters is shown in Figure 21. The voltage experiences a subtle increase, while the equivalent impedance at 100 km almost doubles the one at 0 km.

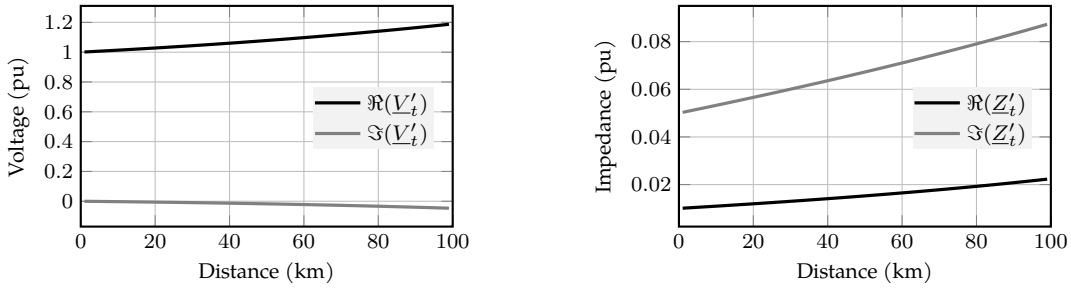

Figure 21: Thévenin voltage and impedance depending on the cable distance.

The four strategies are again evaluated, as depicted in Figure 22, where a line-to-line fault takes place with an impedance between phases a and b of 0.1 pu. Increasing the cable distance causes the negative sequence voltage to grow, while the positive sequence voltage also tends to grow. This phenomenon mostly differs from the profiles obtained in Figure 18 and 19, where both voltages either simultaneously approached the objective value (1 and 0 respectively), or distanced from it. Consequently, in the cases of the grid code implementation, longer distances imply a lower I_{im}^{+} current, while the less convenient growing negative sequence voltages force an increment in I_{im}^{-}. Most of the current capability is precisely devoted to this negative sequence imaginary current. The OPT option achieves a more favorable objective function value than the rest by keeping the positive sequence currents practically constant, increasing I_{re}^{-} (in absolute value), and decreasing I_{im}^{-}, which is the inverse trend followed by GCP and GCN. Again, V^{-} is large for the GC option and consequently there is a non-negligible margin between the objective function f_o of GC and the other strategies.

3.4 Two-converter case study

This Section presents a two-converter case in order to spot the differences in the distribution of currents between both converters, and at the same time, evaluate the feasibility of the suggested strategies. Figure 23 shows a single-phase representation of the system under study. It corresponds to an adaptation of the IEEE 9-bus system where the generators in buses 2 and

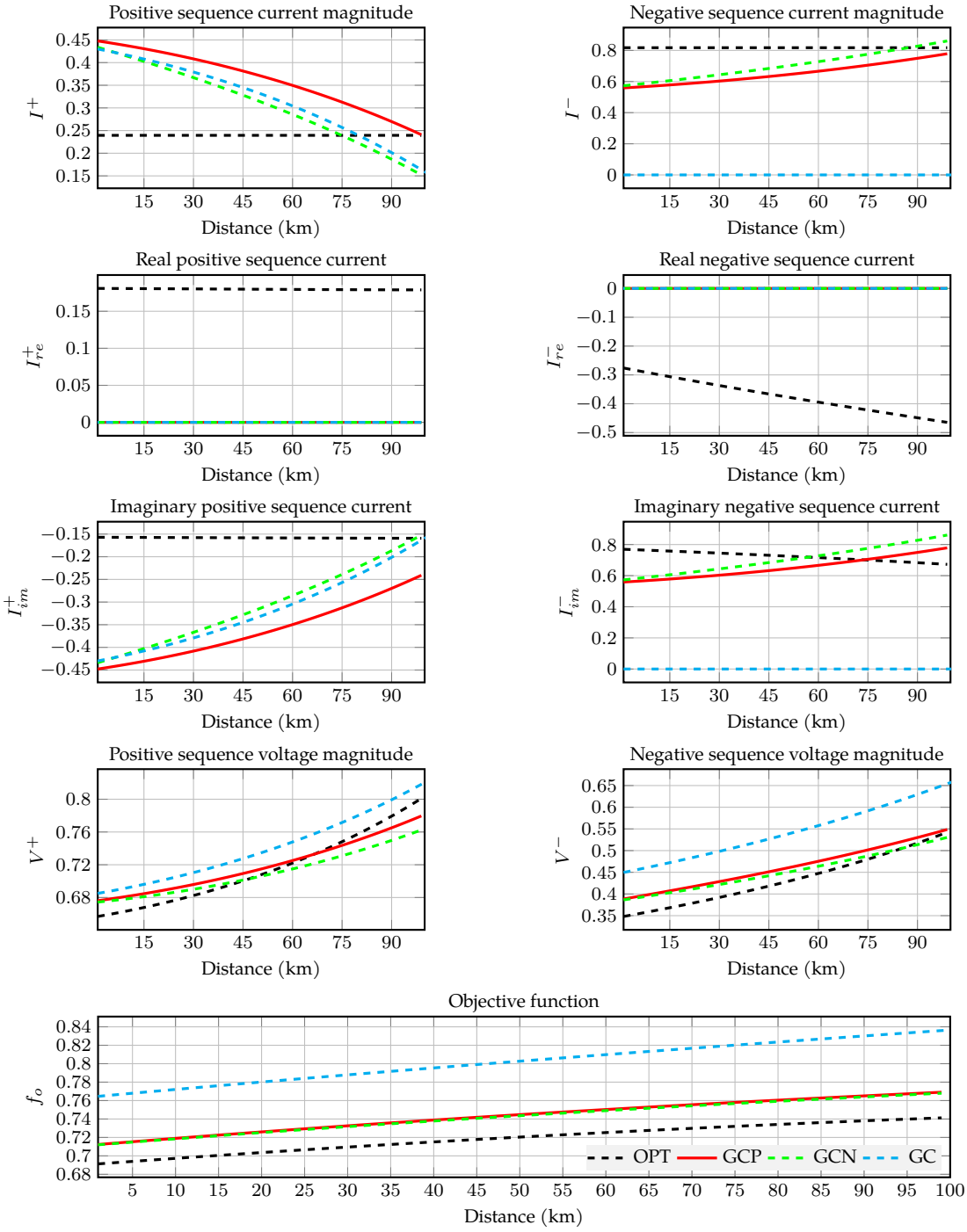

Figure 22: Influence of the currents for a line-to-line fault with $\underline{Z}_{ab} = 0.1$ and a varying cable distance, one-converter case.

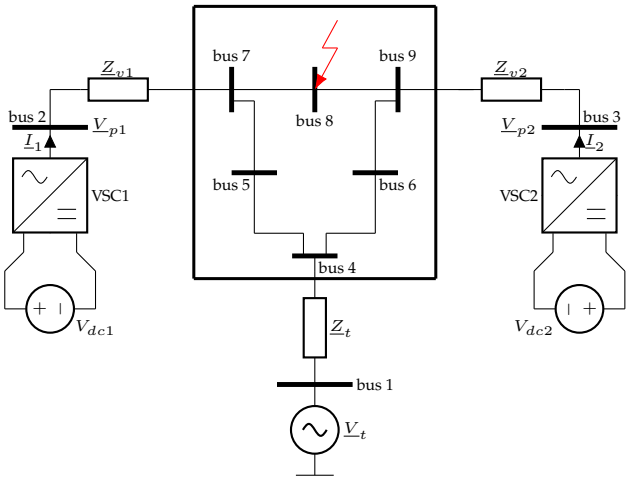

Figure 23: Simplistic single-phase representation of the two-converter IEEE 9-bus system under study.

3 have been replaced by VSCs. PQ loads were originally connected to buses 4 to 9; they have been disconnected during the fault for protection. Bus 1 remains the slack bus. The connections between the converters and the slack bus with respect to the boxed grid are achieved through transformers which are modeled by a single impedance. This boxed grid represents the passive part of the grid. Its internal connections are modeled with an equivalent π circuit. All data have been extracted from [77].

Analogous to the one-converter situation, the optimization problem becomes:

$$\begin{aligned} \min_{\mathbf{I_1},\mathbf{I_2}\in\mathbf{I}} \quad & f_o = \lambda_1^+|(1-V_{p1}^+(\mathbf{I}))| + \lambda_1^-|(0-V_{p1}^-(\mathbf{I}))| \\ & + \lambda_2^+|(1-V_{p2}^+(\mathbf{I}))| + \lambda_2^-|(0-V_{p2}^-(\mathbf{I}))|, \\ \text{s.t.} \quad & \max(I_1^a, I_1^b, I_1^c) \leq I_{\text{max},1} \ , \\ & \max(I_2^a, I_2^b, I_2^c) \leq I_{\text{max},2} \ , \end{aligned} \tag{57}$$

where $\mathbf{I_1}$ and $\mathbf{I_2}$ are respectively the currents injected by converters 1 and 2, $\mathbf{I}$ symbolizes all current injections as in the left-hand side of (43), and all λ have been set to 1.0. The application of the GC, GCP and GCN strategies is the same as before, in the sense that the injection of current $\mathbf{I_1}$ only depends on $\underline{V}_{p1}$, and $\mathbf{I_2}$ is expressed as a function of $\underline{V}_{p2}$.

As can be deduced from Figure 23, a short-circuit fault is provoked in bus 8. Figure 24 shows the most representative results for this line-to-line short-circuit fault with different fault impedances, where the plotted voltages correspond to the positive and negative sequence of $\underline{V}_{p1}$ and $\underline{V}_{p2}$. The OPT choice prioritizes I^+, mainly its imaginary part. This helps to obtain a higher V^+. Contrarily, the suggested grid codes GCP and GCN inject a larger I^- current, which of course, is purely imaginary. Their associated V^+ values are inferior to the ones obtained with OPT, yet their V^- voltage is also smaller. As a result, there is little difference in the objective function,

which makes GCP and GCN near-optimal strategies. The decision to choose between GCP and GCN may be based on other factors such as the limitations the sequence components impose on protective relays. On the other hand, the basic grid code GC injects a small current as the fault is not extremely severe. Only about 25% of the full current capability of the converters is employed. Thus, there are relevant differences in the objective function between GC and the other options.

A dynamic simulation has been performed with Matlab/Simulink to validated the results. Figure 25 shows the evolution of the voltages with time. It is confirmed that the steady-state values are the same, hence the presented steady-state calculation procedure is considered correct.

3.5 Conclusion

The system operation points during the fault achieved with conventional grid codes have been compared with the optimal solution in systems that integrate converters considering limitations. In the optimal solution, the positive and negative sequence voltages approach as much as possible the nominal voltage and a zero voltage respectively. Two strategies have been derived to respectively prioritize positive (GCP) and negative (GCN) currents in saturated conditions, therefore maximizing the voltage-support. These two strategies are superior to the basic grid code. Although there are certain differences in the currents for GCP and GCN, both of them tend to provide almost the same objective function value. Several parameters have been swept, such as the fault impedance, the angle of the interconnecting impedance, and the length of a cable. Generally, the distribution of currents derived from the optimization differs considerably from the currents injected following the conventional grid codes. Nonetheless, the proposed approaches GCP and GCN offer an objective function value that is usually closer to the optimal than to the basic grid code. This work concludes that it is possible to improve the voltage-support with arguably simple rules where only reactive current/power is injected from power converters. The optimal situation is not suitable to be implemented in reality as it requires knowledge about the fault impedance and a high computational effort. However, GCP and GCN can be easily implemented in reality since they are of the same nature as traditional grid codes. Due to the ease of implementation and the near-optimal voltage-support, the adapted grid codes GCP and GCN are considered the most convenient choices.

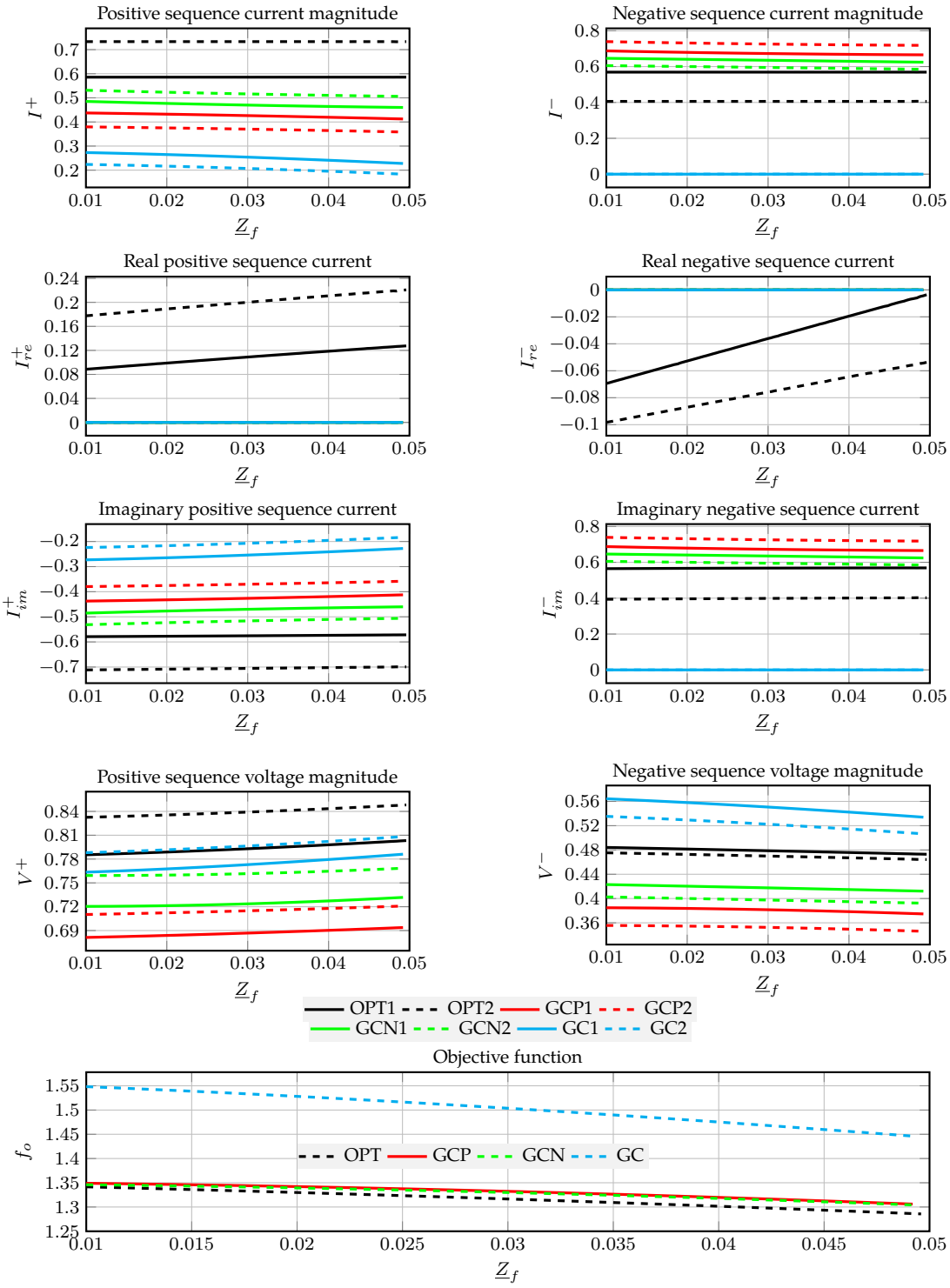

Figure 24: Influence of the currents for the line-to-line fault with a varying fault impedance in bus 8 of the IEEE 9-bus system.

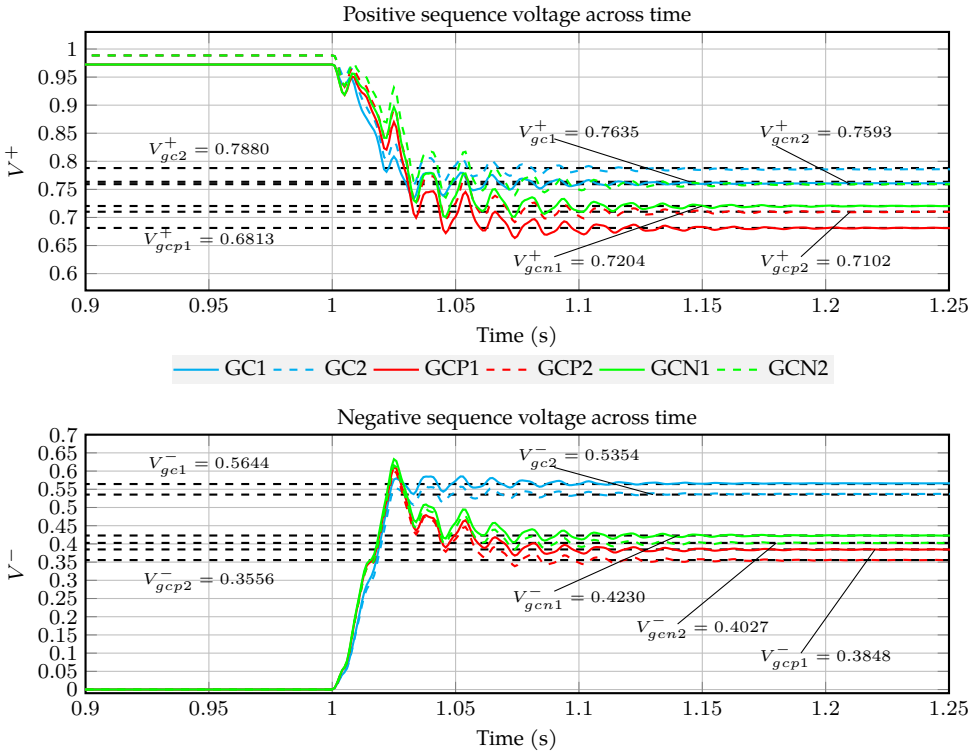

Figure 25: Dynamic validation to check the obtained steady-state results for $\underline{Z}_f = 0.01$ in the IEEE 9-bus system.

4 Galerkin method for parametric studies

4.1 Introduction

The power flow problem is focused on solving a given state under certain conditions. However, in reality, many parameters are prone to change. The powers can evolve over the course of the day, for instance. As these inputs change, the power flow has to be solved again and again. This is an arduous task, especially considering that the topology is expected to remain the same. Ideally, the system should be solved once for all cases. The parametric power flow revolves around this core idea [78].

The first work following the aforementioned direction is the so-called probabilistic power flow [79]. Given some uncertainty in the input parameters, it estimates the probability of output variables such as the power through the lines. Such an approach is limited to working with probabilities. In this sense, there is no deterministic output value to be derived from the inputs. A simple yet arguably inaccurate option is to rely on the Taylor expansion method. The first derivative could estimate the evolution of an output (denoted as a state from now on) depending on the inputs (also called parameters) [80]. Unfortunately, this sensitivity analysis is limited to the usage of linear terms whereas the power flow exhibits a rather quadratic profile. Opting for derivatives of higher order involves a very complex system of equations without a straightforward solution. For more depth in this regard, see the two-bus example system in [43]. A more fundamentally sound possibility is to look for an explicit closed-form expression that links parameters with states (perhaps in the form of a simple polynomial). A set of parameters can be sampled inside a closed predefined range, extract the dependency between parameters and inputs, and fit a polynomial to these points [23]. Eventually, the parameters can be grouped with the Principal Component Analysis so that the states depend only on a few final parameters [81]. Some advantages of this method are its simplicity and freedom to choose a polynomial basis. On the downside, it is heavily dependent on the sampling stage. Even opting for the Latin Hypercube sampling, which produces a realistic representation of the space [82], does not minimize much the error. Fortunately, the Galerkin method avoids the sampling process and achieves smaller errors in the whole domain [83]. If orthogonal bases are selected, the residual will be perpendicular to them, which is said to be optimal [20]. This is the key behind the Galerkin method.

This chapter covers the mathematical formulation of the Galerkin method. Both the decoupled and expanded approaches are explored. The goal of the chapter is to introduce the notation, show explicitly the form that equations take, and get an idea of its practicality. Simple systems are evaluated as well as the IEEE 14-bus system.

4.2 Initial definitions

The parametric power flow and in particular the Galerkin method rely on a set of initial definitions. Objects such as states, parameters, bases and residuals are described as follows:

- **States**: they are the outputs under consideration. In other words, they are the unknowns to be found. In this work, they are denoted by a vector $\boldsymbol{x} \in \mathbb{R}^n$, where n is the length of the $\boldsymbol{x}$ vector, that is, the number of unknowns. States are treated as real numbers because the rectangular power flow is adopted.

- **Parameters**: they are the inputs of the system. Parameters are input variables likely to change. Hence, there is interest in expressing the states as functions of these parameters. They are represented by a vector $\boldsymbol{p} \in \mathbb{R}^{N_d}$, where N_d is the total number of parameters.

- **Bases**: they are a set of polynomials function of the parameters. For example, one basis could be p, another p^2, and so on, where p is a single paremeter. The whole set of bases is denoted by $\boldsymbol{\Phi}$, and has a length of N. States and parameters are eventually defined as a linear combination of bases.

- **Residuals**: they are the equations to be solved expressed as polynomials. The Galerkin method relies on computing the inner product between residuals and bases. Residuals are expressed as a vector $\boldsymbol{R}$, which has a length n, the same as the number of unknowns.

4.3 Decoupled approach

Contrarily to the expanded approach, the decoupled Galerkin deals with less complexity at the expense of larger errors [84]. The bases of the Galerkin method are established, and then, the characteristics of the decoupled procedure are presented.

4.3.1 Formulation

In essence, the power flow looks for a solution to a non-linear system of equations of the form:

$$\mathbf{0} = \boldsymbol{f}(\boldsymbol{x}), \tag{58}$$

where $\boldsymbol{x}$ is the vector of unknowns (usually the voltages), and $\boldsymbol{f}$ is a set of non-linear equations.

Nonetheless, parameters can also be explicitly considered in the parametric power flow. This way, (58) becomes:

$$\mathbf{0} = \boldsymbol{f}(\boldsymbol{x}, \boldsymbol{p}), \tag{59}$$

where $\boldsymbol{p}$ is a vector of parameters. Magnitudes such as powers in PQ buses or the voltage magnitude in PV buses can be treated as parameters. In general, impedances could be parameters as well.

In any case, the power flow equations are implicit. This justifies why a tiny change in a parameter theoretically involves having to solve the whole system of equations. Instead, the parametric power flow looks for the following:

$$\boldsymbol{x} = \boldsymbol{g}(\boldsymbol{p}), \tag{60}$$

where $\boldsymbol{g}$ is a set of equations to be found.

The parametric power flow adopts the treatment of states with polynomial representations involving coefficients and the parameters. This is desirable because as the Weierstrass approximation theorem states, a polynomial function can identify as closely as desired a continuous function inside a closed interval [20], [85]. The concept of approximating the solution with polynomials is not new. For example, the Holomorphic Embedding Load-Flow Method (HELM) is based on it [86].

The approximation of states depends on bases and on coefficients. With the Galerkin method, a set of bases $\boldsymbol{\Phi}$ is chosen. A basis is an object whose value strictly depends on the parameters, and is common for all states. Coefficients, on the other hand, are initially unknown and are particular for each state. Combining bases and coefficients, the definition of states becomes:

$$\boldsymbol{x} = \sum_{i=0}^{N-1} \boldsymbol{c}_i \boldsymbol{\Phi}_i, \tag{61}$$

that is, they are a linear function of the bases, where $\boldsymbol{x}$ denotes the estimated states, and $\boldsymbol{c}_i$ are coefficients to be found. The value of N depends on the chosen order of the polynomials N_p and the amount of parameters N_d (sometimes also referred to as dimensions). Concretely:

$$N = \frac{(N_p + N_d)!}{N_p! N_d!}. \tag{62}$$

The curse of dimensionality ought to be avoided in order to reduce the computational cost. If it is decided that polynomials should reach high orders to better approximate the states or numerous magnitudes are meant to change, then N will inevitably take a very large value. One of the motivations of the decoupled Galerkin is to alleviate somewhat this burden.

A key idea behind the Galerkin method for the parametric power flow is the orthogonality between bases. Let the inner product between two objects x and y (that is, two different linear combinations of the bases) be $\langle x, y \rangle$. It is defined as [83]:

$$\langle x, y \rangle = \int_{\Omega} x(\boldsymbol{p}) y(\boldsymbol{p}) d\boldsymbol{p}, \tag{63}$$

where Ω is the full domain that considers all parameters.

If orthogonal bases are picked, the inner product between two bases Φ_i and Φ_j is:

$$\langle \Phi_i, \Phi_j \rangle = \delta_{ij}, \tag{64}$$

where δ_{ij} is a non-null constant if $i = j$ and 0 if $i \neq j$. While it is not mandatory for the bases to be orthogonal, it is of great practicality. Recall the expressions of the power flow contain the product between voltages. With orthogonal bases, the equations are greatly simplified because most products become null following (64).

The choice of polynomials (in other words, the form that the bases take) is to be decided by the user. In the work that follows, Legendre polynomials are selected due to being bounded in the range $[-1, 1]$. Working in per unit values, most likely the parameters evolve inside this range. If needed, they can be denormalized as well. Supposing a single parameter p is involved, using Rodrigues' formula (which is a particular formula for finding Legendre polynomials), the first polynomials are [87]:

$$\begin{cases} \Phi_0 = 1, \\ \Phi_1 = p, \\ \Phi_2 = (3p^2 - 1)/2, \\ \Phi_3 = (5p^3 - 3p)/2. \end{cases} \tag{65}$$

In the example contained in this chapter, a second parameter is introduced. Let p be the first parameter representing the active power, and q the second parameter that stands for the reactive power. If a maximum order $N_p = 3$ is chosen, then the full set of bases turns out to be the products between polynomials whose resulting maximum order does not exceed 3:

$$\boldsymbol{\Phi} = \left[1, p, q, pq, \frac{3p^2-1}{2}, \frac{3q^2-1}{2}, p\frac{3q^2-1}{2}, q\frac{3p^2-1}{2}, \frac{5p^3-3p}{2}, \frac{5q^3-3q}{2}\right]. \tag{66}$$

To find the coefficients in (61), after being defined the set of bases $\boldsymbol{\Phi}$, the next step is to formulate the residuals $\boldsymbol{R}$. Just as in the traditional power flow, the residuals represent the mismatch between the actual power and the specified power in a given bus. The goal is to minimize these residuals by taking the projection to each basis:

$$\langle \boldsymbol{R}, \boldsymbol{\Phi} \rangle = \mathbf{0}. \tag{67}$$

In principle, this will form a non-linear system of equations to be solved, for example, by the Newton-Raphson method. Suppose the system under study has n unknowns (coinciding with the total number of equations). Since $\boldsymbol{\Phi}$ is formed by N terms, there is a system of size $N \times n$ to be solved all at once.

To avoid solving this potentially huge system in one go, a solution is to decompose it following the decoupled Galerkin method [84]. In it, first the inner product of the residuals $\boldsymbol{R}_0$ only containing 0 order terms and Φ_0 is performed:

$$\langle \boldsymbol{R}_0, \Phi_0 \rangle = \mathbf{0}. \tag{68}$$

As a result of it, the first coefficients $\boldsymbol{c}_0$ are obtained.

Then, the first order terms are considered through:

$$\langle \boldsymbol{R}_1, \Phi_1 \rangle = \mathbf{0}, \tag{69}$$

which involves the already known coefficients $\boldsymbol{c}_0$ and the new coefficients to find $\boldsymbol{c}_1$. Note that the residuals of the form $\boldsymbol{R}_k$ involve coefficients of a maximum order k. In this sense, they are said to be truncated residuals as the high order coefficients are ignored.

The described approach continues until all bases have been exhausted. A total of N systems of equations, each of them formed by n unknowns, are solved sequentially. Thus, all required coefficients to represent the states are found, and the problem is finished. It has to be mentioned that going for this technique has the advantage of having to solve a linear system for orders greater than 0. The associated matrix can be inverted only once, resulting in a saving of time. The decoupled Galerkin cannot compete with the classical Galerkin in terms of precision but yields a high-speed advantage (see [84]).

4.3.2 Fundamental example

The example that follows consists of a two-bus system. One bus is the slack one, while the second acts as a PQ bus. Its powers $p + jq$ are parameters. Figure 26 shows very schematically this system.

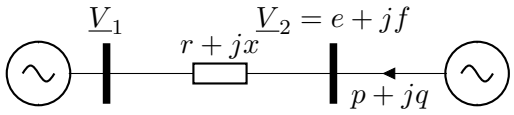

Figure 26: Scheme of the two-bus system.

With the Galerkin method, it is preferable to solve the power flow in rectangular coordinates, as it makes the integrals easier to operate. Assume bus 1 has a set voltage of $\underline{V}_1 = e_1 + jf_1 = 1 + 0j$. Then, the power equations are:

$$\begin{cases} p = ge^2 - ge + gf^2 - bf, \\ -q = gf + be^2 - be + bf^2, \end{cases} \tag{70}$$

where $g + jb = \frac{1}{r+jx}$, and e and f represent respectively the real and imaginary part of the voltage at bus 2.

Considering the polynomial representation of the voltages of the form $\sum_i c_i \Phi_i$, as described in

(61), (70) becomes:

$$\begin{cases} R_p = & -\sum_{i=0}^{N-1} c_i^p \Phi_i + g \sum_{i=0}^{N-1} c_i^e \Phi_i \sum_{i=0}^{N-1} c_i^e \Phi_i - g \sum_{i=0}^{N-1} c_i^e \Phi_i \\ & +g \sum_{i=0}^{N-1} c_i^f \Phi_i \sum_{i=0}^{N-1} c_i^f \Phi_i - b \sum_{i=0}^{N-1} c_i^f \Phi_i, \\ R_q = & \sum_{i=0}^{N-1} c_i^q \Phi_i + g \sum_{i=0}^{N-1} c_i^f \Phi_i + b \sum_{i=0}^{N-1} c_i^e \Phi_i \sum_{i=0}^{N-1} c_i^e \Phi_i \\ & -b \sum_{i=0}^{N-1} c_i^e \Phi_i + b \sum_{i=0}^{N-1} c_i^f \Phi_i \sum_{i=0}^{N-1} c_i^f \Phi_i, \end{cases} \tag{71}$$

where R_p and R_q are the active and reactive power residuals. The powers are parametrized as well with coefficients c_i^p and c_i^q respectively, and the coefficients for the real and imaginary part of the voltages are c^e and c^f respectively. This way, the voltages are explicitly:

$$\begin{cases} e = \sum_{i=0}^{N-1} c_i^e \Phi_i = c_0^e \cdot 1 + c_1^e \cdot p + c_2^e \cdot q + c_3^e \cdot pq + ... \\ f = \sum_{i=0}^{N-1} c_i^f \Phi_i = c_0^f \cdot 1 + c_1^f \cdot p + c_2^f \cdot q + c_3^f \cdot pq + ... \end{cases} \tag{72}$$

where all coefficients are unknowns and have to be found by solving the Galerkin equations.

The power coefficients are found directly assuming that (71) has to be equivalent to (70). Hence:

$$\begin{cases} p = \sum_{i=0}^{N-1} c_i^p \Phi_i = 0 \cdot 1 + 1 \cdot p + 0 \cdot q + 0 \cdot pq + ... \\ q = \sum_{i=0}^{N-1} c_i^q \Phi_i = 0 \cdot 1 + 0 \cdot p + 1 \cdot q + 0 \cdot pq + ... \end{cases} \tag{73}$$

So all their coefficients are zero except for the one that multiplies itself, of course.

To proceed in order to solve for the coefficients of the voltages, first the inner product $\langle \boldsymbol{R}_0, \Phi_0 \rangle = 0$ is calculated:

$$\begin{cases} 0 = g c_0^e c_0^e \int_{-1}^{1} \int_{-1}^{1} dp \cdot dq - g c_0^e \int_{-1}^{1} \int_{-1}^{1} dp \cdot dq + g c_0^f c_0^f \int_{-1}^{1} \int_{-1}^{1} dp \cdot dq - b c_0^f \int_{-1}^{1} \int_{-1}^{1} dp \cdot dq, \\ 0 = g c_0^f \int_{-1}^{1} \int_{-1}^{1} dp \cdot dq + b c_0^e c_0^e \int_{-1}^{1} \int_{-1}^{1} dp \cdot dq - b c_0^e \int_{-1}^{1} \int_{-1}^{1} dp \cdot dq + b c_0^f c_0^f \int_{-1}^{1} \int_{-1}^{1} dp \cdot dq, \end{cases} \tag{74}$$

which simply becomes:

$$\begin{cases} 0 = g c_0^e c_0^e - g c_0^e + g c_0^f c_0^f - b c_0^f, \\ 0 = g c_0^f + b c_0^e c_0^e - b c_0^e + b c_0^f c_0^f. \end{cases} \tag{75}$$

This system of equations is solved with the Newton-Raphson method (note it is non-linear), and coefficients c_0^e and c_0^f are obtained.

The next step involves calculating $\langle \boldsymbol{R}_1, \Phi_1 \rangle = 0$, which only contains coefficients of zero and first order. As a result, the first order coefficients are meant to be obtained with:

$$\begin{cases} 0 = -1 + g(c_0^e c_1^e + c_1^e c_0^e) - g c_1^e + g(c_0^f c_1^f + c_1^f c_0^f) - b c_1^f, \\ 0 = g c_1^f + b(c_0^e c_1^e + c_1^e c_0^e) - b c_1^e + b(c_0^f c_1^f + c_1^f c_0^f). \end{cases} \tag{76}$$

Fortunately, in this case the system is linear, and it will remain linear for the rest of inner products $\langle \boldsymbol{R}_k, \Phi_k \rangle \; \forall k \geq 1$. This way, there is a constant Jacobian, which is just shown for reference:

$$\boldsymbol{J} = \begin{pmatrix} 2gc_0^e - g & 2gc_0^f - b \\ 2bc_0^e - b & 2bc_0^f + g \end{pmatrix}. \tag{77}$$

Explicitly, the inner product $\langle \boldsymbol{R}_2, \Phi_2 \rangle$ becomes:

$$\begin{cases} 0 = g(2c_0^e c_2^e + c_1^e c_1^e) - gc_2^e + g(2c_0^f c_2^f + c_1^f c_1^f) - bc_2^f, \\ 0 = 1 + gc_2^f + b(2c_0^e c_2^e + c_1^e c_1^e) - bc_2^e + b(2c_0^f c_2^f + c_1^f c_1^f). \end{cases} \tag{78}$$

It is solved for the coefficients c_2^e and c_2^f as they are the only unknowns at this stage. The advantage of the decoupled Galerkin becomes clear as it is way simpler to solve step by step these systems of equations than attempting to solve once a large non-linear system.

The rest of coefficients are solved by taking the remaining inner products $\langle \boldsymbol{R}_k, \Phi_k \rangle$ until $k = N$. For this system of example, the non-varying parameters take the values shown in Table 17.

Table 17: Static parameters of the system.

Magnitude	Value
r	0.01
x	0.05
e_1	1.0
f_1	0.0

The dynamic parameters, so to speak, are the powers p and q. They are assumed to take values between 0 and 1. If the procedure described above is followed, taking $N_p = 3$, the coefficients of the voltages at bus 2 are the ones gathered in Table 18.

Graphically, the percentual current error presents a shape as the one in Figure 27.

The average error is around 1%, which concludes that the decoupled Galerkin method is capable of approximating reasonably well the voltages in this simple two-bus case. Opting for the full Galerkin, and not the decoupled, would produce smaller errors by nature. As it is common practice in power systems analysis to admit errors of the order of 10^{-3} pu at least, the decoupled Galerkin may have a limited application in solving real-life grids.

4.4 Expanded approach

The expanded approach of the Galerkin method, simply called Galerkin method, is regarded as a powerful tool to accurately solve the parametric power flow. Having observed the limitations of the decoupled approach, this section concentrates on formulating a generic algorithm to be applied to any realistic grid. The method is then tested on the IEEE 14-bus system.

Table 18: Obtained coefficients for the voltages.

Order	$\boldsymbol{c}^e$	$\boldsymbol{c}^f$
0	1.00000E+00	0.00000E+00
1	1.00000E-02	5.00000E-02
2	4.74000E-02	-1.00000E-02
3	5.20000E-05	0.00000E+00
4	-2.34780E-03	0.00000E+00
5	4.20264E-05	0.00000E+00
6	2.21728E-04	0.00000E+00
7	-8.17450E-06	0.00000E+00
8	-2.63729E-05	0.00000E+00
9	1.47668E-06	0.00000E+00

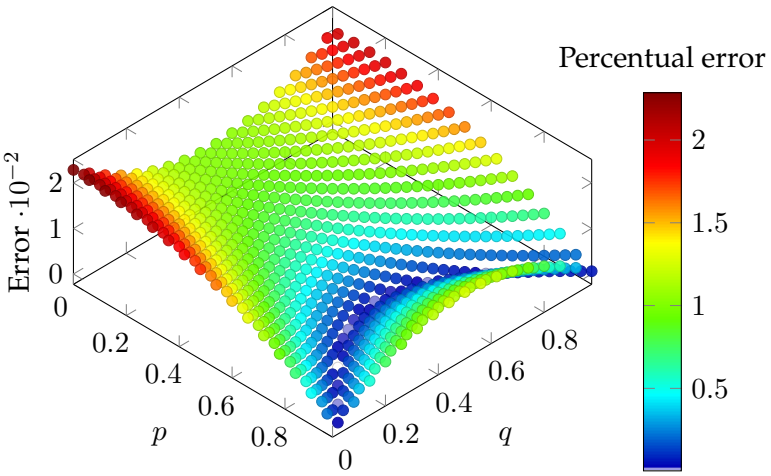

Figure 27: Representation of the current error as a function of the parametrized powers for the decoupled Galerkin with $N_p = 3$.

4.4.1 Formulation

The expanded Galerkin corresponds to the original method where the series are expanded and the coefficients have to be computed in one go. It is considered to be the most rigorous version of the Galerkin method, although it suffers from the curse of dimensionality.

Recall that the Galerkin method relies on a set of orthogonal bases encapsulated in $\boldsymbol{\Phi}$. Also note that the power flow equations take the form of (71). The Galerkin equations are formed with the inner product between the residuals and the bases:

$$\langle R_r, \Phi_k \rangle = 0 \qquad \forall\, R_r \in \boldsymbol{R}, \quad \forall\, \Phi_k \in \boldsymbol{\Phi}, \tag{79}$$

where $\boldsymbol{R}$ is the set of residuals.

Due to the form of the power flow equations, the solution to (79) involves computing integrals such as:

$$\langle R_r, \Phi_k \rangle = ... + \int_\Omega \sum_i c_i \Phi_i(\boldsymbol{p}) \sum_j c_j \Phi_j(\boldsymbol{p}) \Phi_k(\boldsymbol{p}) d\boldsymbol{p} + ... \,, \tag{80}$$

where Ω defines the space (as the integral is potentially multidimensional), and $\boldsymbol{p}$ is the set of parameters. As the terms c are independent from $\boldsymbol{p}$, they can be extracted from the integral:

$$\langle R_r, \Phi_k \rangle = ... + \sum_i c_i \sum_j c_j \int_\Omega \Phi_i(\boldsymbol{p}) \Phi_j(\boldsymbol{p}) \Phi_k(\boldsymbol{p}) d\boldsymbol{p} + ... \,. \tag{81}$$

From (81) it becomes clear that products of three bases are prone to appear (and also of two bases), and no more.

4.4.2 Tensorial representation

A methodology to develop the products between bases has to be introduced considering a system with multiple parameters. For better comprehension, bases are represented as tensors. Tensors are N_d-dimensional objects that involve the cross-products between all primal bases. Primal bases are just the monomial expansion of a parameter such as $[p^0, p^1, p^2, p^3]$. Figure 28 exemplifies the tensor for a 2-dimensional case.

	q^0	q^1	q^2	q^3
p^0	1			
p^1				
p^2	1/2			
p^3				3

$$\Phi(p, q) = 1 + p^2/2 + 3p^3q^3$$

Figure 28: Exemplification of a tensor representing a polynomial. Empty entries are zeros.

The idea behind using tensors (which are no more than multidimensional matrices) is to be able to store systematically the bases information. In addition, the product operator between tensors has to be defined. Let Φ_a and Φ_b be bases that have to be multiplied. Its product is formally written as:

$$\Phi_a \circ \Phi_b = \sum_{a_1}^{|d_1|} \sum_{a_2}^{|d_2|} ... \sum_{a_{N_d}}^{|d_{N_d}|} \sum_{b_1}^{|d_1|} \sum_{b_2}^{|d_2|} ... \sum_{b_{N_d}}^{|d_{N_d}|} c_{a_1,a_2,...,a_{N_d}} c_{b_1,b_2,...,b_{N_d}} p_{d_1}^{a_1+b_1} p_{d_2}^{a_2+b_2} ... p_{d_{N_d}}^{a_{N_d}+b_{N_d}}, \tag{82}$$

where each tensor is formed by N_d dimensions, $|d_1|$ stands for the length of the first dimension, a_1 is the index that goes over all its positions in the Φ_a basis, $c_{a_1,a_2,...,a_{N_d}}$ is the coefficient stored

in the position $[a_1, a_2, .., a_{N_d}]$ of the Φ_a tensor, and p_{d_1} corresponds to the first parameter under consideration.

Let Φ_c be the basis resulting from the product $\Phi_a \circ \Phi_b$. Then, this new basis Φ_c can also be represented with a tensor, although of a larger size. The size of an original basis is $N_d \times (N_p + 1)$, where N_p is the maximum order of the primal bases. For instance, given a system that has $N_d = 3$ parameters, if the maximum order of the primal bases is chosen to be $N_p = 3$, the tensor has a size of $(4, 4, 4)$. Therefore, the new tensor Φ_c will have dimensions of $N_d \times (2N_p + 1)$. In the previous example, this is equivalent to a size of $(7, 7, 7)$.

The full $\mathbf{\Phi}$ bases are the one used to parametrize the states. They are obtained by computing the products between primal bases such that the maximum order of the polynomials is less than or equal to N_p:

$$\mathbf{\Phi} = \left[\sum_{i_1}^{|d_1|} \sum_{i_2}^{|d_2|} ... \sum_{i_{N_d}}^{|d_{N_d}|} \boldsymbol{\Psi_{p_1}}[i_1] \boldsymbol{\Psi_{p_2}}[i_2] ... \boldsymbol{\Psi_{p_{N_d}}}[i_{N_d}] \right] \text{ if } i_1 + i_2 + ... + i_{N_d} \leq N_p, \tag{83}$$

where $\boldsymbol{\Psi_{p_1}}[i_1]$ is the i_1 term in $\boldsymbol{\Psi_{p_1}}$, that is, i_1 is the index of the vector.

4.4.3 Exemplification with Legendre polynomials

Consider a primal basis of the first Legendre polynomials:

$$\boldsymbol{\Psi_{p_1}} = \left[1, p_1, \frac{3}{2}p_1^2 - \frac{1}{2}, \frac{5}{2}p_1^3 - \frac{3}{2}p_1 \right], \tag{84}$$

which contains four terms as it has been decided that $N_p = 3$.

The representation in tensors of all its terms is characterized by null values everywhere except for the row corresponding to the p_1 dimension. Equivalently, the same applies for the rest of dimensions. If a second dimension is assumed to be present:

$$\boldsymbol{\Psi_{p_2}} = \left[1, p_2, \frac{3}{2}p_2^2 - \frac{1}{2}, \frac{5}{2}p_2^3 - \frac{3}{2}p_2 \right]. \tag{85}$$

By applying (83), the complete basis becomes:

$$\mathbf{\Phi} = \left[\sum_{i_1}^{|d_1|} \sum_{i_2}^{|d_2|} \boldsymbol{\Psi_{p_1}}[i_1] \boldsymbol{\Psi_{p_2}}[i_2] \right] \text{ if } i_1 + i_2 \leq N_p. \tag{86}$$

Assuming $N_p = 3$, the resulting full set of bases is equivalent to the one shown in (66). In the

format of tensors, it is given by:

$$\begin{aligned}\mathbf{\Phi} = \Bigg[&\begin{pmatrix} 1 & 0 & 0 & 0 \\ 0 & 0 & 0 & 0 \\ 0 & 0 & 0 & 0 \\ 0 & 0 & 0 & 0 \end{pmatrix}, \begin{pmatrix} 0 & 0 & 0 & 0 \\ 1 & 0 & 0 & 0 \\ 0 & 0 & 0 & 0 \\ 0 & 0 & 0 & 0 \end{pmatrix}, \begin{pmatrix} 0 & 1 & 0 & 0 \\ 0 & 0 & 0 & 0 \\ 0 & 0 & 0 & 0 \\ 0 & 0 & 0 & 0 \end{pmatrix}, \begin{pmatrix} 0 & 0 & 0 & 0 \\ 0 & 1 & 0 & 0 \\ 0 & 0 & 0 & 0 \\ 0 & 0 & 0 & 0 \end{pmatrix} \\ &\begin{pmatrix} -\frac{1}{2} & 0 & 0 & 0 \\ 0 & 0 & 0 & 0 \\ \frac{3}{2} & 0 & 0 & 0 \\ 0 & 0 & 0 & 0 \end{pmatrix}, \begin{pmatrix} -\frac{1}{2} & 0 & \frac{3}{2} & 0 \\ 0 & 0 & 0 & 0 \\ 0 & 0 & 0 & 0 \\ 0 & 0 & 0 & 0 \end{pmatrix}, \begin{pmatrix} 0 & -\frac{1}{2} & 0 & 0 \\ 0 & 0 & 0 & 0 \\ 0 & \frac{3}{2} & 0 & 0 \\ 0 & 0 & 0 & 0 \end{pmatrix}, \\ &\begin{pmatrix} 0 & 0 & 0 & 0 \\ -\frac{1}{2} & 0 & \frac{3}{2} & 0 \\ 0 & 0 & 0 & 0 \\ 0 & 0 & 0 & 0 \end{pmatrix}, \begin{pmatrix} -\frac{1}{2} & 0 & 0 & 0 \\ 0 & 0 & 0 & 0 \\ 0 & 0 & 0 & 0 \\ \frac{5}{3} & 0 & 0 & 0 \end{pmatrix}, \begin{pmatrix} -\frac{1}{2} & 0 & 0 & \frac{5}{3} \\ 0 & 0 & 0 & 0 \\ 0 & 0 & 0 & 0 \\ 0 & 0 & 0 & 0 \end{pmatrix} \Bigg],\end{aligned} \tag{87}$$

where rows correspond to the parameter p_1 and columns to p_2. In any case, this is an arbitrary decision and could be the other way around.

4.4.4 Integrals of tensors

As shown in (81), the inner product between the residual and a given basis involves the integral of the product of up to three bases. Denote the three bases as Φ_a, Φ_b and Φ_c respectively. The result of the integral, represented by I, follows:

$$I = \int_{\Omega} \Phi_a(\boldsymbol{p}) \Phi_b(\boldsymbol{p}) \Phi_c(\boldsymbol{p}) d\boldsymbol{p}. \tag{88}$$

Hence, first of all, the product between the three bases has to be computed. Using the associative property:

$$\Phi_x = \Phi_a \circ (\Phi_b \circ \Phi_c). \tag{89}$$

Then, the integral is simply:

$$I = \int_{\Omega} \Phi_x(\boldsymbol{p}) d\boldsymbol{p}. \tag{90}$$

The integral is calculated over the domain Ω. Assuming the usage of Legendre polynomials, each parameter is bounded between -1 and 1. More explicitly:

$$I = \int_{-1}^{1} \int_{-1}^{1} ... \int_{-1}^{1} \Phi_x(p_1, p_2, ..., p_{N_d}) dp_1 dp_2 ... dp_{N_d}. \tag{91}$$

If the basis Φ_x is further developed:

$$I = \int_{-1}^{1} \int_{-1}^{1} ... \int_{-1}^{1} \sum_{x_1}^{|d_1|} \sum_{x_2}^{|d_2|} ... \sum_{x_{N_d}}^{|d_{N_d}|} c_{x_1, x_2, ..., x_{N_d}} p_1^{x_1} p_2^{x_2} ... p_{N_d}^{x_{N_d}} dp_1 dp_2 ... dp_{N_d}. \tag{92}$$

With this, the whole integral ends up being:

$$I = \sum_{x_1}^{|d_1|} \sum_{x_2}^{|d_2|} \dots \sum_{x_{N_d}}^{|d_{N_d}|} c_{x_1,x_2,\dots,x_{N_d}} \frac{1}{x_1+1} p_1^{x_1+1} \Big|_{-1}^{1} \frac{1}{x_2+1} p_2^{x_2+1} \Big|_{-1}^{1} \dots \frac{1}{x_{N_d}+1} p_{N_d}^{x_{N_d}+1} \Big|_{-1}^{1}, \tag{93}$$

and applying Barrow's rule:

$$I = \sum_{x_1}^{|d_1|} \sum_{x_2}^{|d_2|} \dots \sum_{x_{N_d}}^{|d_{N_d}|} c_{x_1,x_2,\dots,x_{N_d}} \frac{1}{x_1+1} \frac{1}{x_2+1} \dots \frac{1}{x_{N_d}+1} \Gamma, \tag{94}$$

where the compacted term Γ is:

$$\Gamma = \left(1-(-1)^{x_1+1}\right)\left(1-(-1)^{x_2+1}\right)\dots\left(1-(-1)^{x_{N_d}+1}\right). \tag{95}$$

Notice that if one of the indices of the form x_k is odd, then Γ will become zero. With the presence of many parameters, many integrals are likely to be zero as well. This is not an issue as such, but rather, one of the consequences of relying on Legendre polynomials.

4.4.5 Obtention of coefficients

The coefficients that represent the states of the system are the ones that satisfy (79). Let m denote the number of unknown voltages. As each voltage is splitted into a real and an imaginary part, there is a total of $2m \times N$ unknowns to compute. Here N denotes the length of $\mathbf{\Phi}$, and recall from (62) that it is equal to $(N_d+N_p)!/(N_d!N_p!)$. The structure of the vector of unknowns is:

$$\boldsymbol{x} = [c^e, c^f]^T = [c_0^{e_1}, c_1^{e_1}, ..., c_{N-1}^{e_m}, c_0^{f_1}, c_1^{f_1}, ..., c_{N-1}^{f_m}]^T, \tag{96}$$

where the superscript of the coefficients identifies the unknown state whereas the subscript indexes the term of the coefficient expansion.

Among the various options to solve the system of equations, the Newton-Raphson method is implemented. It aims to linearize a system of the form:

$$\boldsymbol{f} = \langle \boldsymbol{R}(\boldsymbol{x}, \boldsymbol{p}), \mathbf{\Phi}(\boldsymbol{p}) \rangle = 0. \tag{97}$$

In its generic form, the equation that follows has to be solved repeatedly until a small enough error (smaller than a preset tolerance ϵ) is obtained:

$$-\boldsymbol{f} = \boldsymbol{J}\boldsymbol{\Delta x}, \tag{98}$$

where $\boldsymbol{J}$ is the Jacobian matrix, and $\boldsymbol{\Delta x}$ represents the variation of the unknowns. The Jacobian $\boldsymbol{J}$ is defined as $\frac{d\boldsymbol{f}}{d\boldsymbol{x}}$. In other words, it contains the derivatives of the functions with respect to the unknowns.

Figure 29 depicts the full scheme of the algorithm. First, the bases are computed. Then, the system of equations formed by taking the inner product of the residuals with each basis is solved

with the Newton-Raphson method. Its output is the set of coefficients that identify a given unknown. Once the coefficients have been calculated, the problem is said to be parametrized. The states can be evaluated for multiple values of the parameters with a low computational effort.

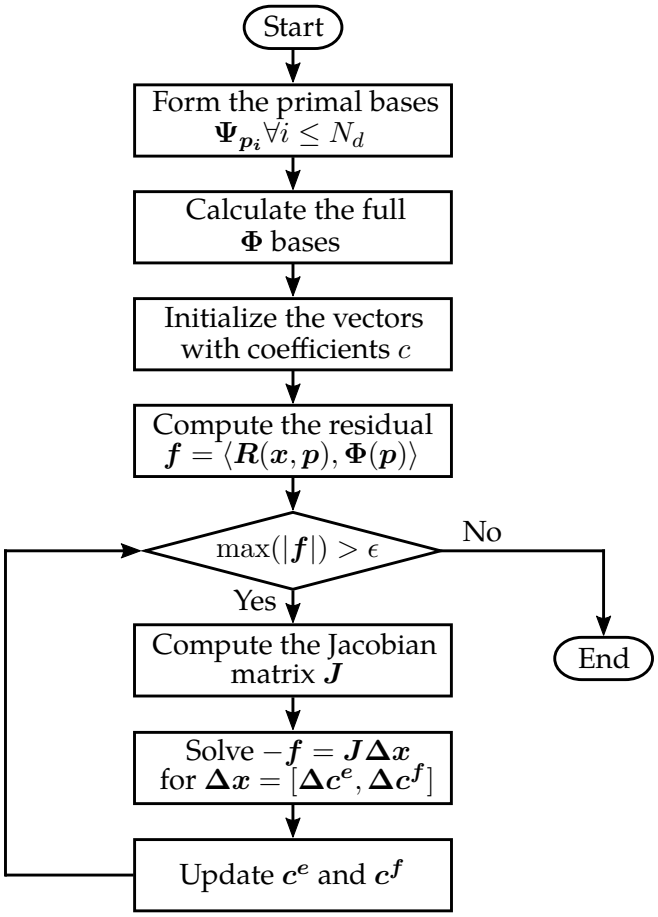

Figure 29: Process to obtain the coefficients of the states.

4.4.6 Basic example

The fundamentals of the expanded Galerkin method are exemplified in the solution of a simple equation such as:

$$R(x, p) = x^2 - p - 2 = 0, \tag{99}$$

where x is the unknown and p a parameter that takes values inside the $[-1, 1]$ range.

The solution to (99) is simply $x = \pm\sqrt{p+2}$, so there would be no point in parametrizing it. However, the power flow equations are implicit, and therefore, it is beneficial to parametrize them. Leaving aside these core differences, this simple case will be useful to show the procedure behind the expanded Galerkin.

Since there is a single parameter p, the primal basis $\mathbf{\Psi}$ coincides with the full bases $\mathbf{\Phi}$. With Legendre polynomials, assuming $N_p = 2$:

$$\mathbf{\Psi} = \mathbf{\Phi} = \left[1, p, \frac{3}{2}p^2 - \frac{1}{2}\right]. \tag{100}$$

This implies that the unknown x is given by:

$$x = c_0 + c_1 p + c_2 \left(\frac{3}{2}p^2 - \frac{1}{2}\right), \tag{101}$$

and hence the equation to solve can be further developed as:

$$\begin{aligned} R(x,p) = c_0c_0 + c_1c_1p^2 + \frac{9}{4}c_2c_2p^4 + \frac{1}{4}c_2c_2 - \frac{3}{2}c_2c_2p^2 + 2c_0c_1p \\ +3c_0c_2p^2 - c_0c_2 + 3c_1c_2p^3 - c_1c_2p - p - 2 = 0 \end{aligned} \tag{102}$$

Next, the inner product of the residual with each basis in $\mathbf{\Phi}$ has to be equal to zero. The system of equations that provides the solution is:

$$\begin{cases} \langle R(x,p), 1\rangle = 0, \\ \langle R(x,p), p\rangle = 0, \\ \langle R(x,p), (\frac{3}{2}p^2 - \frac{1}{2})\rangle = 0. \end{cases} \tag{103}$$

The inner product involves calculating the definite integral in the domain of study, in this case, between -1 and 1. To exemplify the calculation of the inner product, the operation $\langle R(x,p), 1\rangle = 0$ is developed below:

$$\begin{aligned} 0 = c_0c_0\int_{-1}^{1} dp + c_1c_1\int_{-1}^{1} p^2\cdot dp + \frac{9}{4}\int_{-1}^{1} p^4\cdot dp + \frac{1}{4}c_2c_2\int_{-1}^{1} dp \\ -\frac{3}{2}c_2c_2\int_{-1}^{1} p^2\cdot dp + 2c_0c_1\int_{-1}^{1} p\cdot dp + 3c_0c_2\int_{-1}^{1} p^2\cdot dp - c_0c_2\int_{-1}^{1} dp \\ +3c_1c_2\int_{-1}^{1} p^3\cdot dp - c_1c_2\int_{-1}^{1} p\cdot dp - \int_{-1}^{1} p\cdot dp - 2\int_{-1}^{1} dp. \end{aligned} \tag{104}$$

Notice that the coefficients leave the integral. This way, the integrals simply behave as scalar factors. Computing the inner products results in the transformation of (103) into:

$$\begin{cases} 2c_0c_0 + \frac{2}{3}c_1c_1 + \frac{4}{10}c_2c_2 - 4 = 0, \\ \frac{4}{3}c_0c_1 + \frac{8}{15}c_1c_2 - \frac{2}{3} = 0, \\ \frac{4}{15}c_1c_2 + \frac{4}{35}c_2c_2 + \frac{4}{5}c_0c_2 = 0. \end{cases} \tag{105}$$

The application of the Newton-Rapshon method in solving (105) yields the solution:

$$[c_0, c_1, c_2] = [1.39873, 0.36067, -0.03110]. \tag{106}$$

Figure 30 depicts the curve obtained with the parametrization and the actual solution. Notice that only the positive solution to (99) is obtained. This has to do with the initialization of the coefficients. While the parametrized solution does not exactly match the desired value, the mean relative error is found to be 0.12%. Visually speaking the difference is hard to perceive as both curves overlap.

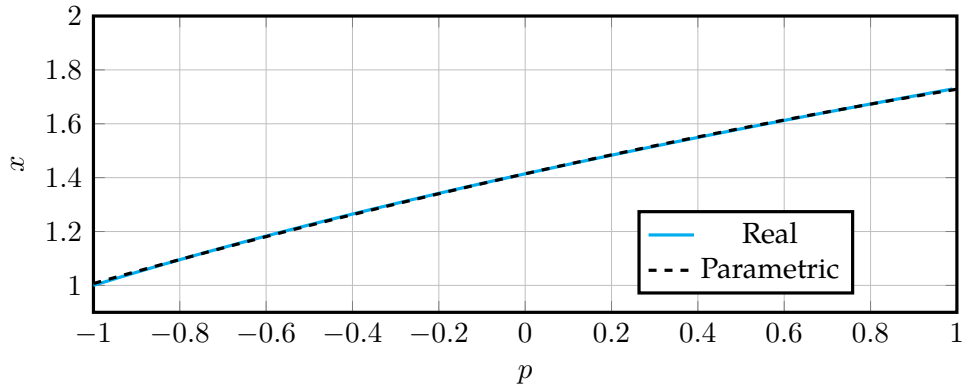

Figure 30: Comparison of the real and parametrized solution to $x = \sqrt{p+2}$ for $N_p = 2$.

According to Weierstrass approximation theorem, this error is meant to be improved the larger N_p becomes [88]. Table 19 displays the mean relative error for various N_p values, showing that Weierstrass approximation theorem is validated.

Table 19: Mean relative error as a function of the order of the polynomial for $x = \sqrt{p+2}$.

N_p	Mean relative error
1	$9.21 \cdot 10^{-3}$
2	$1.24 \cdot 10^{-3}$
3	$2.08 \cdot 10^{-4}$
4	$3.91 \cdot 10^{-5}$
5	$7.86 \cdot 10^{-6}$

4.4.7 Two-bus system

The same two-bus system shown in Figure 26, whose values are captured in Table 17, is solved with the fully expanded Galerkin method. The employed methodology is the one described in Figure 29, where the set of equations is solved with the Newton-Raphson method. While this approach tends to be reliable, it is crucial to initialize the arrays of coefficients c^e and c^f appropriately. As the voltage at the slack bus is set to $1.0 + 0.0j$, e should not differ much from 1.0 whereas f should be close to 0.0. Hence, $c_0^e = 1.0$, while the rest of the coefficients are initialized at 0. Similarly as before, the absolute current error is plotted in Figure 31 as a function of the parameters p and q.

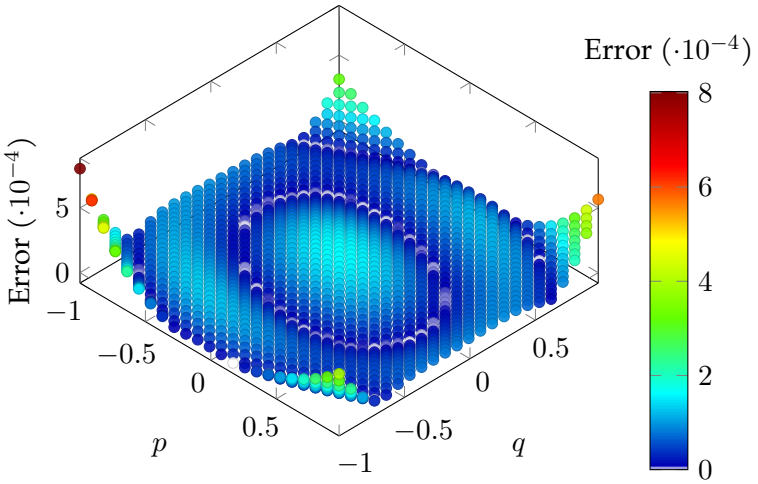

Figure 31: Representation of the absolute current error as a function of the parametrized powers with the expanded Galerkin for $N_p = 3$ applied to a two-bus system.

The error is usually in the order of $1 \cdot 10^{-4}$ pu. It increases when the parameters take extreme values, yet it is much more acceptable than the error obtained with the decoupled Galerkin represented in Figure 27. As a summary, the expanded Galerkin is significantly more accurate as it is guaranteed to provide the optimal polynomial given orthogonal bases. This does not imply that the error will be null, but it ensures the obtention of the best possible polynomial representation. On the other side, the computational scalability of the method is worse. Contrarily to the parametric power flow computed with sampling, here the parameters should be limited to a few.

4.4.8 Generalized algorithm

This section covers the generalized formulation of the extended Galerkin to be applied in real-life grids. The rectangular power flow is employed as it becomes simpler to calculate the integrals. Consider the well-known equations of the power flow problem for PQ and PV buses [89]:

$$\begin{cases} P_i = \sum_k \left[G_{ik}e_ie_k + G_{ik}f_if_k - B_{ik}e_if_k + B_{ik}e_kf_i\right] & \forall i \in \text{PQ} \cup \text{PV}, \\ -Q_i = \sum_k \left[G_{ik}e_if_k - G_{ik}e_kf_i + B_{ik}e_ie_k + B_{ik}f_if_k\right] & \forall i \in \text{PQ}, \\ V_i^2 = e_ie_i + f_if_i & \forall i \in \text{PV}, \end{cases} \tag{107}$$

where G_{ik} and B_{ik} represent the real and imaginary components of the (i,k) term of the bus admittance matrix, i is an index that identifies the bus under consideration, and k is an index that goes over all buses, including i.

The development of (107) taking into consideration the representation of unknowns as polyno-

mials yields the following residuals:

$$\begin{cases} R_i^p = \sum_k \Big[G_{ik} \sum_r c_r^{e_i} \Phi_r \sum_m c_m^{e_k} \Phi_m + G_{ik} \sum_r c_r^{f_i} \Phi_r \sum_m c_m^{f_k} \Phi_m \\ -B_{ik} \sum_r c_r^{e_i} \Phi_r \sum_m c_m^{f_k} \Phi_m + B_{ik} \sum_r c_r^{e_k} \Phi_r \sum_m c_m^{f_i} \Phi_m \Big] - \sum_r c_r^{p_i} \Phi_r, \\ R_i^q = \sum_k \Big[G_{ik} \sum_r c_r^{e_i} \Phi_r \sum_m c_m^{f_k} \Phi_m - G_{ik} \sum_r c_r^{e_k} \Phi_r \sum_m c_m^{f_i} \Phi_m \\ +B_{ik} \sum_r c_r^{e_i} \Phi_r \sum_m c_m^{e_k} \Phi_m + B_{ik} \sum_r c_r^{f_i} \Phi_r \sum_m c_m^{f_k} \Phi_m \Big] + \sum_r c_r^{q_i} \Phi_r, \\ R_i^v = \sum_r c_r^{e_i} \Phi_r \sum_m c_m^{e_i} \Phi_m + \sum_r c_r^{f_i} \Phi_r \sum_m c_m^{f_i} \Phi_m - V_i^2. \end{cases} \tag{108}$$

Notice the powers are parametrized via coefficients of the form c^{p_i} and c^{q_i}, while the voltage at PV buses is treated as a set value, hence as a constant.

To formulate the Galerkin equations, the inner product between the residuals in (108) and the bases $\mathbf{\Phi}$ has to be computed. When expanded, the equations to solve are as follows. For the active power, the inner product $f_{i,x}^p = \langle R_i^p, \Phi_x \rangle = 0$ becomes:

$$\begin{aligned} f_{i,x}^p = \sum_k \Big[& G_{ik} \sum_r \sum_m c_r^{e_i} c_m^{e_k} \int_\Omega \Phi_r \Phi_m \Phi_x d\boldsymbol{p} + G_{ik} \sum_r \sum_m c_r^{f_i} c_m^{f_k} \int_\Omega \Phi_r \Phi_m \Phi_x d\boldsymbol{p} \\ & - B_{ik} \sum_r \sum_m c_r^{e_i} c_m^{f_k} \int_\Omega \Phi_r \Phi_m \Phi_x d\boldsymbol{p} + B_{ik} \sum_r \sum_m c_r^{e_k} c_m^{f_i} \int_\Omega \Phi_r \Phi_m \Phi_x d\boldsymbol{p} \Big] \\ & - \sum_r c_r^{p_i} \int_\Omega \Phi_r \Phi_x d\boldsymbol{p}. \end{aligned} \tag{109}$$

Similarly, for the reactive power equation:

$$\begin{aligned} f_{i,x}^q = \sum_k \Big[& G_{ik} \sum_r \sum_m c_r^{e_i} c_m^{f_k} \int_\Omega \Phi_r \Phi_m \Phi_x d\boldsymbol{p} - G_{ik} \sum_r \sum_m c_r^{e_k} c_m^{f_i} \int_\Omega \Phi_r \Phi_m \Phi_x d\boldsymbol{p} \\ & + B_{ik} \sum_r \sum_m c_r^{e_i} c_m^{e_k} \int_\Omega \Phi_r \Phi_m \Phi_x d\boldsymbol{p} + B_{ik} \sum_r \sum_k c_r^{f_i} c_m^{f_k} \int_\Omega \Phi_r \Phi_m \Phi_x d\boldsymbol{p} \Big] \\ & + \sum_r c_r^{q_i} \int_\Omega \Phi_r \Phi_x d\boldsymbol{p}. \end{aligned} \tag{110}$$

For the residuals of voltage at the PV buses:

$$f_{i,x}^v = \sum_r \sum_m c_r^{e_i} c_m^{e_i} \int_\Omega \Phi_r \Phi_m \Phi_x d\boldsymbol{p} + \sum_r \sum_m c_r^{f_i} c_m^{f_i} \int_\Omega \Phi_r \Phi_m \Phi_x d\boldsymbol{p} - V_i^2 \int_\Omega \Phi_x d\boldsymbol{p}. \tag{111}$$

The slack bus voltage, which is part of the input data, can be represented by a polynomial whose terms are known. In fact, all its terms are null except for the one multiplying the basis $\Phi = 1$.

The structure of the Newton-Raphson method applied to the expanded Galerkin power flow is given by:

$$\begin{pmatrix} \boldsymbol{f_p} \\ \boldsymbol{f_q} \\ \boldsymbol{f_v} \end{pmatrix} = - \begin{pmatrix} \frac{d\boldsymbol{f_p}}{d\boldsymbol{c^e}} & \frac{d\boldsymbol{f_p}}{d\boldsymbol{c^f}} \\ \frac{d\boldsymbol{f_q}}{d\boldsymbol{c^e}} & \frac{d\boldsymbol{f_q}}{d\boldsymbol{c^f}} \\ \frac{d\boldsymbol{f_v}}{d\boldsymbol{c^e}} & \frac{d\boldsymbol{f_v}}{d\boldsymbol{c^f}} \end{pmatrix} \begin{pmatrix} \Delta \boldsymbol{c^e} \\ \Delta \boldsymbol{c^f} \end{pmatrix}, \tag{112}$$

where $\boldsymbol{c^e}$ and $\boldsymbol{c^f}$ both exclude the slack bus as it is not an unknown. More compactly, (112) turns out to be:

$$\begin{pmatrix} \boldsymbol{f_p} \\ \boldsymbol{f_q} \\ \boldsymbol{f_v} \end{pmatrix} = - \begin{pmatrix} \boldsymbol{J1} & \boldsymbol{J2} \\ \boldsymbol{J3} & \boldsymbol{J4} \\ \boldsymbol{J5} & \boldsymbol{J6} \end{pmatrix} \begin{pmatrix} \Delta \boldsymbol{c^e} \\ \Delta \boldsymbol{c^f} \end{pmatrix}. \tag{113}$$

Note that $\boldsymbol{c^e}$ and $\boldsymbol{c^f}$ contain the terms for all PQ and PV buses. The chosen order is the following:

$$\boldsymbol{c^e} = [\underbrace{c_0^{e_0}, c_1^{e_0}, ..., c_{N-1}^{e_0}}_{\text{bus } 0}, \underbrace{c_0^{e_1}, c_1^{e_1}, ..., c_{N-1}^{e_1}}_{\text{bus } 1}, ..., \underbrace{c_0^{e_w}, c_1^{e_w}, ..., c_{N-1}^{e_w}}_{\text{bus } w}], \tag{114}$$

where $w+1$ is the number of non-slack buses. The same structure shown in (114) applies to $\boldsymbol{c^f}$.

The submatrices from $\boldsymbol{J1}$ to $\boldsymbol{J6}$ compose the full Jacobian matrix. They are calculated as:

$$\boldsymbol{J1} = \begin{cases} \frac{df_{i,x}^p}{dc_z^{e_y}} = G_{iy} \sum_r c_r^{e_i} \int_\Omega \Phi_r \Phi_z \Phi_x d\boldsymbol{p} + B_{iy} \sum_r c_r^{f_i} \int_\Omega \Phi_r \Phi_z \Phi_x d\boldsymbol{p} & \text{if } y \neq i, \\ \frac{df_{i,x}^p}{dc_z^{e_y}} = \sum_{k \neq i} G_{ik} \sum_r c_r^{e_k} \int_\Omega \Phi_r \Phi_z \Phi_x d\boldsymbol{p} - \sum_k B_{ik} \sum_r c_r^{f_k} \int_\Omega \Phi_r \Phi_z \Phi_x d\boldsymbol{p} & \\ +2G_{ii} \sum_r c_r^{e_i} \int_\Omega \Phi_r \Phi_z \Phi_x d\boldsymbol{p} + B_{ii} \sum_r c_r^{f_i} \int_\Omega \Phi_r \Phi_z \Phi_x d\boldsymbol{p} & \text{if } y = i. \end{cases} \tag{115}$$

$$\boldsymbol{J2} = \begin{cases} \frac{df_{i,x}^p}{dc_z^{f_y}} = G_{iy} \sum_r c_r^{f_i} \int_\Omega \Phi_r \Phi_z \Phi_x d\boldsymbol{p} - B_{iy} \sum_r c_r^{e_i} \int_\Omega \Phi_r \Phi_z \Phi_x d\boldsymbol{p} & \text{if } y \neq i, \\ \frac{df_{i,x}^p}{dc_z^{f_y}} = \sum_{k \neq i} G_{ik} \sum_r c_r^{f_k} \int_\Omega \Phi_r \Phi_z \Phi_x d\boldsymbol{p} + \sum_k B_{ik} \sum_r c_r^{e_k} \int_\Omega \Phi_r \Phi_z \Phi_x d\boldsymbol{p} & \\ +2G_{ii} \sum_r c_r^{f_i} \int_\Omega \Phi_r \Phi_z \Phi_x d\boldsymbol{p} - B_{ii} \sum_r c_r^{e_i} \int_\Omega \Phi_r \Phi_z \Phi_x d\boldsymbol{p} & \text{if } y = i. \end{cases} \tag{116}$$

$$\boldsymbol{J3} = \begin{cases} \frac{df_{i,x}^q}{dc_z^{e_y}} = B_{iy} \sum_r c_r^{e_i} \int_\Omega \Phi_r \Phi_z \Phi_x d\boldsymbol{p} - G_{iy} \sum_r c_r^{f_i} \int_\Omega \Phi_r \Phi_z \Phi_x d\boldsymbol{p} & \text{if } y \neq i, \\ \frac{df_{i,x}^q}{dc_z^{e_y}} = \sum_{k \neq i} B_{ik} \sum_r c_r^{e_k} \int_\Omega \Phi_r \Phi_z \Phi_x d\boldsymbol{p} + \sum_k G_{ik} \sum_r c_r^{f_k} \int_\Omega \Phi_r \Phi_z \Phi_x d\boldsymbol{p} & \\ +2B_{ii} \sum_r c_r^{e_i} \int_\Omega \Phi_r \Phi_z \Phi_x d\boldsymbol{p} - G_{ii} \sum_r c_r^{f_i} \int_\Omega \Phi_r \Phi_z \Phi_x d\boldsymbol{p} & \text{if } y = i. \end{cases} \tag{117}$$

$$\boldsymbol{J4} = \begin{cases} \frac{df_{i,x}^q}{dc_z^{f_y}} = G_{iy} \sum_r c_r^{e_i} \int_\Omega \Phi_r \Phi_z \Phi_x d\boldsymbol{p} + B_{iy} \sum_r c_r^{f_i} \int_\Omega \Phi_r \Phi_z \Phi_x d\boldsymbol{p} & \text{if } y \neq i, \\ \frac{df_{i,x}^q}{dc_z^{f_y}} = \sum_{k \neq i} B_{ik} \sum_r c_r^{f_k} \int_\Omega \Phi_r \Phi_z \Phi_x d\boldsymbol{p} - \sum_k G_{ik} \sum_r c_r^{e_k} \int_\Omega \Phi_r \Phi_z \Phi_x d\boldsymbol{p} & \\ +2B_{ii} \sum_r c_r^{f_i} \int_\Omega \Phi_r \Phi_z \Phi_x d\boldsymbol{p} + G_{ii} \sum_r c_r^{e_i} \int_\Omega \Phi_r \Phi_z \Phi_x d\boldsymbol{p} & \text{if } y = i. \end{cases} \tag{118}$$

$$\boldsymbol{J5} = \begin{cases} \frac{df_{i,x}^v}{dc_z^{e_y}} = 0 & \text{if } y \neq i, \\ \frac{df_{i,x}^v}{dc_z^{e_y}} = 2 \sum_r c_r^{e_i} \int_\Omega \Phi_r \Phi_z \Phi_x d\boldsymbol{p} & \text{if } y = i. \end{cases} \tag{119}$$

$$\boldsymbol{J6} = \begin{cases} \frac{df_{i,x}^v}{dc_z^{f_y}} = 0 & \text{if } y \neq i, \\ \frac{df_{i,x}^v}{dc_z^{f_y}} = 2 \sum_r c_r^{f_i} \int_\Omega \Phi_r \Phi_z \Phi_x d\boldsymbol{p} & \text{if } y = i. \end{cases} \tag{120}$$

The Jacobian matrices can also be computed with differences [90]. This approach is arguably simpler but sacrifices speed in the calculations. Following the definition of a derivative, the terms of $\boldsymbol{J1}$ are found with:

$$\frac{df_{i,x}^p}{dc_z^{e_y}} = \frac{f_{i,x}^p(c_z^{e_y} + \delta) - f_{i,x}^p(c_z^{e_y})}{\delta}. \tag{121}$$

where δ represents a small difference ($1 \cdot 10^{-10}$ for instance). The same procedure is analogously applied to the rest of the submatrices from $\boldsymbol{J2}$ to $\boldsymbol{J6}$.

The process as such, with the main steps to follow, is summarized in Algorithm 5.

Algorithm 5: Procedure to solve the expanded Galerkin applied to the power flow.

Data: $\boldsymbol{Y}_{\text{bus}}$, $\boldsymbol{S}_{\text{bus}}$, $\boldsymbol{V}_{\text{bus}}$, ϵ, N_p, $\boldsymbol{p}$, pq and pv buses
Result: Set of coefficients $\mathbf{c^e}$ and $\mathbf{c^f}$
$\boldsymbol{G}_{\text{bus}} \leftarrow \Re(\boldsymbol{Y}_{\text{bus}})$; $\boldsymbol{B}_{\text{bus}} \leftarrow \Im(\boldsymbol{Y}_{\text{bus}})$;
$\boldsymbol{\Phi} \leftarrow \text{g}(\boldsymbol{p}, N_p)$;
Initialize $\boldsymbol{c^e} \leftarrow \mathbf{0}$, $\boldsymbol{c^f} \leftarrow \mathbf{0}$, $\boldsymbol{c_0^e} \leftarrow \mathbf{1}$;
Compute $\boldsymbol{f^p}$, $\boldsymbol{f^q}$ and $\boldsymbol{f^v}$ with (109), (110) and (111) ;
while $\max(|\boldsymbol{f^p}|, |\boldsymbol{f^q}|, |\boldsymbol{f^v}|) > \epsilon$ **do**
  Calculate $\boldsymbol{J}$ with (115) up to (120) ;
  $[\Delta \boldsymbol{c^e}, \Delta \boldsymbol{c^f}] \leftarrow \text{-}\boldsymbol{J^{-1}}[\boldsymbol{f^p}, \boldsymbol{f^q}, \boldsymbol{f^v}]$;
  $\boldsymbol{c^e} \leftarrow \boldsymbol{c^e} + \Delta \boldsymbol{c^e}$, $\boldsymbol{c^f} \leftarrow \boldsymbol{c^f} + \Delta \boldsymbol{c^f}$;
  Update $\boldsymbol{f^p}$, $\boldsymbol{f^q}$ and $\boldsymbol{f^v}$ with (109), (110) and (111) ;
end

The algorithm starts with passing the data such as the admittance matrix, the vector of powers, the vector of voltages, the classification of buses, the parameters stored in $\boldsymbol{p}$, the desired order of the polynomials N_p, and the tolerance ϵ. Then, the admittance matrix is split into its real and imaginary parts. The full bases $\boldsymbol{\Phi}$ are formed with the so-called function g, which fundamentally comes from the application of (83). The voltages of PQ and PV buses are supposed to not be far from the slack bus voltage. Hence, it is a good practice to initialize all the coefficients to 0 except for the first order coefficients of $\boldsymbol{c^e}$, as they should be close to 1 pu. This aids substantially in reaching convergence in the Newton-Raphson algorithm that follows. The iterations stop once the error is small enough. At this stage, the system of Galerkin equations is said to be solved, and with this the coefficients $\boldsymbol{c^e}$ and $\boldsymbol{c^f}$.

4.4.9 Results in a standardized grid

The generalized algorithm is applied to a well-known standardized grid such as the IEEE 14-bus system. The goal is to show that the Galerkin method can be extended to more complex systems than two-bus grids while retaining its accuracy. Figure 32 shows the topology of the grid, where the active power in bus 4 and the reactive power in bus 5 are treated as parameters. The input data are extracted from [91].

Figure 33 illustrates the maximum power error in all buses as a function of the two parameters. Just as it happened in the two-bus case, larger errors appear to be in the extremes. This is a consequence of employing the Galerkin method, as it is concerned with minimizing the error

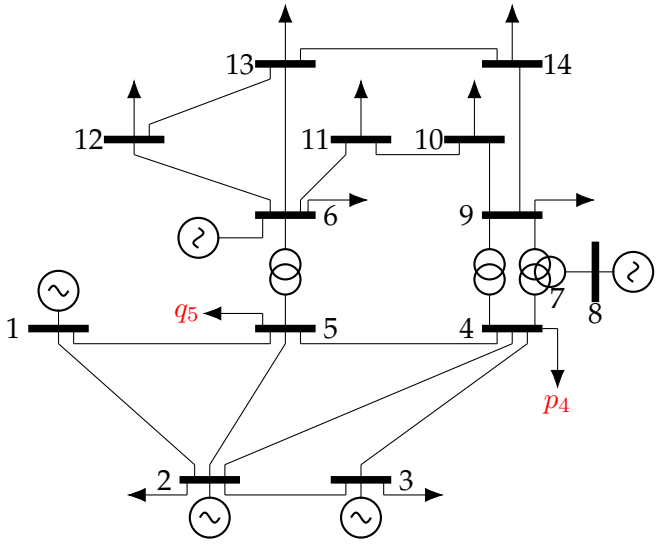

Figure 32: Scheme of the IEEE 14-bus system, where the parameters are marked in red. Adapted from [92].

over the full integration space Ω.

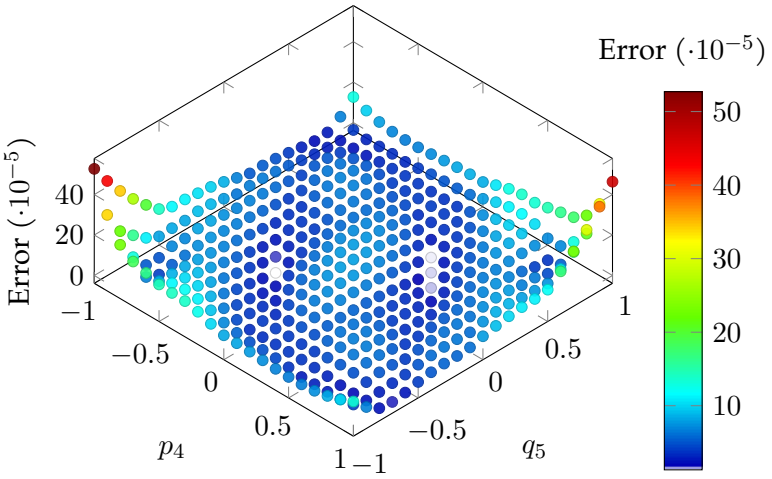

Figure 33: Representation of the maximum power error as a function of the parametrized powers with the expanded Galerkin for $N_p = 3$ applied to the IEEE 14-bus system.

The beauty of the expanded Galerkin is found in the capability of parametrizing the unknowns considering whatever the number of parameters is. In other words, its usage is not restricted to only two parameters, Even if the results shown are extracted assuming only two powers are parameters, the program has been successfully tested for a greater number of parameters. The downside of the expanded Galerkin method is the fact that it suffers from the curse of dimensionality. It is recommended to operate with 5 parameters at most, as otherwise the computational effort and subsequent time are extremely high.

As an example, the coefficients of the voltage at bus 7 are captured in Table 20.

Table 20: Voltage coefficients for the voltage at bus 7 of the IEEE 14-bus system.

Φ	c^{e_7}	c^{f_7}
1	1.036E+00	-2.226E-01
q_5	1.058E-02	-5.884E-03
$\frac{3}{2}q_5^2 - \frac{1}{2}$	-4.234E-04	-3.275E-04
$\frac{5}{2}q_5^3 - \frac{3}{2}q_5$	2.087E-05	1.918E-05
p_4	2.920E-02	9.972E-02
$p_4 q_5$	-2.885E-04	-1.568E-03
$p_4(\frac{3}{2}q_5^2 - \frac{1}{2})$	7.768E-05	8.773E-05
$\frac{3}{2}p_4^2 - \frac{1}{2}$	-4.043E-03	-4.588E-04
$q_5(\frac{3}{2}p_4^2 - \frac{1}{2})$	2.004E-04	7.048E-05
$\frac{5}{2}p_4^3 - \frac{3}{2}p_4$	1.054E-04	-1.640E-05

Notice that the real and imaginary coefficients for $\Phi = 1$ may very well represent the solution to the power flow in a base case. That is, $c_0^{e_7}$ is close to the slack voltage and $c_0^{f_7}$ takes a small negative value, typical in inductive power systems. The rest of the coefficients are significantly smaller and represent the influence of the parametrized powers on the solution. This is a pattern that repeats for the other buses, just as expected.

A simple test to check the validity of the solution has been performed. The active power injection p_4 has been set to 0 while the reactive power injection q_5 is swept. The voltage magnitude V_7 is obtained by substituting into the extracted polynomial, and also with a conventional power flow solver such as GridCal. Figure 34 plots the variation it experiences as a function of q_5.

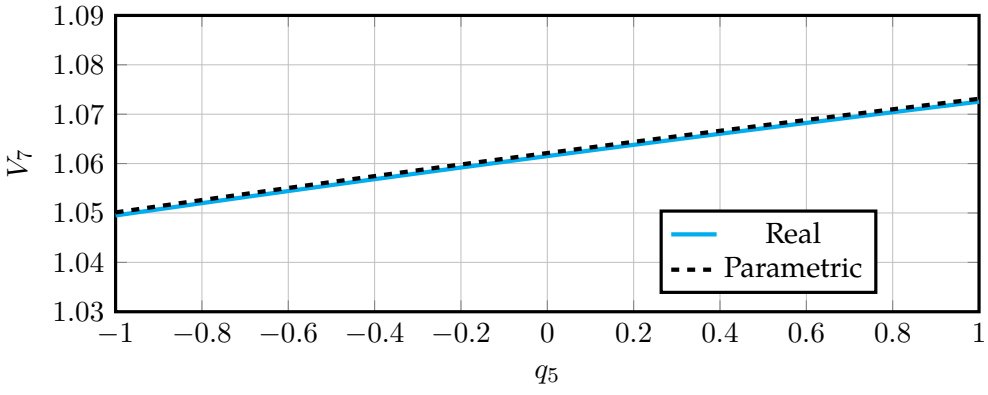

Figure 34: Comparison of the real and parametrized solution for V_7 in the IEEE 14-bus system with a varying q_5 and $p_4 = 0$.

Both curves follow the same pattern, i.e., V_7 increases the higher the reactive power injection becomes. The results make physical sense as it is well-known that reactive power injections boost

the voltage in inductive systems. Although the curves are not exactly the same, they tend to overlap. This is expectable with an overall error in the order of $1 \cdot 10^{-4}$. In any case, the extended Galerkin can capture the solution with acceptable accuracy.

4.5 Conclusion

The mathematical concepts behind the Galerkin method have been covered. It has been shown that the decoupled Galerkin approach is relatively simple and less complex than the expanded Galerkin method. However, its error may turn out to be unacceptable. By contrast, the expanded Galerkin requires an elaborated formulation for generic cases. Part of the contribution from this chapter details the formation of bases and operations of tensors. A general algorithm that can be used for any realistic grid has been presented. Regarding the results, the expanded Galerkin permits obtaining highly accurate solutions despite the complexity. For these reasons, it can become useful to study grids in an offline manner. The polynomials can be precomputed and then employed for crossing scenarios, for instance, in the design phase of a system.

5 Efficient parametric power flow techniques

5.1 Introduction

It is a well-known fact that the power flow in power systems is represented by non-linear equations. Multiple solvers have been applied during these past decades. Some of them have been intentionally created for such purpose, while others are based on common numerical methods, being the Newton-Raphson the most popular. At their core, all these solvers are intended to be used with deterministic input data, that is, they leave no room for variation. If an input changes, the power flow has to be recalculated. With this conventional approach, given a power system where there are m uncertain parameters and each of them takes n values, the solver would have to be called n^m times in order to extract all solutions. Thus, an increase in the number of parameters involves a meteoric rise in the computational effort, which is most likely unjustified. Parametrization solve this issue, but it is crucial to be fast. Efficient techniques are required to provide satisfactory solutions to the parametric power flow.

Efficient approaches sacrifice a bit of precision compared to the Galerkin method in order to obtain a satisfactory approximation, much more computationally efficient. The parametric power flow has been implemented in conjunction with an optimal power flow formulation [93], yet for the most part, it has remained an unexplored methodology. García-Blanco et al. have formulated the so-called Proper Generalized Decomposition, which manages to obtain all n^m solutions reasonably fast and accurately [94], [95]. Nevertheless, the methodology is not scalable. It is tied to a traditional power system formed by PQ buses and a single slack bus. There are workarounds to add PV buses but they are prone to cause divergence. Thus, as power systems tend to incorporate controllable power electronic devices, there is little relevance to this technique. A much more appealing methodology, formulated by Shen et al., approaches the problem from a statistical standpoint [96]. The method is capable of compacting the parameters, hence being substantially more efficient.

This chapter presents an efficient formulation of the parametric power flow and justifies how dimensions can be reduced. Then, a basic 5-bus system is tackled to exemplify the methodology. In addition, an optimization problem is solved with the aid of the parametric power flow. Some thoughts on the implications of this technique are also verbalized. Finally, conclusions are extracted along with the conceptualization of potential research ideas.

5.2 Proper Generalized Decomposition

The Proper Generalized Decomposition (PGD) is a technique to efficiently solve a multidimensional problem. It relies on progressive enrichments performed not on each individual case of the problem, but on the structure of the problem as a whole [97], [98]. The outcome of the PGD becomes a potentially well-refined solution for various scenarios that have not been computed

directly. Indeed, this comes with an associated saving of time. Backed by its mathematical proof, the notation is presented, along with a practical algorithm overview.

It is a well-known fact that the power flow problem is mainly concerned with four magnitudes: voltages denoted by $\boldsymbol{V}$, currents represented by $\boldsymbol{I}$, complex powers given by $\boldsymbol{S}$ and the bus admittance matrix $\boldsymbol{Y}$. The usage of bold variables indicates that these are multidimensional objects.

The first novelty of the PGD has to do with its tensorial representation. This arises from the crossing of multiple vectors, each describing a dimension of the form:

$$\boldsymbol{Z}(\boldsymbol{x}, \boldsymbol{t}, \boldsymbol{p_1}, \boldsymbol{p_2}, ..., \boldsymbol{p_D}) = \sum_{i=1}^{n} X(\boldsymbol{x}) \otimes T(\boldsymbol{t}) \otimes P_1(\boldsymbol{p_1}) \otimes P_2(\boldsymbol{p_2}) \otimes ... \otimes P_D(\boldsymbol{p_D}) \,, \tag{122}$$

where $\boldsymbol{Z}$ represents either $\boldsymbol{V}$, $\boldsymbol{I}$ or $\boldsymbol{S}$. Note the dependence on position ($\boldsymbol{x}$), time ($\boldsymbol{t}$) and the parameters meant to change ($\boldsymbol{p_1}$ to $\boldsymbol{p_D}$). In the power flow problem, $\boldsymbol{x}$ stands for the indices attributed to the buses while the parameters can be for instance variations in power in several buses. Changes in impedance could also be parametrized, although it is not clear how the PGD should be adapted to it. Notice also that the final tensor is the result of the sum of multiple tensors with the same dimensions. One tensor could represent the predicted stationary power, while another one could stand for the variations we introduce, for instance.

Recall that by definition solving the power flow means finding the solution to:

$$\boldsymbol{Y}\boldsymbol{V} = \frac{\boldsymbol{S}^*}{\boldsymbol{V}^*} \,, \tag{123}$$

where $\boldsymbol{V}$ is unknown. Considering the presence of a slack bus, where the voltage is already known and its current injection to the rest of the buses is symbolized by $\boldsymbol{I_0}$, (123) becomes:

$$\boldsymbol{Y}\boldsymbol{V} = \boldsymbol{I_0} + \frac{\boldsymbol{S}^*}{\boldsymbol{V}^*} \,. \tag{124}$$

which translates into the following in compact form:

$$\boldsymbol{V} = \boldsymbol{Y}^{-1}(\boldsymbol{I_0} + \boldsymbol{S}^* \oslash \boldsymbol{V}) \,, \tag{125}$$

where $\oslash$ denotes the Hadamard division, that is, the element-wise division. As described in [99], the power flow problem can be solved with the so-called alternating search directions (ASD) method. This has the advantage of combining quite adequately with the PGD methodology due to its speed, but mainly, because of the linear relationship between voltages and currents during one of the two steps in which the PGD is divided.

The first of the mentioned two-step process is the non-linear connection between voltages and currents:

$$\boldsymbol{I} = \boldsymbol{S}^* \oslash \boldsymbol{V}^{*[\gamma]} \,. \tag{126}$$

where γ indicates the outer loop iteration number. Here the variables are in fact tensors. Note that the traditional way to solve (126) would be to compute all the cases, one by one. However, this is not beneficial and it is not the point of the PGD. In fact, the PGD circumvents this problem.

The second step to perform is described by:

$$\boldsymbol{V}^{[\gamma+1]} = \boldsymbol{Y}^{-1}(\boldsymbol{I} + \boldsymbol{I_0}) \, . \tag{127}$$

The procedure consists of first computing $\boldsymbol{I}$ from (126) using the PGD method. Once this is done, the tensor $\boldsymbol{V}$ is meant to be updated. In the end, $\boldsymbol{V}$ follows the same structure as $\boldsymbol{I}$ because they are related by a linear transformation, which saves computational time.

The complexity of solving this problem lies in (126). The second step given by (127) is direct. Recall that the tensor $\boldsymbol{Z}$ shown in (122) represents in a general form $\boldsymbol{S}$, $\boldsymbol{V}$ and $\boldsymbol{I}$. The redefinition of $\boldsymbol{I}$ is:

$$\boldsymbol{I} = \sum_{i=1}^{n-1} \boldsymbol{i_1} \otimes \boldsymbol{i_2} \otimes ... \otimes \boldsymbol{i_D} + \boldsymbol{R_1} \otimes ... \otimes \boldsymbol{R_D} \, . \tag{128}$$

The so-called test field is introduced as follows:

$$\boldsymbol{u} = \boldsymbol{R_1^*} \otimes \boldsymbol{R_2} \otimes ... \otimes \boldsymbol{R_D} + ... + \boldsymbol{R_1} \otimes \boldsymbol{R_2} \otimes ... \otimes \boldsymbol{R_D^*} \, . \tag{129}$$

The compact system of equations to solve becomes:

$$\boldsymbol{u^T V^* I} = \boldsymbol{u^T S^*}. \tag{130}$$

At this stage, a greedy algorithm is implemented [100]. This technique serves the purpose to find the multiple $\boldsymbol{R_i^{[\Gamma]}}$ for $i = 1, ..., D$, where Γ represents the iteration number of the most inner loop. This way, there are three loops. The outer one is the ASD as such, that is, the algorithm responsible for solving the power flow problem. The intermediate one deals with finding the residues at every superposition of the $\boldsymbol{I}$ tensor. To do so, the last and most inner loop is the one that goes over the several Γ indices to iterate and find convenient residues. This can be summarized by:

- Outer loop: iterate on γ to solve the power flow as such.
- Intermediate loop: iterate on i to find the superposition of terms of the $\boldsymbol{I}$ tensor.
- Inner loop: iterate on Γ to find the residues $\boldsymbol{R_k^\Gamma}$ $\forall k \in [1, ..., D]$.

Once all residuals k are found, an inner iteration Γ is said to be finished. The residuals are computed from the previously known residues, which are also going to be updated. In essence, this replicates the Gauss-Seidel method. It is recommended to iterate several times in this inner loop to refine the solution. Usually, around 10 to 20 times is more than enough. The same applies to the intermediate loop, where the number of iterations can change at each step according to

the necessities [99]. Once $\boldsymbol{I}$ is fully built, the voltages are updated and the iteration procedure continues until a satisfactory solution has been generated.

The steps involved in the PGD are schematically shown in Algorithm 6 for a generic case with arbitrary parameters.

Algorithm 6: Procedure to solve the PGD.

Data: N_γ, n, N_Γ, $\boldsymbol{S}$, $\boldsymbol{V}^{[0]}$, $\boldsymbol{I_0}$, $\boldsymbol{Y}$
Result: Fully updated tensor $\boldsymbol{V}$
for $\gamma \leftarrow 1$ **to** N_γ **do**
  Calculate the power side of the problem with PGD: $\boldsymbol{I} = \boldsymbol{S^*} \oslash \boldsymbol{V^{*[\gamma]}}$;
  for $i \leftarrow 1$ **to** $n-1$ **do**
    Define $\boldsymbol{I} = \sum_{i=1}^{n-1} \boldsymbol{P_1^{(i)}} \otimes \boldsymbol{P_2^{(i)}} \otimes ... \otimes \boldsymbol{P_D^{(i)}} + \boldsymbol{P_1^{(n)}} \otimes \boldsymbol{P_2^{(n)}} \otimes ... \otimes \boldsymbol{P_D^{(n)}}$;
    for $\Gamma \leftarrow 1$ **to** N_Γ **do**
      Compute $\boldsymbol{P_1^{(n)[\Gamma+1]}}$ with $\boldsymbol{P_2^{(n)[\Gamma]}}$,...,$\boldsymbol{P_D^{(n)[\Gamma]}}$;
      Compute $\boldsymbol{P_2^{(n)[\Gamma+1]}}$ with $\boldsymbol{P_1^{(n)[\Gamma+1]}}$ and $\boldsymbol{P_3^{(n)[\Gamma]}}$,...,$\boldsymbol{P_D^{(n)[\Gamma]}}$;
      ... ;
      Compute $\boldsymbol{P_D^{(n)[\Gamma+1]}}$ with $\boldsymbol{P_1^{(n)[\Gamma+1]}}$,...,$\boldsymbol{P_{D-1}^{(n)[\Gamma+1]}}$;
    end
  end
  Calculate admittances side of the problem directly: $\boldsymbol{V^{[\gamma+1]}} = \boldsymbol{Y^{-1}}(\boldsymbol{I} + \boldsymbol{I_0})$;
end

Solving the power flow for each variation in the parameters with the classical Newton-Raphson is without a doubt more straightforward than following the procedure summarized in Algorithm 6. The price to pay for this simplicity is in the time required, which in computational terms is usually called complexity. The Newton-Raphson involves at least one inversion of the Jacobian matrix, and usually between three to five in order to obtain results with appropriate precision. It is a well-known fact that the complexity of a $n \times n$ inverse matrix increases exponentially with its size [101], and in principle, it is $\mathcal{O}(n^3)$. Therefore, having to compute the inverse so many times in power flow problems where parameters change slightly becomes a computationally intensive task.

On the contrary, the PGD becomes a much more efficient methodology. There are no inverse matrices involved (apart from the impedance matrix, which can be precomputed) and it is able to decouple the dimensions of the problem. Take for instance a system where three parameters p_1, p_2 and p_3 vary in ranges of n_1, n_2 and n_3 values. If the total number of non-slack buses in the system is n_b, the number of calculations N_u turns out to be [94]:

$$N_u \propto M(n_b + n_1 + n_2 + n_3) \,, \tag{131}$$

where M is the so-called number of modes and corresponds to the number of iterations performed in the intermediate loop. Instead, a Newton-Raphson-based algorithm would require to compute N_r unknowns, where:

$$N_r \propto n_b n_1 n_2 n_3 \, . \tag{132}$$

When the dimensions of the system tend to large values, the PGD becomes considerably faster than the Newton-Raphson. For example, [98] reported solving in a matter of minutes a time-series power flow which took a couple of hours with the Newton-Raphson method.

5.3 Parametrization in the Holomorphic Embedding Load-Flow Method

The Holomorphic Embedding Load-Flow Method (HELM) was developed as a tool to guarantee the obtention of a solution when it exists, and to signal when no solution is present [86]. Its strong mathematical properties have made it a competitive algorithm that achieves similar computational times as the classical Newton-Raphson [102]. The essence of HELM consists of submerging (or embedding) the initial problem under another problem arguably simple to solve [103]. The embedded power balance at a given bus i becomes:

$$\sum_j \underline{Y}_{ij}\underline{V}_j(s) = s\frac{\underline{S}_i^*}{\underline{V}_i(s)}, \tag{133}$$

where s is by definition a complex variable, although by convention it is not represented as such.

The voltages of the form $\underline{V}_k(s)$ are the unknowns of the problem. These voltages are represented by coefficients in the following manner:

$$\underline{V}_k(s) = \sum_r \underline{c}_{k,r} s^r, \tag{134}$$

where the coefficients $\underline{c}$ have to be found. They are computed by substituting the definition shown in (134) into (133). First of all, s is set to 0 and the first coefficients are obtained. They are typically initialized at 1. Afterwards, s takes a value of 1 and the polynomial equations derived from (133) are solved. More details about the procedure can be found in [43].

In this regard, HELM can be seen as a pseudo-parametric method. The states are represented by polynomials. The major complexity of the method is finding the coefficients, just like it happens for the Galerkin method. Once they are known, the voltages can be evaluated by simply substituting the values of the parameters. Nonetheless, the major difference between the conventional parametric power flow and HELM lies on the type of parameters. In parametric techniques, the parameters are for instance the power injections which are known to vary inside an interval. In HELM, there is a single parameter: the complex variable s. The voltages are evaluated for $s \to 1$, and hence the method does not capture the dependence with the real parameters.

Another major difference between HELM and other parametric techniques is the fact that the coefficients vary depending on the inputs. That is, the inputs are not seen as parameters but rather as values taken as if they were part of a snapshot. The arrays with coefficients $\underline{c}$ will undoubtedly change. This makes the method not suitable to track the dependence voltages have with parameters. All in all, HELM is not a good candidate for parametrizing the power flow.

5.4 Principal Component Analysis with dimension reduction

5.4.1 Summary of states, parameters and dimensions

States are denoted by $\mathbf{x}$ and stand for the unknowns of the power flow, such as the voltage magnitude. The traditional power flow looks to obtain a solution for all states; in the parametric power flow, this is not necessarily the case, as there might be only one bus under study.

Parameters are defined as the input data which are meant to vary. Powers are part of this category, since loads change over time and most generation sources also experience variations. Considering a total of m parameters, grouped under $\mathbf{p} = [p_1, p_2, ..., p_m]$, each parameter $p_k \; \forall k \in \{1, ..., m\}$ takes values inside the $[a_k, b_k]$ range.

This way, the power flow problem can be written as:

$$\mathbf{f}(\mathbf{x}, \mathbf{p}) = \mathbf{0}, \tag{135}$$

where $\mathbf{f}$ symbolizes all implicit functions involved in the solution of the problem. The formulation that follows is generic, in the sense that the methodology would be equally valid for other problems. Hence, this technique is not limited to the traditional power flow.

The parametric approach looks to express a certain state as a function of the parameters:

$$x = g(\mathbf{p}), \tag{136}$$

where g is a function pending to be found.

From (136) it becomes clear that all parameters will potentially affect a given state. Visually speaking, Figure 35.a shows a representation of a state as a function of a single parameter, that is, assuming that only one input changes. Figure 35.b presents a similar visualization with two parameters involved. This justifies why, when viewed as a spatial representation, parameters are also denoted as dimensions. Each one of them stands for a new independent axis, and thus, orthogonal to the rest.

More than two dimensions are expected to be present in a typical analysis of the parametric power flow. In a mid-size system, assuming all powers are treated as parameters, there could be hundreds of dimensions. If $m \approx 100$, opting for the naive approach with n^m cases would be painful to compute. This is often called the curse of dimensionality.

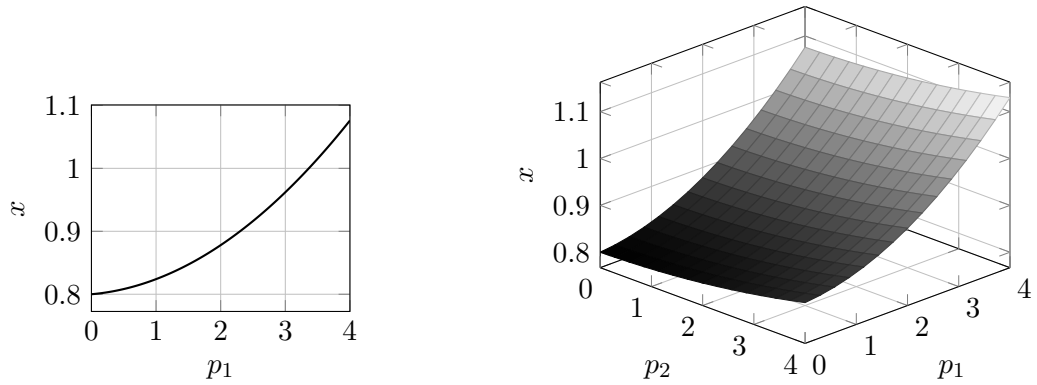

(a) one-axis representation.

(b) two-axis representation.

Figure 35: Representation of a state with one or two parameters.

One fundamental step to circumvent this challenge is to reduce the dimensions. Note that in Figure 35 the value of x is more or less the same in both Figure 35.a and Figure 35.b. That is, p_1 has a larger influence than p_2. The essence of dimensionality reduction lies in compacting all dimensions into a few. A prerequisite is to determine the impact all parameters have on the state.

The Galerkin method is based on solving a large and complex system of equations. The technique shown here relies on obtaining some samples, determining the influence of the parameters, and fitting the polynomials to represent the states. It exchanges precision for speed and simplicity.

5.4.2 Principal Component Analysis technique

The Principal Component Analysis (PCA) weights the parameters according to their influence. To do so, the first step is concerned with computing the gradient:

$$\nabla_{\mathbf{p}} g = \left[\frac{\partial x}{\partial p_1}, ..., \frac{\partial x}{\partial p_k}, ..., \frac{\partial x}{\partial p_m} \right]^T. \tag{137}$$

Calculating the gradient numerically is probably the most beneficial option because it allows to operate with implicit functions, just like the power flow is commonly presented. Hence, for all k in $[1, ..., m]$:

$$\frac{\partial x}{\partial p_k} = \frac{g(p_1, ..., p_k + \delta, ..., p_m) - g(p_1, ..., p_k, ..., p_m)}{\delta}, \tag{138}$$

where δ is an arbitrary small number, such as $\delta = 1 \cdot 10^{-10}$ for instance. Computing the gradient with this approach means that the power flow solver has to be called $m + 1$ times.

Let $\mathbf{C} \in \mathbb{R}^{m \times m}$ be the covariance matrix. Its elements identify the influence of the parameters on the states. Large elements represent that the involved parameters have a significant impact on the state, whereas small elements mean that these parameters are potentially irrelevant. Since a parameter p_k can take any value inside its corresponding range $[a_k, b_k]$, several samples have to

be extracted to have a representative $\mathbf{C}$ matrix:

$$\mathbf{C} \approx \frac{1}{M} \sum_{i=1}^{M} \nabla_{\mathbf{p}} g (\nabla_{\mathbf{p}} g)^T, \tag{139}$$

where M is the total number of samples and takes a relatively arbitrary value.

The parameters take random values in each sample. The power flow solver would have to be called $M(m+1)$ times in total. Although it largely depends on the number of initial dimensions, M can take values in the order of a hundred. As a consequence, it can be foreseen that calculating $M(m+1)$ power flows is generally way faster than computing n^m cases. The reason is that there is no dependence on the discretized n values and this methodology provides a continuous solution (in the form of a polynomial).

Matrix $\mathbf{C}$ is symmetrical by definition, which means it can be diagonalized by orthogonal matrices:

$$\mathbf{C} = \mathbf{WAW}^T, \tag{140}$$

where $\mathbf{A}$ is a diagonal $m \times m$ matrix formed by eigenvalues $[\lambda_1, ..., \lambda_k, ..., \lambda_m]$ sorted in order of relevance, and $\mathbf{W}$ contains their respective eigenvectors, denoted as $[\mathbf{w}_1, ..., \mathbf{w}_k, ..., \mathbf{w}_m]$, in the form of columns.

The eigenvectors in $\mathbf{W}$ can be understood as dimensions. The idea behind the PCA is to determine the impact of a given dimension, which ends up being proportional to its eigenvalue [96]. Since eigenvalues are sorted by order of importance, $\mathbf{w}_1$ is more representative than $\mathbf{w}_2$, $\mathbf{w}_2$ is more important than $\mathbf{w_3}$, and so on. This process of determining the relevant dimensions is the core of the Proper Orthogonal Decomposition (POD), which has been widely employed in the field of fluid dynamics [104], [105].

If some dimensions are more influential than others, it makes sense to eliminate the insignificant ones. Although this is a subjective step, the truncation error can be defined as:

$$e_t = \frac{\lambda_{k+1} + ... + \lambda_m}{\lambda_1 + ... + \lambda_m}, \tag{141}$$

which implies that only eigenvalues $[\lambda_1, ..., \lambda_k]$ have been selected. The user ought to select a desired error (e.g., $e_t = 10\%$) and identify the eigenvalues that allow obtaining a similar truncation error. The lower the truncation error, the more accurate and complex the model will be, and vice versa.

5.4.3 Dimension reduction approach

Up to this point, the most relevant dimensions have been identified. The next step is to reduce the dimensions:

$$\mathbf{y} = \mathbf{W_y}^T \mathbf{p}, \tag{142}$$

where ${\mathbf{W_y}}^T$ is formed by the rows of eigenvectors $[\mathbf{w}_1, ..., \mathbf{w}_k]$. As ${\mathbf{W_y}}^T \in \mathbb{R}^{k\times m}$, it transforms all m directions into k impactful directions.

Consequently, the initial parametric power flow of the form $x = g(\mathbf{p})$ is transformed into:

$$x \approx h(\mathbf{y}), \tag{143}$$

where h is a function that has yet to be found. In more detail, it will consist of a polynomial. Working with $\mathbf{y}$, which symbolizes k directions, instead of $\mathbf{p}$ where there are m directions involved, is not mandatory. The state x could still be approximated by a polynomial function $h(\mathbf{p})$. However, if m tends to a large number, the method would suffer from the curse of dimensionality.

More details are provided in the following section, but for now, it will be assumed that the number of terms N in the function h is given by [96], [106]:

$$N = \binom{N_p + m}{m} = \frac{(N_p + m)!}{m!\,(N_p + m - m)!} = \frac{(N_p + m)!}{m!\,N_p!}, \tag{144}$$

where N_p denotes the expansion order and it usually does not have to exceed 3. From (144), if $N_p = 3$ and $m = 5$, $N = 56$; if $N_p = 3$ while $m = 10$, $N = 286$. The computational effort would have increased by a factor of approximately 5 even though the number of dimensions has only doubled. This numerical example indicates why it is appropriate to reduce the number of dimensions in spite of losing a bit of accuracy.

5.4.4 Polynomial function representation

Function h is a polynomial function of degree N_p at most. It is formed by a succession of terms such as:

$$x \approx h(\mathbf{y}) = \sum_{j=0}^{N} {\mathbf{c_j}}^T \phi_{\mathbf{j}}(\mathbf{y}), \tag{145}$$

where $\mathbf{c_j}$ is a vector of coefficients with the same length as $\phi_{\mathbf{j}}$, which contains all bases functions of degree j. All coefficients have to be found in order to determine h. Once this is achieved, h will be fully defined and ready to be used to compute the state for whatever values the parameters take.

As (145) might be too compact, it is exemplified in the case where $k = 3$ (that is, there are 3 meaningful directions) and $N_p = 2$. The three significant directions are denoted by y_1, y_2, y_3. The rule is that all three parameters have to be multiplied between them, and the degree of the resulting function has to be equal to j. Thus, when $j = 0$:

$$\begin{aligned} f_0(\mathbf{y}) &= [c_{0,1}] \cdot \left[y_1^0 y_2^0 y_3^0\right]^T \\ &= c_{0,1} \cdot 1, \end{aligned} \tag{146}$$

where $c_{0,1}$ stands for the first (and only) coefficient of the basis function with degree 0, and it is unknown. The values of y_1, y_2, y_3 are known since they are treated as inputs.

When $j = 1$:

$$\begin{aligned} f_1(\mathbf{y}) &= [c_{1,1}, c_{1,2}, c_{1,3}] \cdot \left[y_1^1 y_2^0 y_3^0, y_1^0 y_2^1 y_3^0, y_1^0 y_2^0 y_3^1\right]^T \\ &= c_{1,1} \cdot y_1 + c_{1,2} \cdot y_2 + c_{1,3} \cdot y_3. \end{aligned} \tag{147}$$

When $j = 2$:

$$\begin{aligned} f_2(\mathbf{y}) = [c_{2,1}, c_{2,2}, c_{2,3}, c_{2,4}, c_{2,5}, c_{2,6}] \cdot \big[&y_1^1 y_2^1 y_3^0, y_1^1 y_2^0 y_3^1, y_1^0 y_2^1 y_3^1, \\ &y_1^2 y_2^0 y_3^0, y_1^0 y_2^2 y_3^0, y_1^0 y_2^0 y_3^2\big]^T \\ = c_{2,1} \cdot y_1 y_2 + c_{2,2} \cdot y_1 y_3 + c_{2,3} \cdot y_2 y_3 + c_{2,4} \cdot y_1^2 + c_{2,5} \cdot y_2^2 + c_{2,6} \cdot y_3^2. \end{aligned} \tag{148}$$

Finally, all f are added:

$$x \approx h(\mathbf{y}) = f_0(\mathbf{y}) + f_1(\mathbf{y}) + f_2(\mathbf{y}). \tag{149}$$

Note that taking into account (146), (147) and (148), there are a total of $N = 10$ terms, just like (144) indicates when $N_p = 2$ and $m = 3$.

Recall that a total of M samples, where the parameters take random values, are needed to build the covariance matrix. Now these samples have to be used in order to compute the coefficients $\mathbf{c}$. Let $\mathbf{Q} \in \mathbb{R}^{M \times N}$ denote the matrix where the terms that multiply the coefficients $\mathbf{c}$ are stored, and $\mathbf{h_x}$ the vector that contains the value of the state x at each sample. Then, the goal is to minimize the error ϵ in the generic expression:

$$\mathbf{h_x} = \mathbf{Q}\mathbf{c} + \epsilon, \tag{150}$$

where $\mathbf{c}$ is constituted by the N coefficients.

Several ways to calculate the coefficients in $\mathbf{c}$ exist [96]. If the least squares regression method is chosen [107], the best estimate of $\mathbf{c}$ is:

$$\mathbf{c} = \left(\mathbf{Q}^T\mathbf{Q}\right)^{-1}\mathbf{Q}^T\mathbf{h_x}. \tag{151}$$

To apply this least squares regression, it is necessary to have $M \geq N$, and as a rule of thumb, M should be around 1.5 to 3 times N [107]. This concludes the calculation process, as $h(\mathbf{y})$ is fully known.

5.4.5 Procedure overview

The steps to take in order to obtain the reduced dimension model are summarized below:

1. Compute the gradients for the M samples to calculate the covariance matrix $\mathbf{C}$ with (139).

2. Perform the orthogonal decomposition of $\mathbf{C}$ and select the most influential dimensions according to the desired truncation error.

3. With the random samples, transform $\mathbf{p}$ into $\mathbf{y}$ with (142).

4. Build the $\mathbf{Q}$ matrix, the $\mathbf{h_x}$ vector, and find the coefficients with (151).

Once the coefficients $\mathbf{c}$ are calculated, the procedure yields an explicit function that relates the state x with any value of the parameters.

5.4.6 Fundamental case study

This section aims to show more in detail the calculation procedure. The methodology is applied to a basic power system such as the 5-bus system from the GridCal tutorial [108], shown in Figure 36.

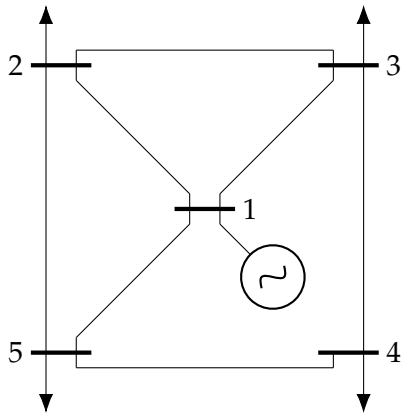

Figure 36: High-level representation of the 5-bus system.

The system is formed by four PQ buses and one slack bus, corresponding to node 1. Lines are originally modeled with a π equivalent. Nevertheless, the parallel capacitances are removed to have voltages below the level imposed by the slack bus, which should help in obtaining a more intuitive result.

The state of interest will be the voltage magnitude at bus 5, thus, $x = V_5$. Choosing the parameters is rather a subjective choice which largely depends on the scope of the study. However, they are chosen to be the four active powers and the four reactive powers in this case:

$$[p_1, p_2, p_3, p_4, p_5, p_6, p_7, p_8] = [P_2, Q_2, P_3, Q_3, P_4, Q_4, P_5, Q_5], \tag{152}$$

where P and Q stand for the loads of active and reactive power.

These powers can take any value inside a predefined range of values. In a realistic scenario, this range could comprise a high confidence interval. Table 21 shows the chosen lower and upper bounds for all powers.

Table 21: Lower and upper limit for all parameters, in the order of MVA.

Limit	P_2	Q_2	P_3	Q_3	P_4	Q_4	P_5	Q_5
Lower	0	0	0	0	0	0	0	0
Upper	40	30	30	45	25	20	30	20

The calculation process obeys the four steps summarized in Section 5.4.5. Each of them is numerically detailed below.

1. Compute the gradients for the M samples to calculate the covariance matrix $\mathbf{C}$ with (139).

A total of $M = 10$ samples is chosen. This becomes a reasonable amount considering that the expansion order is set to $N_p = 3$. Moreover, as it will be shown in the next step, all eight parameters will be encapsulated in a single meaningful direction, so $k = 1$. Thus, $N = 4$ in accordance with (144). The requirements are being met since M should be between 1.5 to 3 times N at least.

There is no complexity in generating the samples. All parameters take random values between the limits set in Table 21. The power flow is solved $M(m+1) = 10(8+1) = 90$ times. With it, a total of 10 gradients are obtained by following (138). The covariance matrix $\mathbf{C}$ is built by adding the products of gradients, as shown in (139). In this particular case, it becomes:

$$\mathbf{C} = 10^{-8} \cdot \begin{pmatrix} 1.39 & 3.18 & 1.93 & 4.40 & 5.00 & 11.16 & 1.92 & 4.57 \\ 3.18 & 7.27 & 4.40 & 10.05 & 11.41 & 25.48 & 4.39 & 10.43 \\ 1.93 & 4.40 & 2.66 & 6.08 & 6.91 & 15.43 & 2.66 & 6.31 \\ 4.40 & 10.05 & 6.08 & 13.89 & 15.77 & 35.21 & 6.07 & 14.41 \\ 5.00 & 11.41 & 6.91 & 15.77 & 17.91 & 39.98 & 6.89 & 16.36 \\ 11.16 & 25.48 & 15.43 & 35.21 & 39.98 & 89.28 & 15.39 & 36.54 \\ 1.92 & 4.39 & 2.66 & 6.07 & 6.89 & 15.39 & 2.65 & 6.30 \\ 4.57 & 10.43 & 6.31 & 14.41 & 16.36 & 36.54 & 6.30 & 14.95 \end{pmatrix}. \tag{153}$$

It is symmetrical, with tiny values as the voltage does not change much with variations in the powers.

2. Perform the orthogonal decomposition of $\mathbf{C}$ and select the most influential dimensions according to the desired truncation error.

The orthogonal decomposition of the covariance matrix follows (140). The eight eigenvalues are presented in Table 22.

The first eigenvalue is significantly more relevant than the others. Choosing $k = 1$ impactful dimensions translates into a minuscule truncation error. This shows that going from 8 to 1

Table 22: Ordered eigenvalues obtained from the orthogonal decomposition.

	λ_1	λ_2	λ_3	λ_4	λ_5	λ_6	λ_7	λ_8
Value ($\cdot 10^{-12}$)	$1.5 \cdot 10^6$	67	28	21	5	3	1	0

dimension is possible without making a notorious mistake.

As $k = 1$, $\mathbf{W}_y$ is a single-column matrix containing the eigenvector $\mathbf{w}_1$ associated with λ_1:

$$\mathbf{W}_y = \begin{pmatrix} 0.09651 \\ 0.22017 \\ 0.13332 \\ 0.30426 \\ 0.34549 \\ 0.77142 \\ 0.13303 \\ 0.31575 \end{pmatrix}. \tag{154}$$

This matrix weights all parameters. Notice how the sixth parameter, the one corresponding to Q_4, is the largest by far. This could also have been observed in the $\mathbf{C}$ matrix shown in (153), where the sixth column/row has significantly greater values than the rest. It makes sense that Q_4 has a notable impact on V_5 because bus 4 is the only one not directly connected to the slack bus, and the impedance between bus 4 and 5 is small.

3. With the random samples, transform $\mathbf{p}$ into $\mathbf{y}$ with (142).

Then, the $\mathbf{p}$ vector with the random samples and the matrix $\mathbf{W}_y^T$ are multiplied for all samples. This is a straightforward step since the two involved objects are already known. The goal is to transform the 8 dimensions in $\mathbf{p}$ to just one dimension stored in $\mathbf{y}$. In the end, the procedure looks for $h(\mathbf{y})$, so $\mathbf{p}$ always has to be transformed. Since there is only one dimension in $\mathbf{y}$, the basis function expansion turns out to be simplified. If $N_p = 3$:

$$h(y) = c_0 + c_1 \cdot y^1 + c_2 \cdot y^2 + c_3 \cdot y^3, \tag{155}$$

where $y \in \mathbb{R}$ and the coefficients c have to be calculated.

4. Build the $\mathbf{Q}$ matrix, the $\mathbf{h_x}$ vector, and find the coefficients with (151).

The $\mathbf{h_x}$ vector has been previously computed. It simply gathers the 10 solutions (one for each

sample) of V_5, and is equal to:

$$\mathbf{h_x} = \begin{pmatrix} 0.95990 \\ 0.95690 \\ 0.95676 \\ 0.96470 \\ 0.95795 \\ 0.96585 \\ 0.97307 \\ 0.96149 \\ 0.95658 \\ 0.96660 \end{pmatrix}. \tag{156}$$

The $\mathbf{Q}$ matrix has dimensions 10×4, and it is formed by the four elements that are multiplied by the coefficients in (155), with each sample constituting a row. It is not shown here for simplicity.

Finally, the coefficients in $\mathbf{c}$ are computed with (151). The resulting equation becomes:

$$V_5 \approx h(y) = 1.00004 - 1.14716 \cdot 10^{-3} y - 1.10118 \cdot 10^{-6} y^2 - 3.24401 \cdot 10^{-9} y^3. \tag{157}$$

To calculate the approximated voltage in every possible situation it is enough to convert the vector of parameters $\mathbf{p}$ to y and input its value to (157). Figure 37 shows the value V_5 takes depending on y.

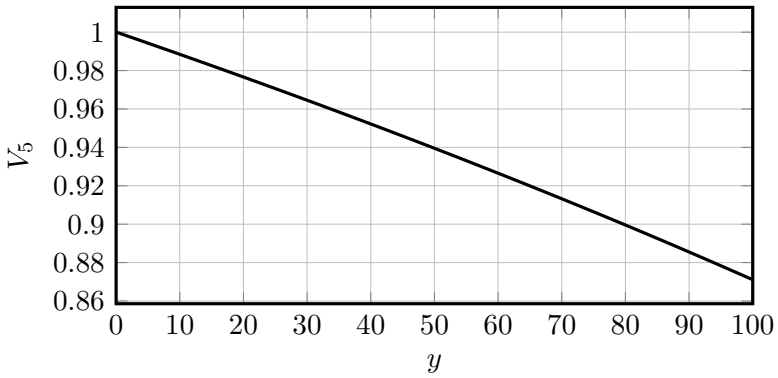

Figure 37: Graphical interpretation of $V_5 \approx h(y)$.

If the horizontal axis were to be extended, it would become clear how $V_5(y)$ follows a parabolic profile, similar to the typical P-V curves. Also, it is relevant to mention that the values of $\mathbf{h_x}$ are around 0.95 to 0.98 approximately. This is due to the lower and upper bounds defined in Table 21. Therefore, the computed value of y should be between 15 and 40 more or less.

The methodology has been tested for several cases with satisfactory results. Table 23 compares the results obtained with $V_5 \approx h(y)$ and the results provided by the power flow solver in case $\mathbf{p} = [25, 12, 8, 33, 21, 4, 17, 11]$ MVA.

Table 23: Comparison of results when $\mathbf{p} = [25, 12, 8, 33, 21, 4, 17, 11]$ MVA.

Magnitude	Value
V_5 from (157)	0.9618089
V_5 from the power flow solver	0.9618607
Error	$5.1800583 \cdot 10^{-5}$

It can be concluded that by only calling the power flow 90 times, a satisfactory model has been obtained. It can reproduce with great accuracy the actual V_5 value as a function of the parameters. Errors in the order of 10^{-4} have been typically obtained. In essence, the methodology is based on computing the gradients at different operating points. It may seem equally valid to calculate the gradient at a random operating point and estimate the state from this. While this basic approach could work for grids where the loads are at their lower levels, it is not suitable for higher load levels. Intuitively speaking, the operating points would move closer to the nose of the P-V curves, which are quadratic. As a consequence, a simple linearization at a random point becomes sub-optimal.

5.4.7 Case study about the optimal placement of capacitors

This section covers the analysis of a well-known system to test the accuracy of the parametric analysis applied to an optimization problem. As shown in Figure 38, this particular system consists of a radial distribution grid with 100 PQ buses [95], [109]. A capacitor bank of a certain capacity has to be installed in a single bus with the goal of minimizing power losses. The data of the system are captured in Table 24.

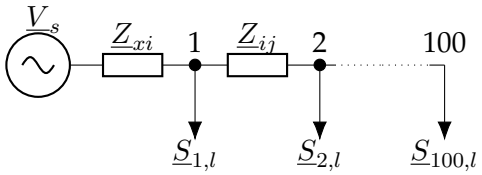

Figure 38: High-level representation of the radial distribution system.

Table 24: Data for the radial distribution system, in pu values.

Magnitude	Value
$\underline{V}_s$	$1.0/\underline{0^\circ}$
$\underline{S}_{i,l}$	$0.007500 + j0.003632$
$\underline{Z}_{xi}$	$0.0005 + j0.001$
$\underline{Z}_{ij}$	$0.0005 + j0.001$

Thus, there are two unknowns: the reactive power provided by the capacitor bank, and its

position. Mathematically:

$$\begin{aligned} \min_{x,Q} \quad & P_g(x,Q) - \sum_{i=1}^{n} P_{i,l} \\ \text{s.t.} \quad & x \in \mathbb{Z} \cap [1,n] \\ & \sum_{k=0}^{n} \underline{Y}_{ik}\underline{V}_k = \frac{\underline{S}_i^*}{\underline{V}_i^*}, \ \forall i \in \mathbb{Z} \cap [1,n] \end{aligned} \tag{158}$$

where P_g denotes the power generated by the slack bus, x stands for the position, Q symbolizes the reactive of the capacitor, $P_{i,l}$ identifies the active power load of the i bus, $n = 100$ buses, $\underline{Y}_{ik}$ is the (i,k) element of the nodal admittance matrix, $\underline{V}_k$ is the voltage at the k bus, and $\underline{S}_i$ corresponds to the injected complex power at bus i.

One approach to solve the optimization problem involves computing the losses for thousands of (x,Q) pairs of values. Figure 39 shows that there is indeed a global minimum with x around two thirds of the total length, which is proved in [109].

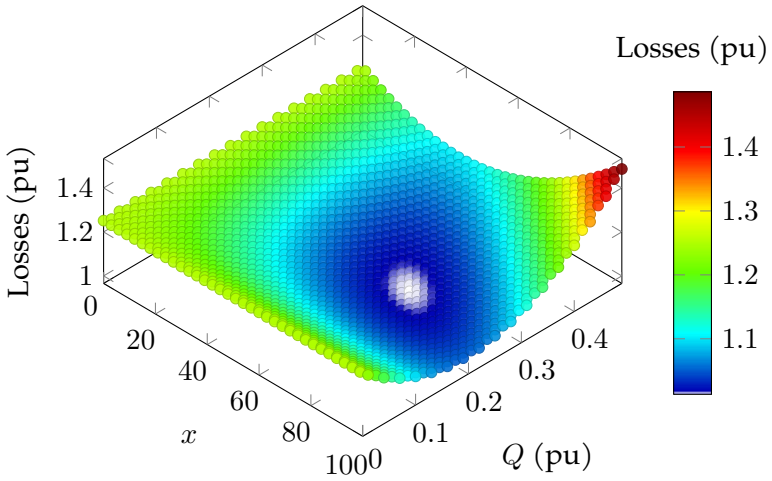

Figure 39: Representation of the losses as a function of the distance and the reactive power.

Note that Figure 39 is obtained by tediously computing the losses for various (x,Q) pairs of values. Say Q takes 50 different values, and x ranges from 1 to 100. This results in 5000 power flow calls. On the contrary, the parametric approach further reduces the number of power flow calls (up to 25, although there is some arbitrariness on that). States and parameters are introduced as follows:

$$\begin{cases} \mathbf{x} = [P_g(\mathbf{p}) - \sum_{i=1}^{n} P_{i,l}] \\ \mathbf{p} = [x, Q] \end{cases} \tag{159}$$

where $\mathbf{p}$ represents the parameters, and $\mathbf{x}$ stands for the states. In this case, there is a single state: the active power losses. It is worth mentioning that the position x has not to be confused with the array of states $\mathbf{x}$. The optimization problem described in (158) preserves its validity.

The usage of the parametric power flow yields a continuous expression to relate the parameters with the active power losses. Although this relationship has a certain degree of randomness due to the sampling stage, one solution with the corresponding permutations is presented in Table 25. Recall that given two meaningful directions and an expansion order equal to 3, the state of interest obeys:

$$\mathbf{x} = \left[\sum_{i=1}^{10} c_i y_1^k y_2^j \right], \tag{160}$$

where $k \in \mathbb{Z}$, $j \in \mathbb{Z}$, and $k + j \leq 3$.

Magnitudes y_1 and y_2 are derived from the normalized parameters $\hat{x}$ and $\hat{Q}$:

$$\begin{pmatrix} y_1 \\ y_2 \end{pmatrix} = \begin{pmatrix} -1.0000 & -1.3505 \cdot 10^{-6} \\ +1.3505 \cdot 10^{-6} & -1.0000 \end{pmatrix} \begin{pmatrix} \hat{x} \\ \hat{Q} \end{pmatrix}. \tag{161}$$

Essentially, $y_1 \approx -\hat{x}$ and $y_2 \approx -\hat{Q}$. It makes sense to have two meaningful directions as these two parameters do not share the same nature. Had it been a case where the only parameters are powers, they could have been grouped under a single direction. Besides, since the method uses the orthogonal decomposition concept, the column vectors in the matrix are perpendicular.

In turn, the normalized parameters $\hat{x}$ and $\hat{Q}$ are obtained from the natural x and Q values by stretch and translation. In other words, their initial ranges of values are mapped to the $[0, 1]$ range. This facilitates the obtention of well-conditioned coefficients (usually below 1.0) as depicted in Table 25.

Table 25: Solution obtained from the parametric power flow.

i	(k, j)	c
1	$(0, 1)$	$+0.082508$
2	$(1, 2)$	-1.243129
3	$(2, 1)$	-0.989375
4	$(0, 0)$	$+1.265757$
5	$(1, 1)$	-1.928269
6	$(0, 3)$	$+0.046238$
7	$(2, 0)$	$+0.156790$
8	$(3, 0)$	$+0.095222$
9	$(0, 2)$	$+0.102589$
10	$(1, 0)$	$+0.083469$

With the closed-form expression of the losses as a function of the parameters shown in (160), the next step consists of inputting the data to an optimization solver. Another option is to sweep for various values of $\hat{x}$ and $\hat{Q}$, which would probably take less time than computing the power

flow again and again as in the traditional approach. In any case, the Mystic package [74], based on Python, is employed.

The optimization solver yields the following results:

$$\begin{cases} \mathbf{x} = [1.013995] \\ \hat{x} = 0.642838 \\ \hat{Q} = 0.527806 \end{cases} \tag{162}$$

Visually speaking, the optimal result seems to be in line with the plot in Figure 39. Numerically, it differs about 0.083% from the optimal result found by sweeping. A fairer comparison would use the AC OPF result, but despite this, it has been shown that the parametric approach obtains a satisfactory solution. Regarding the optimal position, it would have to be denormalized and take its integer value. Doing this results in $x = 65$, which roughly speaking is equivalent to saying that the capacitor has to be placed at two thirds of the total length. Similarly, the denormalized reactive power becomes $Q = 0.26390$ pu.

The calculation of the optimal position and reactive power has taken under 1 second with a custom Python code. Its speed remains to be tested in a time-series power flow, where loads vary with time. In this latter case, an analogous system has been studied in [109] and in [95]. They reported computational times in the order of hours and minutes, respectively.

5.4.8 Time complexity and errors discussion

The speed of the PCA in combination with the dimension reduction is compared to the fully expanded Galerkin method. Table 26 shows the required computational time and the associated error. The PCA seems to be a better fitting choice, as substantially less time is needed in order to obtain a similar error. Two powers have been parametrized in each case, and an expansion order of $N_p = 3$ has been chosen.

Table 26: Time and error comparison between PCA and Galerkin for standard grids.

Grid	**PCA**		**Galerkin**	
	Time (s)	**Average error (pu)**	**Time (s)**	**Average error (pu)**
IEEE 5	0.91	$1.62 \cdot 10^{-4}$	50.61	$3.30 \cdot 10^{-5}$
IEEE 9	1.01	$1.21 \cdot 10^{-3}$	511.64	$4.24 \cdot 10^{-5}$
IEEE 14	1.35	$3.26 \cdot 10^{-3}$	1906.33	$5.72 \cdot 10^{-5}$

The usage of the PCA with the dimension reduction approach produces tolerable errors (mostly in the order of 10^{-3}) in a relatively short amount of time. On the other side, the expanded Galerkin requires significantly more time but yields acceptable errors in the order of 10^{-5}. The Galerkin method suffers greatly from the curse of dimensionality since the computational time

scales exponentially with the number of buses. All in all, the PCA with dimension reduction becomes the most convenient approach to study large-scale systems, as long as extremely low errors are not obligatory.

5.4.9 Application fields

The time-series power flow is likely the most natural application regarding the parametric analysis of power systems. The topology is preserved, and powers act as parameters. The case study can be treated as a situation where powers vary inside a range of values, with an enormous number of combinations. With just a few samples, obtaining a representative expression for the state of interest is arguably simple. This contrasts with the inconvenient approach where the power flow would have to be called n^m times.

When integrating renewables, it becomes potentially attractive to have a closed-form expression of the state as a function of the input parameters. The system operator would be able to build a solid estimate about the value of the state in real-time, rather than relying on probabilistic studies, which have been the norm (see [110]–[112]).

On the other hand, the DC load flow has been the state of the art for power systems planning. It computes a fast result at the expense of a very approximate solution. In addition, it may not be appropriate for distribution grids since the resistive part of the lines is neglected [113]. The efficient parametric analysis, in contrast, generates a much more precise result with a function that can be recycled over and over. The covered parametric power flow may suppose a paradigm shift.

Fault analysis can be regarded as a sub-field inside the power systems planning field. In its basic form, powers could be seen as static values and grid impedances treated as parameters. Since the methodology is not tied to the form of the power flow equations, the parametric analysis could be performed for varying impedances. Three-phase faults would imply that the power flow equations remain unchanged. Unbalanced faults introduce some more complexity because the three phases would have to be analyzed separately. Nonetheless, as the equations would still be continuously differentiable, there should be no issues in implementing the parametric analysis.

Power electronics are prone to suffer from saturation. That is, apart from the natural limitation of not being able to provide more power than the generated from the renewable energy source, voltages and currents have to be kept inside the limits. This means that power electronic devices can operate in various states, such as unsaturated, partially saturated, or fully saturated, which in turn are defined by different equations [114]. It may very well be that the parametric analysis becomes incapable of tracking saturated states. This will mostly depend on the sampling. If all parameters yield an unsaturated converter state, the final explicit function will of course not

contemplate a saturated state. Thus, it is recommended to keep the upper and lower bounds close together, and if possible, previously ensure that the converter always operates in the same state. There is much work to be done in order to integrate power electronics devices.

5.5 Conclusion

This chapter has reviewed some of the most popular efficient parametric techniques. An efficient methodology aimed at the parametric analysis of power systems has been presented. It allows obtaining a polynomial that relates a state of interest with the parameters. It achieves so by reducing the dimensions of the initial problem to a few meaningful dimensions. Thus, a bit of precision is sacrificed so as to generate a fast and generic solution, ideal for systems planning.

It has to be mentioned that for the most part, the application of this technique remains unpopular. It borrows well-known concepts such as the orthogonal decomposition, widely used in other fields. However, up to now, there are almost no studies on how it performs when analyzing power systems. It seems to be a promising technique, with potential applications in time series, real-time computing, and fault analysis. More diverse case studies are required in order to properly assess its potential.

6 Conclusions

The thesis has covered the formulation and implementation of techniques to solve power systems in steady-state. This chapter summarizes the main contributions of the work and potentially rewarding ideas to further develop in the future.

6.1 Contributions

The most relevant findings, organized by chapter, are the following:

- Chapter 2 presents a new classification of buses considering the saturated states of converters. Related to this, a Newton-Raphson method aimed at integrating saturated converters has been introduced. The structure of the algorithm does not differ considerably from the one employed in the traditional power flow. The program has been found to be scalable and computationally efficient. The associated case study is centered on a 2000-bus system whose solution has been validated with a dynamic simulation. Compared to other existing pieces of software, the proposed modeling is concluded to be accurate. In addition to that, the chapter formulates and tests a Lagrangian to algebraically include the converter's limits in a simple system.

- Chapter 3 analyzes the operation of power converters under short-circuit fault conditions. The goal is to maximize the voltage-support, that is, to inject currents that cause voltages to approach the optimal values. The optimal solution is obtained to serve as a benchmark. Compared to it, the traditional grid code is a suboptimal choice. The thesis proposes two adapted grid codes (GCP and GCN) that tend to be near-optimal. The implementation of these modified grid codes is arguably simple, and hence, they could substitute conventional grid codes.

- Chapter 4 is focused on the Galerkin method to solve the power flow problem. First, the mathematical bases of the Galerkin method are covered. Then, the decoupled Galerkin is analyzed in order to assess its viability. Although it is advantageous in terms of speed, the error it provides is considered to be excessive. Hence, the complete Galerkin method is derived. The thesis develops a generalized formulation of the complete Galerkin so that it can be employed in generic grids. Despite the complexity, its usage yields a more than acceptable error in a standardized grid such as the IEEE-14 bus system.

- Chapter 5 reviews less computationally intensive techniques to solve the parametric power flow. Especially, the Principal Component Analysis is useful to capture the weight each parameter has on the states. Combined with a reduction of dimensions, this becomes a much more efficient approach to solve the parametric power flow than the Galerkin method. The obtained explicit functions are then employed in an optimization problem

with considerable accuracy.

It has to be mentioned that all results, except for the dynamic simulations, have been generated with custom Python codes.

6.2 Future work

Numerical tools applied to solving power systems in steady-state form a vast field. This thesis has covered a specific set of techniques aimed at the challenges linked to modern grids. Some research lines and several aspects that would benefit from an in-depth analysis have emerged:

- The states of converters are uncertain a priori. Since a given combination of states may yield no solution, it is convenient to develop heuristics that indicate which states should be modified. This could have a tremendous benefit in systems constituted by a large number of converters.

- The efficacy of the Lagrangian expression to algebraically include the limits has been tested in a small-scale system. It remains to be seen how well it would perform in large AC systems with potentially multiple solutions. The power flow could then be solved in one go without having to switch the states of the converters.

- Regarding the modified grid codes GCP and GCN, they assume the system is mostly inductive, and hence only reactive current is meant to be injected. This assumption may become inappropriate in distribution grids since the resistive component of the grid becomes more relevant. Finding the right balance between active and reactive current could boost the voltage-support.

- The proposed Galerkin method relies on Legendre polynomials given their orthogonality property. Chebyshev polynomials are also known to be orthogonal. A comparison between the performance of the method with one or the other family of polynomials would be of interest. Storing the bases in the form of sparse multidimensional matrices could suppose an improvement as well.

- The parametric power flow is solved in an offline manner in this thesis. That is to say, first the polynomials are obtained, and then the approximated results are extracted. Depending on the problem, the program may need to recalculate the polynomials as new information is gathered. Modifying the algorithm to operate in this online fashion could be rewarding in optimizations with rolling horizons, among others.

- Instead of only parametrizing the powers, certain admittances could also act as parameters. This way, faults at various buses and with different impedances could be parametrized.

Acknowledgements

Són moltes les persones que d'una forma directa o indirecta han contribuït en aquest treball.

En primer lloc, m'agradaria expressar el meu agraïment a l'Oriol, per la seva visió, dedicació i suport. Per descomptat, també em sento grat per l'oportunitat de formar part del CITCEA i en l'actualitat d'eRoots. Igualment, agraeixo a l'Edu el seu entusiasme, saber estar, i totes les gestions realitzades. Així mateix, dono les gràcies a en Marc per la seva paciència i positivisme.

Agradezco a Santiago todo lo que me ha permitido aprender a su lado, y por ser clave en adentrarme en el mundo de los sistemas de potencia.

I would also like to show my gratitude towards Jie, for the numerous fruitful discussions, and to Luis and Esteban, for being able to work alongside them. I am also indebted to the rest of the CITCEA team, for the good times.

My gratitude also goes towards César, for his help at making it possible to publish my first article.

Vull reconèixer l'ajuda dels diversos companys amb qui he coincidit com a estudiant tant a Girona com a Barcelona. En especial a en Jon, en Pablo i també en Yassine, per la convivència.

Querría mostrar mi agradecimiento a Jesús y al resto de las nuevas incorporaciones de eRoots, por todo lo que queda por venir.

Gràcies a tots els amics de la Bisbal i voltants, sobretot a en David, en Pol, l'Adrià, en Ricard i en Genís. Per moltes més estones plegats.

En últim lloc voldria agrair als pares, a la Maria, i al meu germà, per tot el que han representat.

A Environmental impact

The present chapter considers the environmental impact of modern grids with the inclusion of power converters. This is no easy task to carry out as particular cases should be analyzed. Power systems differ in size, elements and topology, so a generic description is given.

A.1 Impact on the transmission system

Power systems that incorporate power electronics equipment are likely to depend less on centralized generation units. This makes it possible for the system to have loads closer to generation points. The topology of the system is expected to become more meshed, and therefore, the current through the lines diminishes. The losses are reduced as a consequence. Hence, the system becomes more efficient. Less generation is required to supply the same load. Thus, systems that integrate power converters are inclined to have an inferior environmental impact than traditional grids.

Besides, power converters offer the capability of controlling the exchanged active and reactive powers. Services such as voltage-support or frequency-support can be provided by generation units coupled to the grid through power converters. By doing so, the participation of generators powered by fossil fuels is prone to diminish.

A.2 Integration of renewable energy

Power converters are essential for integrating renewables at the grid level. They are the interface that connects the renewable resource to the grid, and it achieves this by adapting the electrical magnitudes. Converters are capable of increasing the efficiency by operating at the point of maximum efficiency. In the case of photovoltaics (PV), converters employ the so-called technique of maximum power point tracking (MPPT). The ratio between the voltage and the current is optimized so that the generation achieves maximum efficiency. For wind turbines, converters are capable of regulating the speed of rotation. Similarly, the generation source can work at the point of maximum efficiency as a result. Overall, the environmental impact ought to be reduced given that more power from renewable sources is injected into the grid.

A.3 Replacement of fossil fuel generators

The progressive integration of renewable sources of energy reduces the participation in the generation mix of units powered by fossil fuels. At the current moment, the European electricity emission factor sits at approximately 230 gCO_2/kWh [115], which is less than half of what it used to be in the 90s. Decarbonizing the system means following this trajectory, and ideally achieving carbon neutrality. Even though this scenario may not be reached in the short to medium term, a much higher renewable penetration is required to approach these levels. The evolution towards

modern and decarbonized grids will probably have to be accompanied by storage solutions as well as demand response mechanisms, among others.

A.4 Reflection on the direct impact

This thesis has covered, first of all, the analysis of short-circuits for systems with power converters. The contribution derived from this could imply not having to oversize power lines and protections as more accurate results are provided. Thus, some replacements of the aforementioned elements could be avoided. Besides, the analysis of grid codes indicates that power converters can boost the voltage-support. The installation of more renewable power plants would have a positive impact not only on the voltage-support but also on the environmental level. Moreover, the parametrization of the power flow could also be translated to a higher renewable penetration. The effect that powers from renewable resources have on the grid could be studied. In particular, the parametric power flow allows a precise assessment of the contribution that the renewable penetration level has on the bus voltages and loadings of the lines. For this reason, more renewables are expected to be installed.

B Time planning

Figure 40 shows the temporal evolution of the various tasks that have constituted the project.

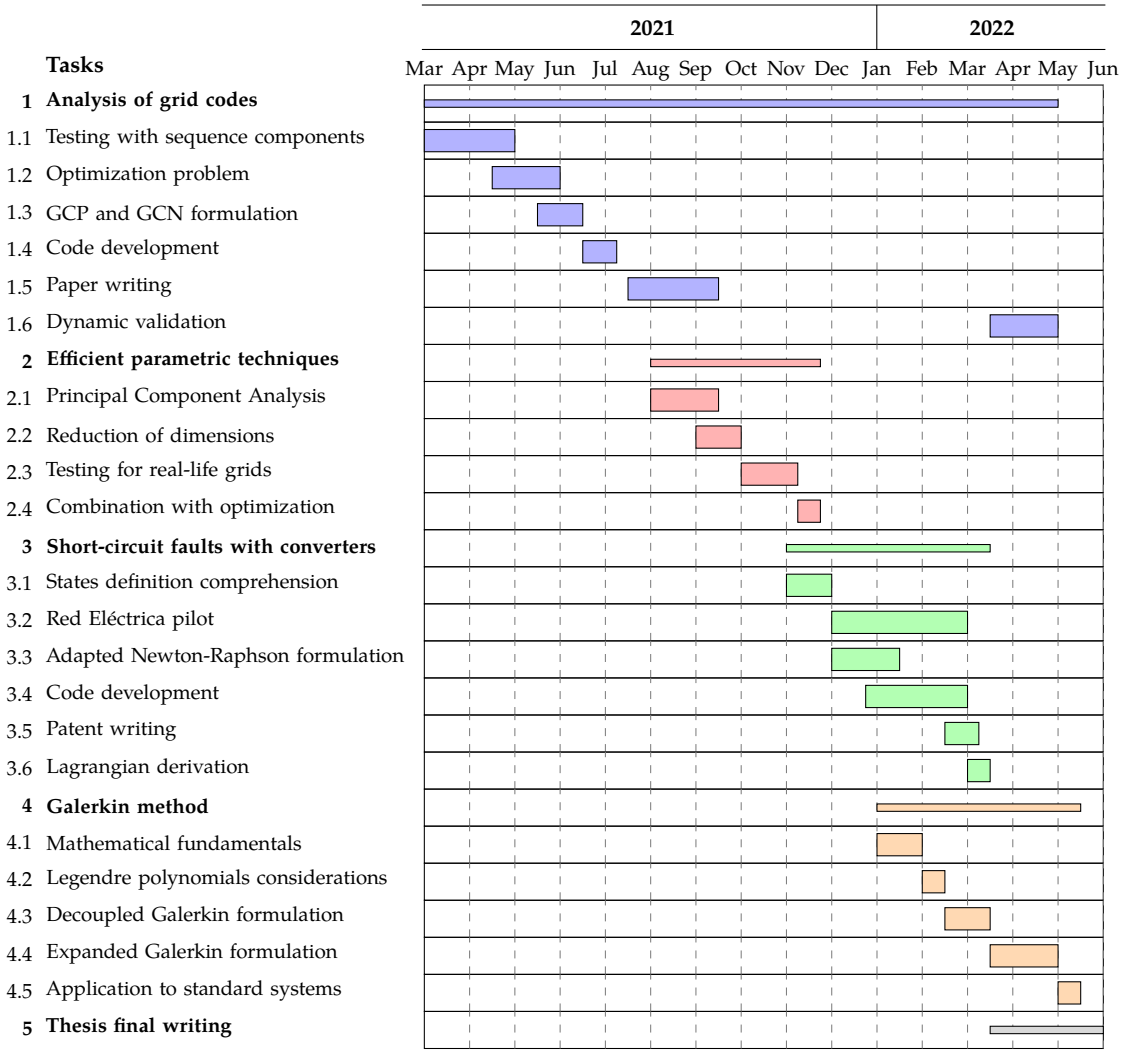

Figure 40: Gantt diagram illustrating the project evolution.

C Budget

C.1 Equipment

The costs of machinery and digital tools required in the project development appear in Table 27.

Table 27: Equipment costs.

Concept	Unit cost (€)	Quantity	Total (€)
Personal computer	1000.00	1	1000.00
PSS/E license for 4 months	11840.00	1	11840.00
Matlab individual annual license	2000.00	1	2000.00
Total			14840.00

C.2 Human resources

The working hours spent on the thesis and related work are captured in Table 28. It also includes the cost linked to the supervision process.

Table 28: Human resources costs.

Concept	Unit cost (€/h)	Quantity (h)	Total (€)
Research	20.00	450	9000.00
Code development	20.00	400	8000.00
Testing	20.00	100	2000.00
Writing	20.00	150	3000.00
Supervision	30.00	50	1500.00
Total			23500.00

C.3 Total budget

The total budget formed by aggregating equipment and human resources is shown in Table 29. No Value Added Tax (VAT) is considered in the budget.

Table 29: Total budget of the thesis.

Concept	Total (€)
Equipment	14840.00
Human resources	23500.00
Total	38340.00

4th of June, 2022

Josep Fanals i Batllori

Bibliography

[1] X. Yu, C. Cecati, T. Dillon, and M. G. Simoes, "The new frontier of smart grids," *IEEE Industrial Electronics Magazine*, vol. 5, no. 3, pp. 49–63, 2011.

[2] E. F. Camacho, T. Samad, M. Garcia-Sanz, and I. Hiskens, "Control for renewable energy and smart grids," *The Impact of Control Technology, Control Systems Society*, vol. 4, no. 8, pp. 69–88, 2011.

[3] M. Hossain, N. Madlool, N. Rahim, J. Selvaraj, A. Pandey, and A. F. Khan, "Role of smart grid in renewable energy: An overview," *Renewable and Sustainable Energy Reviews*, vol. 60, pp. 1168–1184, 2016.

[4] C. Cecati, G. Mokryani, A. Piccolo, and P. Siano, "An overview on the smart grid concept," in *IECON 2010-36th Annual Conference on IEEE Industrial Electronics Society*, IEEE, 2010, pp. 3322–3327.

[5] S. K. Rathor and D. Saxena, "Energy management system for smart grid: An overview and key issues," *International Journal of Energy Research*, vol. 44, no. 6, pp. 4067–4109, 2020.

[6] J. M. Carrasco, L. G. Franquelo, J. T. Bialasiewicz, *et al.*, "Power-electronic systems for the grid integration of renewable energy sources: A survey," *IEEE Transactions on industrial electronics*, vol. 53, no. 4, pp. 1002–1016, 2006.

[7] M. Sandhu and T. Thakur, "Issues, challenges, causes, impacts and utilization of renewable energy sources-grid integration," *International Journal of Engineering Research and Applications*, vol. 4, no. 3, pp. 636–643, 2014.

[8] I. Colak, E. Kabalci, G. Fulli, and S. Lazarou, "A survey on the contributions of power electronics to smart grid systems," *Renewable and Sustainable Energy Reviews*, vol. 47, pp. 562–579, 2015.

[9] M. Manojkumar, K. Porkumaran, and C. Kathirvel, "Power electronics interface for hybrid renewable energy system—a survey," in *2014 International Conference on Green Computing Communication and Electrical Engineering (ICGCCEE)*, IEEE, 2014, pp. 1–9.

[10] K. T. Chi, M. Huang, X. Zhang, D. Liu, and X. L. Li, "Circuits and systems issues in power electronics penetrated power grid," *IEEE Open Journal of Circuits and Systems*, vol. 1, pp. 140–156, 2020.

[11] J. Song, M. Cheah-Mane, E. Prieto-Araujo, and O. Gomis-Bellmunt, "On the solution of equilibrium points of power systems with penetration of power electronics considering converter limitation," *IEEE access*, vol. 9, pp. 67 143–67 153, 2021.

[12] F. Barrero-Gonzalez, *Sistemas de energía eléctrica*. Editorial Paraninfo, 2004.

[13] J. J. Grainger, *Power system analysis*. McGraw-Hill, 1999.

[14] International Electrotechnical Commission, "Short-circuit currents in three-phase ac systems," *Standard IEC 60909-0:2016*, 2016.

[15] R. Aljarrah, H. Marzooghi, V. Terzija, and J. Yu, "Issues and challenges of steady-state fault calculation methods in power systems with a high penetration of non-synchronous generation," in *2019 IEEE Milan PowerTech*, IEEE, 2019, pp. 1–6.

[16] O. Gomis-Bellmunt, J. Song, M. Cheah-Mane, and E. Prieto-Araujo, "Steady impedance mapping in grids with power electronics: What is grid strength in modern power systems?" *International Journal of Electrical Power & Energy Systems*, vol. 136, p. 107 635, 2022.

[17] M. N. I. Sarkar, L. G. Meegahapola, and M. Datta, "Reactive power management in renewable rich power grids: A review of grid-codes, renewable generators, support devices, control strategies and optimization algorithms," *IEEE Access*, vol. 6, pp. 41 458–41 489, 2018.

[18] R. Garcıa-Blanco, D. Borzacchiello, F. Chinesta, and P. Diez, "Monitoring a pgd solver for parametric power flow problems with goal-oriented error assessment," *International Journal for Numerical Methods in Engineering*, vol. 111, no. 6, pp. 529–552, 2017.

[19] F. Q. Hu, M. Y. Hussaini, and P. Rasetarinera, "An analysis of the discontinuous galerkin method for wave propagation problems," *Journal of Computational Physics*, vol. 151, no. 2, pp. 921–946, 1999.

[20] H. Wu, D. Shen, B. Xia, Y. Qiu, Y. Zhou, and Y. Song, "Parametric problems in power system analysis: Recent applications of polynomial approximation based on galerkin method," *Journal of Modern Power Systems and Clean Energy*, vol. 9, no. 1, pp. 1–12, 2020.

[21] Y. Sun, R. Mao, Z. Li, and W. Tian, "Constant jacobian matrix-based stochastic galerkin method for probabilistic load flow," *Energies*, vol. 9, no. 3, p. 153, 2016.

[22] F. Y. Kuo and I. H. Sloan, "Lifting the curse of dimensionality," *Notices of the AMS*, vol. 52, no. 11, pp. 1320–1328, 2005.

[23] D. Shen, H. Wu, B. Xia, and D. Gan, "A principal component analysis-based dimension reduction method for parametric power flow," in *2020 12th IEEE PES Asia-Pacific Power and Energy Engineering Conference (APPEEC)*, IEEE, 2020, pp. 1–5.

[24] T. Kulworawanichpong, "Simplified newton–raphson power-flow solution method," *International journal of electrical power & energy systems*, vol. 32, no. 6, pp. 551–558, 2010.

[25] J. Song, M. Cheah-Mane, E. Prieto-Araujo, and O. Gomis-Bellmunt, "Short-circuit analysis of grid-connected pv power plants considering inverter limits and grid-support," in *11th Solar Storage Power System Integration Workshop (SIW 2021)*, vol. 2021, 2021, pp. 154–160.

[26] H. Margossian, J. Sachau, and G. Deconinck, "Short circuit calculation in networks with a high share of inverter based distributed generation," in *2014 IEEE 5th International Symposium on Power Electronics for Distributed Generation Systems (PEDG)*, IEEE, 2014, pp. 1–5.

[27] A. Kumar, B. K. Jha, D. Singh, and R. K. Misra, "Current injection-based newton–raphson power-flow algorithm for droop-based islanded microgrids," *IET Generation, Transmission & Distribution*, vol. 13, no. 23, pp. 5271–5283, 2019.

[28] R. D. Zimmerman, "Ac power flows, generalized opf costs and their derivatives using complex matrix notation," *MATPOWER Technical Note 2*, 2010.

[29] J. Song, M. Cheah-Mane, E. Prieto-Araujo, and O. Gomis-Bellmunt, "On the solution of equilibrium points of power systems with penetration of power electronics considering converter limitation," *IEEE Access*, vol. 9, pp. 67 143–67 153, 2021. DOI: 10.1109/ACCESS.2021.3077087.

[30] D. P. Kothari and I. Nagrath, *Modern power system analysis*. Tata McGraw-Hill Education, 2003.

[31] N. Tleis, *Power systems modelling and fault analysis: theory and practice*. Elsevier, 2007.

[32] I. Kasikci, *Short circuits in power systems: A practical guide to IEC 60909-0*. John Wiley & Sons, 2018.

[33] A. Egea-Alvarez, S. Fekriasl, F. Hassan, and O. Gomis-Bellmunt, "Advanced vector control for voltage source converters connected to weak grids," *IEEE Transactions on Power Systems*, vol. 30, no. 6, pp. 3072–3081, 2015.

[34] K. Schönleber, E. Prieto-Araujo, S. Ratés-Palau, and O. Gomis-Bellmunt, "Extended current limitation for unbalanced faults in mmc-hvdc-connected wind power plants," *IEEE Transactions on Power Delivery*, vol. 33, no. 4, pp. 1875–1884, 2017.

[35] K. M. Sambarapu and S. M. Halpin, "Sparse matrix techniques in power systems," in *2007 Thirty-Ninth Southeastern Symposium on System Theory*, IEEE, 2007, pp. 194–198.

[36] H. Abbasi, "Sparse: A more modern sparse array library," in *Proceedings of the 17th python in science conference*, 2018, pp. 27–30.

[37] H. Li, J. H. Yeo, J. L. Wert, and T. J. Overbye, "Steady-state scenario development for synthetic transmission systems," in *2020 IEEE Texas Power and Energy Conference (TPEC)*, IEEE, 2020, pp. 1–6.

[38] A. Birchfield, "Activsg2000: 2000-bus synthetic grid on footprint of texas," 2019.

[39] Comptroller Texas, *Texas state expenditures by council of government region. map of texas council of governments regions*, https://comptroller.texas.gov/transparency/reports/expenditures-by-county/2012/cogs/cogmap.php, Accessed: 2022-02-04.

[40] F. L. Alvarado, "Computational complexity in power systems," *IEEE Transactions on Power Apparatus and Systems*, vol. 95, no. 4, pp. 1028–1037, 1976.

[41] J. Alman and V. V. Williams, "A refined laser method and faster matrix multiplication," in *Proceedings of the 2021 ACM-SIAM Symposium on Discrete Algorithms (SODA)*, SIAM, 2021, pp. 522–539.

[42] T. A. Davis *et al.*, *Suitesparse: A suite of sparse matrix software*, 2015.

[43] A. Trias *et al.*, "Helm: The holomorphic embedding load-flow method. foundations and implementations," *Foundations and Trends® in Electric Energy Systems*, vol. 3, no. 3-4, pp. 140–370, 2018.

[44] M. Imhof and G. Andersson, "Power system stability control using voltage source converter based hvdc in power systems with a high penetration of renewables," in *2014 Power Systems Computation Conference*, IEEE, 2014, pp. 1–7.

[45] S. Eren, A. Bakhshai, and P. Jain, "Control of three-phase voltage source inverter for renewable energy applications," in *2011 IEEE 33rd International Telecommunications Energy Conference (INTELEC)*, IEEE, 2011, pp. 1–4.

[46] F. Blaabjerg, Y. Yang, K. Ma, and X. Wang, "Power electronics-the key technology for renewable energy system integration," in *2015 International Conference on Renewable Energy Research and Applications (ICRERA)*, IEEE, 2015, pp. 1618–1626.

[47] A. Abdou, A. Abu-Siada, and H. Pota, "Improving the low voltage ride through of doubly fed induction generator during intermittent voltage source converter faults," *Journal of Renewable and Sustainable Energy*, vol. 5, no. 4, p. 043 110, 2013.

[48] J. Morren, *Grid support by power electronic converters of Distributed Generation units*. 2006.

[49] I. Erlich, W. Winter, and A. Dittrich, "Advanced grid requirements for the integration of wind turbines into the german transmission system," in *2006 IEEE Power Engineering Society General Meeting*, IEEE, 2006, 7–pp.

[50] X. Zhang, Z. Wu, M. Hu, X. Li, and G. Lv, "Coordinated control strategies of vsc-hvdc-based wind power systems for low voltage ride through," *energies*, vol. 8, no. 7, pp. 7224–7242, 2015.

[51] M. Mohseni and S. M. Islam, "Review of international grid codes for wind power integration: Diversity, technology and a case for global standard," *Renewable and Sustainable Energy Reviews*, vol. 16, no. 6, pp. 3876–3890, 2012.

[52] M. Tsili and S. Papathanassiou, "A review of grid code technical requirements for wind farms," *IET Renewable power generation*, vol. 3, no. 3, pp. 308–332, 2009.

[53] J. Conroy and R. Watson, "Low-voltage ride-through of a full converter wind turbine with permanent magnet generator," *IET Renewable power generation*, vol. 1, no. 3, pp. 182–189, 2007.

[54] S. F. Zarei, H. Mokhtari, M. A. Ghasemi, and F. Blaabjerg, "Reinforcing fault ride through capability of grid forming voltage source converters using an enhanced voltage control scheme," *IEEE Transactions on Power Delivery*, vol. 34, no. 5, pp. 1827–1842, 2018.

[55] A. Haddadi, I. Kocar, J. Mahseredjian, U. Karaagac, and E. Farantatos, "Negative sequence quantities-based protection under inverter-based resources challenges and impact of the german grid code," *Electric Power Systems Research*, vol. 188, p. 106 573, 2020.

[56] L. Wieserman and T. McDermott, "Fault current and overvoltage calculations for inverter-based generation using symmetrical components," in *2014 IEEE Energy Conversion Congress and Exposition (ECCE)*, IEEE, 2014, pp. 2619–2624.

[57] A. Camacho, M. Castilla, J. Miret, L. G. de Vicuña, and R. Guzman, "Positive and negative sequence control strategies to maximize the voltage support in resistive–inductive grids

during grid faults," *IEEE Transactions on Power Electronics*, vol. 33, no. 6, pp. 5362–5373, 2017.

[58] M. M. Shabestary, S. Mortazavian, and Y. I. Mohamed, "Overview of voltage support strategies in grid-connected vscs under unbalanced grid faults considering lvrt and hvrt requirements," in *2018 IEEE International Conference on Smart Energy Grid Engineering (SEGE)*, IEEE, 2018, pp. 145–149.

[59] Red Eléctrica de España. "Información sobre implementación de códigos de red de conexión. textos de los códigos de red de conexió europeos. reglamento 2016/631." (2016), [Online]. Available: https://www.esios.ree.es/es/pagina/codigos-red-conexion (visited on 04/25/2020).

[60] A. G. Paspatis and G. C. Konstantopoulos, "Voltage support under grid faults with inherent current limitation for three-phase droop-controlled inverters," *Energies*, vol. 12, no. 6, p. 997, 2019.

[61] A. Camacho, M. Castilla, J. Miret, J. C. Vasquez, and E. Alarcon-Gallo, "Flexible voltage support control for three-phase distributed generation inverters under grid fault," *IEEE transactions on industrial electronics*, vol. 60, no. 4, pp. 1429–1441, 2012.

[62] X. Guo, X. Zhang, B. Wang, W. Wu, and J. M. Guerrero, "Asymmetrical grid fault ride-through strategy of three-phase grid-connected inverter considering network impedance impact in low-voltage grid," *IEEE Transactions on Power Electronics*, vol. 29, no. 3, pp. 1064–1068, 2013.

[63] M. M. Shabestary and Y. A.-R. I. Mohamed, "An analytical method to obtain maximum allowable grid support by using grid-connected converters," *IEEE Transactions on Sustainable Energy*, vol. 7, no. 4, pp. 1558–1571, 2016.

[64] Z. Dai, H. Lin, H. Yin, and Y. Qiu, "A novel method for voltage support control under unbalanced grid faults and grid harmonic voltage disturbances," *IET power Electronics*, vol. 8, no. 8, pp. 1377–1385, 2015.

[65] M. M. Shabestary and Y. A.-R. I. Mohamed, "Asymmetrical ride-through and grid support in converter-interfaced dg units under unbalanced conditions," *IEEE Transactions on Industrial Electronics*, vol. 66, no. 2, pp. 1130–1141, 2018.

[66] J. Peralta, H. Saad, S. Dennetière, and J. Mahseredjian, "Dynamic performance of average-value models for multi-terminal vsc-hvdc systems," in *2012 IEEE Power and Energy Society General Meeting*, IEEE, 2012, pp. 1–8.

[67] M. T. Andani, H. Pourgharibshahi, Z. Ramezani, and H. Zargarzadeh, "Controller design for voltage-source converter using lqg/ltr," in *2018 IEEE texas power and energy conference (TPEC)*, IEEE, 2018, pp. 1–6.

[68] M. G. Taul, S. Golestan, X. Wang, P. Davari, and F. Blaabjerg, "Modeling of converter synchronization stability under grid faults: The general case," *IEEE Journal of Emerging and Selected Topics in Power Electronics*, 2020.

[69] C. L. Fortescue, "Method of symmetrical co-ordinates applied to the solution of polyphase networks," *Transactions of the American Institute of Electrical Engineers*, vol. 37, no. 2, pp. 1027–1140, 1918.

[70] National Grid, *The grid code, issue 6, revision 1*, https://www.nationalgrideso.com/document/162271/download, 2021.

[71] M. Moschakis and N. Hatziargyriou, "Analytical calculation and stochastic assessment of voltage sags," *IEEE Transactions on Power Delivery*, vol. 21, no. 3, pp. 1727–1734, 2006.

[72] M. Mohseni, M. A. Masoum, and S. Islam, "Emergency control of dfig-based wind turbines to meet new european grid code requirements," in *ISGT 2011*, IEEE, 2011, pp. 1–6.

[73] M. M. McKerns, L. Strand, T. Sullivan, A. Fang, and M. A. Aivazis, "Building a framework for predictive science," *arXiv preprint arXiv:1202.1056*, 2012.

[74] M. McKerns, P. Hung, and M. Aivazis, *Mystic: Highly-constrained non-convex optimization and uq, 2009*.

[75] Z. Bian and Z. Xu, "Fault ride-through capability enhancement strategy for vsc-hvdc systems supplying for passive industrial installations," *IEEE Transactions on Power Delivery*, vol. 31, no. 4, pp. 1673–1682, 2016.

[76] M. Cheah, "Offshore wind integration through high voltage direct current systems," Ph.D. dissertation, Cardiff University, 2017.

[77] PSCAD, *Knowledge base. ieee 09 bus system*, https://www.pscad.com/knowledge-base/article/25, 2021.

[78] K. d. Almeida, F. Galiana, and S. Soares, "A general parametric optimal power flow," *IEEE Transactions on Power Systems*, vol. 9, no. 1, pp. 540–547, 1994.

[79] R. Allan, B. Borkowska, and C. Grigg, "Probabilistic analysis of power flows," in *Proceedings of the Institution of Electrical Engineers*, IET, vol. 121, 1974, pp. 1551–1556.

[80] H. Choi, P. J. Seiler, and S. V. Dhople, "Propagating uncertainty in power-system dae models with semidefinite programming," *IEEE Transactions on Power Systems*, vol. 32, no. 4, pp. 3146–3156, 2016.

[81] P. G. Constantine, E. Dow, and Q. Wang, "Active subspace methods in theory and practice: Applications to kriging surfaces," *SIAM Journal on Scientific Computing*, vol. 36, no. 4, A1500–A1524, 2014.

[82] M. D. McKay, R. J. Beckman, and W. J. Conover, "A comparison of three methods for selecting values of input variables in the analysis of output from a computer code," *Technometrics*, vol. 42, no. 1, pp. 55–61, 2000.

[83] Y. Zhou, H. Wu, C. Gu, and Y. Song, "Global optimal polynomial approximation for parametric problems in power systems," *Journal of Modern Power Systems and Clean Energy*, vol. 7, no. 3, pp. 500–511, 2019.

[84] Y. Zhou, H. Wu, C. Gu, and Y. Song, "A novel method of polynomial approximation for parametric problems in power systems," *IEEE Transactions on Power Systems*, vol. 32, no. 4, pp. 3298–3307, 2016.

[85] L. N. Trefethen, *Approximation Theory and Approximation Practice, Extended Edition*. SIAM, 2019.

[86] A. Trias, "The holomorphic embedding load flow method," in *2012 IEEE Power and Energy Society General Meeting*, IEEE, 2012, pp. 1–8.

[87] P. McCarthy, J. Sayre, and B. Shawyer, "Generalized legendre polynomials," *Journal of mathematical analysis and applications*, vol. 177, no. 2, pp. 530–537, 1993.

[88] D. Pérez and Y. Quintana, "A survey on the weierstrass approximation theorem," *arXiv preprint math/0611038*, 2006.

[89] S. Abhyankar, Q. Cui, and A. J. Flueck, "Fast power flow analysis using a hybrid current-power balance formulation in rectangular coordinates," in *2014 IEEE PES T&D Conference and Exposition*, IEEE, 2014, pp. 1–5.

[90] A. Meseguer, *Fundamentals of Numerical Mathematics for Physicists and Engineers*. John Wiley & Sons, 2020.

[91] University of Washington, Electrical Engineering Department, *Power systems test case archive*, http://labs.ece.uw.edu/pstca/pf14/pg_tca14bus.htm, Accessed: 2010-09-30.

[92] E. N. Azadani, S. Hosseinian, P. H. Divshali, and B. Vahidi, "Stability constrained optimal power flow in deregulated power systems," *Electric Power Components and Systems*, vol. 39, no. 8, pp. 713–732, 2011.

[93] K. d. Almeida, F. Galiana, and S. Soares, "A general parametric optimal power flow," *IEEE Transactions on Power Systems*, vol. 9, no. 1, pp. 540–547, 1994.

[94] R. García-Blanco, "Efficient solvers for power flow equations: Parametric solutions with accuracy control assessment," 2017.

[95] R. G. Blanco, "Efficient solvers for power flow equations: Parametric solutions with accuracy control assessment," Ph.D. dissertation, Universitat Politècnica de Catalunya (UPC), 2017.

[96] D. Shen, H. Wu, B. Xia, and D. Gan, "A principal component analysis-based dimension reduction method for parametric power flow," in *2020 12th IEEE PES Asia-Pacific Power and Energy Engineering Conference (APPEEC)*, 2020, pp. 1–5. DOI: 10.1109/APPEEC48164.2020.9220420.

[97] F. Chinesta, A. Ammar, and E. Cueto, "Recent advances and new challenges in the use of the proper generalized decomposition for solving multidimensional models," *Archives of Computational methods in Engineering*, vol. 17, no. 4, pp. 327–350, 2010.

[98] R. G. Blanco, "Efficient solvers for power flow equations: Parametric solutions with accuracy control assessment," Ph.D. dissertation, Universitat Politècnica de Catalunya (UPC), 2017.

[99] R. García-Blanco, P. Díez, D. Borzacchiello, and F. Chinesta, "A reduced order modeling approach for optimal allocation of distributed generation in power distribution systems," in *2016 IEEE International Energy Conference (ENERGYCON)*, IEEE, 2016, pp. 1–6.

[100] P. E. Black, "Greedy algorithm," *Dictionary of Algorithms and Data Structures*, vol. 2, p. 62, 2005.

[101] Y. He, Y. Song, G. Du, and D. Zhang, "Research of matrix inversion acceleration method," in *2009 International Conference on Computational Intelligence and Software Engineering*, IEEE, 2009, pp. 1–4.

[102] A. Trias, "Fundamentals of the holomorphic embedding load-flow method," *arXiv preprint arXiv:1509.02421*, 2015.

[103] S. Rao, Y. Feng, D. J. Tylavsky, and M. K. Subramanian, "The holomorphic embedding method applied to the power-flow problem," *IEEE Transactions on Power Systems*, vol. 31, no. 5, pp. 3816–3828, 2015.

[104] G. Berkooz, P. Holmes, and J. L. Lumley, "The proper orthogonal decomposition in the analysis of turbulent flows," *Annual review of fluid mechanics*, vol. 25, no. 1, pp. 539–575, 1993.

[105] J. Weiss, "A tutorial on the proper orthogonal decomposition," in *AIAA Aviation 2019 Forum*, 2019, p. 3333.

[106] Y. Zhou, H. Wu, C. Gu, and Y. Song, "A novel method of polynomial approximation for parametric problems in power systems," *IEEE Transactions on Power Systems*, vol. 32, no. 4, pp. 3298–3307, 2016.

[107] Y. Shin and D. Xiu, "Nonadaptive quasi-optimal points selection for least squares linear regression," *SIAM Journal on Scientific Computing*, vol. 38, no. 1, A385–A411, 2016.

[108] S. Peñate-Vera, *Gridcal. 5-node grid creation script*, version 4.1.0, Aug. 22, 2021. [Online]. Available: https://github.com/SanPen/GridCal.

[109] J. A. Martinez and G. Guerra, "Optimum placement of distributed generation in three-phase distribution systems with time varying load using a monte carlo approach," in *2012 IEEE Power and Energy Society General Meeting*, IEEE, 2012, pp. 1–7.

[110] J. M. Morales, L. Baringo, A. J. Conejo, and R. Mínguez, "Probabilistic power flow with correlated wind sources," *IET generation, transmission & distribution*, vol. 4, no. 5, pp. 641–651, 2010.

[111] M. Fan, V. Vittal, G. T. Heydt, and R. Ayyanar, "Probabilistic power flow studies for transmission systems with photovoltaic generation using cumulants," *IEEE Transactions on Power Systems*, vol. 27, no. 4, pp. 2251–2261, 2012.

[112] T. Boehme, A. R. Wallace, and G. P. Harrison, "Applying time series to power flow analysis in networks with high wind penetration," *IEEE transactions on power systems*, vol. 22, no. 3, pp. 951–957, 2007.

[113] H. Seifi and M. S. Sepasian, *Electric power system planning: issues, algorithms and solutions*. Springer Science & Business Media, 2011.

[114] J. Song, M. Cheah-Mane, E. Prieto-Araujo, and O. Gomis-Bellmunt, "Short-circuit analysis of ac distribution systems dominated by voltage source converters considering converter limitations," *IEEE Transactions on Smart Grid*, pp. 1–1, 2021. DOI: 10.1109/TSG.2021.3102011.

[115] European Environment Agency, *Greenhouse gas emission intensity of electricity generation in europe*, https://www.eea.europa.eu/ims/greenhouse-gas-emission-intensity-of-1, Accessed: 2022-03-04.